arXiv:0709.3709v1 [hep-ph] 24 Sep 2007

UNIVERSITY OF CRETE
DEPARTMENT OF PHYSICS

# On vortices and solitons in Goldstone and abelian-Higgs models

C.G.K. Doudoulakis

Heraklion, Greece, 11 October 2007

*Ευχαριστώ το Θεό...*

Christos G. K. Doudoulakis

# *Δίνες και σολιτόνια στο μοντέλο Goldstone και σε αβελιανά μοντέλα Higgs*

Thesis
submitted to the Department of Physics, University of Crete
for the Degree of Doctor of Philosophy in Physics

Heraklion, Greece, 11 October 2007

# On vortices and solitons in Goldstone and abelian-Higgs models

## *Δίνες και σολιτόνια στο μοντέλο Goldstone και σε αβελιανά μοντέλα Higgs*

| | |
|---|---|
| Thesis author | Christos G. K. Doudoulakis |
| Thesis supervisor | Prof. T. N. Tomaras |
| Thesis committee | T. N. Tomaras<br>E. Kiritsis<br>N. Tsamis<br>X. Zotos<br>G. Tsironis<br>P. Ditsas<br>A. Petkou |

Department of Physics, University of Crete
Heraklion, Greece

11 October 2007

# Contents

Acknowledgements . . . . . . . . . . . . . . . . . . . . . . . . . . . . 12
Abstract . . . . . . . . . . . . . . . . . . . . . . . . . . . . . . . . 13

**1 Introduction 14**
1.1 Formation of defects: The Kibble mechanism . . . . . . . . . . 16
1.2 Classification of defects . . . . . . . . . . . . . . . . . . . . . 18
1.3 Superconducting cosmic strings . . . . . . . . . . . . . . . . . . 20
1.4 Brief history of research on defects . . . . . . . . . . . . . . . 21
1.5 Solitons . . . . . . . . . . . . . . . . . . . . . . . . . . . . . . 23

**PART I: THEORETICAL FRAMEWORK 26**

**2 Cosmic string field theory 27**
2.1 Spontaneous symmetry breaking . . . . . . . . . . . . . . . . . . 28
  2.1.1 Spontaneous breaking of a global symmetry . . . . . . 28
  2.1.2 Spontaneous breaking of a gauge symmetry . . . . . . 29
2.2 Effective potential . . . . . . . . . . . . . . . . . . . . . . . . 30
2.3 Phase transitions . . . . . . . . . . . . . . . . . . . . . . . . . 31
  2.3.1 First order phase transition . . . . . . . . . . . . . . 31
  2.3.2 Second order phase transition . . . . . . . . . . . . . 32
2.4 Superconductivity and penetration depth . . . . . . . . . . . . 33
2.5 Nielsen-Olesen vortex . . . . . . . . . . . . . . . . . . . . . . . 36
  2.5.1 Introduction . . . . . . . . . . . . . . . . . . . . . . . 36
  2.5.2 The model . . . . . . . . . . . . . . . . . . . . . . . . 36
  2.5.3 Ansatz and equations . . . . . . . . . . . . . . . . . . 38

2.5.4 Virial theorem . . . . . . . . . . . . . . . . . . . . . . . 39
2.5.5 Numerical solution . . . . . . . . . . . . . . . . . . . . 42
2.6 Straight bosonic superconducting string . . . . . . . . . . . . 43
2.6.1 Introduction . . . . . . . . . . . . . . . . . . . . . . . . 43
2.6.2 The model . . . . . . . . . . . . . . . . . . . . . . . . . 43
2.6.3 Ansatz and equations . . . . . . . . . . . . . . . . . . . 45
2.6.4 Numerical solution . . . . . . . . . . . . . . . . . . . . 47

**PART II: SEARCH FOR STRINGS AND SOLITONS 49**

**3 Antiperiodic solitons of the Goldstone model on $S^1$ 50**
3.1 Introduction . . . . . . . . . . . . . . . . . . . . . . . . . . . 51
3.2 The classical solutions . . . . . . . . . . . . . . . . . . . . . . 51
3.3 The trivial solution . . . . . . . . . . . . . . . . . . . . . . . 52
3.4 Three types of non-trivial solutions . . . . . . . . . . . . . . . 53
3.5 Stability Analysis . . . . . . . . . . . . . . . . . . . . . . . . 57
3.5.1 Type-I solutions . . . . . . . . . . . . . . . . . . . . . . 57
3.5.2 Type-II and Type-III solutions . . . . . . . . . . . . . . 61
3.6 Conclusions . . . . . . . . . . . . . . . . . . . . . . . . . . . 62
3.7 APPENDIX . . . . . . . . . . . . . . . . . . . . . . . . . . . . 64
3.7.1 Part I: Jacobi elliptic functions . . . . . . . . . . . . . 64

**4 $U(1)$ model for straight strings 66**
4.1 Introduction . . . . . . . . . . . . . . . . . . . . . . . . . . . 67
4.2 The $U(1)_A$ model . . . . . . . . . . . . . . . . . . . . . . . . 68
4.3 The $U(1)_A$ model: Search for stable vortices . . . . . . . . . . 70
4.4 The $U(1)_A$ model: Numerical results . . . . . . . . . . . . . . 71
4.4.1 Analysis for $2.13 \leq \beta \leq 2.2$ . . . . . . . . . . . . . . . 74
4.4.2 Reasons for instability when $\beta > 2.2$ . . . . . . . . . . . 74
4.4.3 Reasons for instability when $\beta \leq \beta_{crit}$ . . . . . . . . . 75
4.5 Conclusions . . . . . . . . . . . . . . . . . . . . . . . . . . . 77

**5 On axially symmetric solitons in Abelian-Higgs models 79**

5.1 Introduction . . . . . . . . . . . . . . . . . . . . . . . . . . . . 80
5.2 The $U(1)_A \times U(1)_W$ model . . . . . . . . . . . . . . . . . . . . . 81
5.3 The $U(1)_A \times U(1)_W$ model: Search for superconducting vortex rings . . . . . . . . . . . . . . . . . . . . . . . . . . . . . . . 83
5.4 The $U(1)_A \times U(1)_W$ model: Numerical results . . . . . . . . . 93
5.5 Explanation concerning the instability of the vortex ring . . . 97
5.6 $U(1)_W$ model: Vortex ring without supercurrent . . . . . . . . 101
5.7 Conclusions . . . . . . . . . . . . . . . . . . . . . . . . . . . . 102
5.8 APPENDIX . . . . . . . . . . . . . . . . . . . . . . . . . . . . 103
    5.8.1 Part I: Derivation of the formula $\mathcal{I}^{\psi}_{max} \leq \sqrt{\sigma} eu$ . . . . . 103
    5.8.2 Part II: Toroidal coordinate system . . . . . . . . . . . 104
    5.8.3 Part III: Cylindrical coordinate system . . . . . . . . . 104
    5.8.4 Part IV: Field profiles in different $z$ levels . . . . . . . 105

**6 The extended $U(1) \times U(1)$ model for vortex rings 107**
6.1 Introduction . . . . . . . . . . . . . . . . . . . . . . . . . . . . 108
6.2 The $U(1)_A \times U(1)_W$ model . . . . . . . . . . . . . . . . . . . . 108
6.3 The extended $U(1)_A \times U(1)_W$ model . . . . . . . . . . . . . 109
6.4 The extended $U(1)_A \times U(1)_W$ model: Numerical results . . . 116
6.5 Discussion . . . . . . . . . . . . . . . . . . . . . . . . . . . . . 120
6.6 Conclusions . . . . . . . . . . . . . . . . . . . . . . . . . . . . 121

**7 Conclusions 122**
7.1 Conclusions . . . . . . . . . . . . . . . . . . . . . . . . . . . . 123

**PART III: NUMERICAL METHODS 125**

**8 Summary of the algorithms used 126**
8.1 Relaxation . . . . . . . . . . . . . . . . . . . . . . . . . . . . . 127
8.2 Runge-Kutta . . . . . . . . . . . . . . . . . . . . . . . . . . . . 127
8.3 Newton-Raphson . . . . . . . . . . . . . . . . . . . . . . . . . . 129
8.4 Energy minimization . . . . . . . . . . . . . . . . . . . . . . . 130

# Acknowledgements

It is a great pleasure to thank my advisor, Professor Theodore N. Tomaras. His great experience and ability to answer my questions in a simple and attractive way, were very helpful for me.

I would like to thank the Physics Department of the University of Crete for its warm hospitality and financial support all these years.

I would like to thank Dr. M.D.Kapetanakis for useful discussions, advice and support in difficult moments. We've passed together 11 years since our first day in Physics department. I would also like to thank N.Lagos for useful discussions and support in difficult moments.

I would like to thank Dr. E.D.M.Kavoussanaki for collaboration, useful discussions and advice.

Finally, I would like to thank my parents, for their love and support.

# Abstract

In the present work we discuss non-linear physics problems such as Nielsen-Olesen strings, superconducting bosonic straight strings and static vortex rings. We start with a toy model. We search for antiperiodic solitons of the Goldstone model on a circle. Such models provide the basis as well as useful hints for further research on three-dimensional more realistic problems. We proceed with a full research on a $U(1)$ model which admits stable straight string solutions in a small, numerically determined area. That model has a Ginzburg-Landau potential with a cubic term added to it and can be found in condensed matter problems as well. The next part of our research, has to do with a $U(1) \times U(1)$ model which is the main subject of our interest. There, we search for stable axially symmetric solutions which are solitons, which can represent particles, the mass of which is of the order of TeV. The confirmation or rejection of the existence of those defects is of great interest if we consider that LHC will work in the same energy range. In our study, we find out that due to current quenching, these vortex rings seem to be unstable. We also extend the model of vortex rings by adding higher derivative terms which are favorable for stability. After the extensive analysis we performed, we conclude that these objects don't seem to be stable. The reasons which brought us to this conclusion are explained.

# Chapter 1

# Introduction

In order to study topological defects, in general we need to define the order parameter, to identify the pattern of broken symmetries and to classify the defects we have. A *defect* is defined as a space region containing the discontinuity of the order parameter. In field theory, the order parameter is represented by scalar fields. The topological defect is the singularity in the continuum that cannot be removed by continuous deformation of the local region in the vicinity of the singularity. Strings, monopoles, textures, domain walls or combination of them are some examples of defects. Strings especially are of interest to us.

Current theories of particle physics place chronologically the formation of topological defects on the violent stages of the early evolution of the universe. If somehow their existence is observationally proved, that would be of great importance for particle physics and cosmology, as the notion of topological defects exists in most interesting models of high energy physics trying to describe the early universe. Those defects would be a direct consequence of events of the very early universe.

The same notion is also present in condensed matter physics. Simple examples are the domains in a ferromagnet or the magnetic vortices in thin ferromagnetic films [1] or the vortices in Ginzburg-Landau superconductors [2]. Domains are regions in which the magnetic dipoles are aligned, separated by domain walls. Liquid crystals exhibit an array of topological defects, such as strings and monopoles. Defects can also been found in biochemistry, notably in the process of protein folding. A more specific example is that when liquid helium is quickly pressure-quenched around a critical temperature, namely $T_c$, Zurek argued that vortices carrying rotation in quantized amounts form and represent defects analogous to cosmic strings. More re-

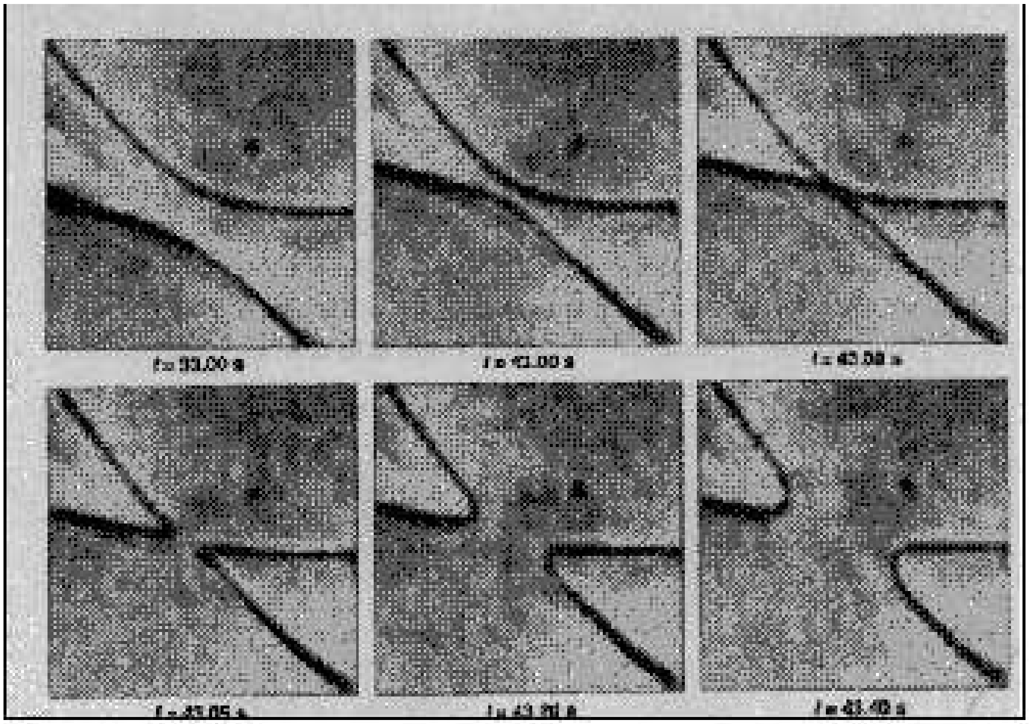

Figure 1.1: String intercommutation in a nematic liquid crystal. Further details can be found in [11].

cently, the existence of vorton solutions is involved in sectors such as QCD [3] and high-$T_c$ superconductivity [4]. There are differences from the cosmological case where relativistic dynamics must be used and gravity is important, but their formation can offer interesting hints for cosmology [5, 6, 7]. One can also think of Bose-Einstein condensates (BEC) (i.e. see [8]), vortices in superfluid Helium-3 and Helium-4 [9, 10] , or nematic liquid crystals [11, 12] (see also figs.1.1, 1.2).

Interest in such defects appears in many branches of theoretical and experimental physics such as particle physics models, experimental high energy physics, cosmology, observational astrophysics, experimental condensed matter physics and, recently, superstring theory. In contrast to other branches of physics, it is established that **no** such topologically stable defects can exist in the Standard Model (SM) of Particle Physics. But, as pointed out in [13], there is the possibility of quasi-topological metastable defects in popular extensions of the SM such as the two-Higgs Standard Model (2HSM) [14]. This was proved to be the case for codimension one and two defects [14], but the search for particle-like solitons of this kind was not so far succesfull [15].

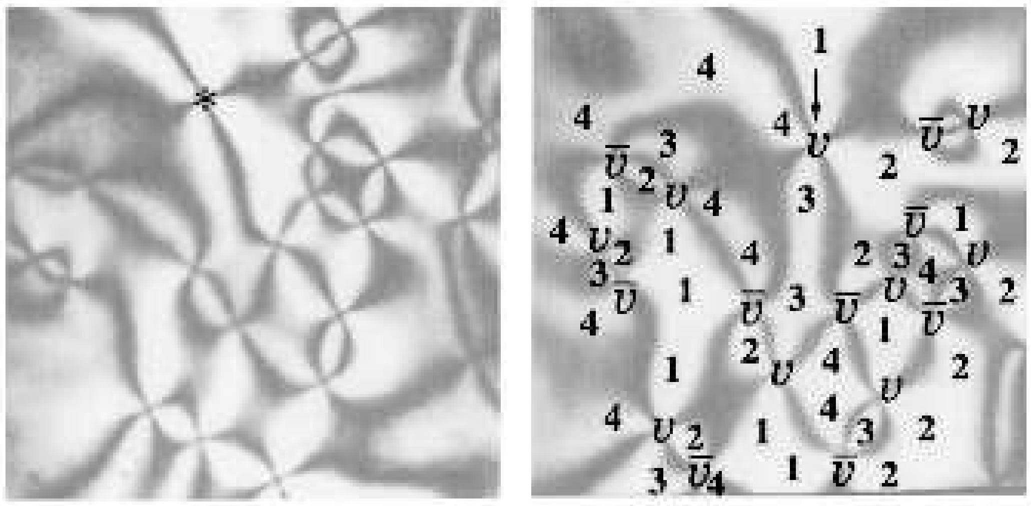

Figure 1.2: Vortex-antivortex formation in a nematic liquid crystal. Further details can be found in [12].

Such solitons, if they exist, in the electroweak theory are very interesting. They will have a mass of a few TeV, and should soon be produced in the LHC at CERN. Search for such objects is the main topic of the present work.

## 1.1 Formation of defects: The Kibble mechanism

The explanation of the formation of topological defects, uses a very important notion of particle physics which is that of *spontaneous symmetry breaking*. This phenomenon appears when the ground state of the system is characterised by a non-zero expectation value of the Higgs field and does not exhibit the full symmetry of the Lagrangian. It is believed that the way to unification of all fundamental natural forces involves this notion. The *Higgs field*, named after the British physicist Peter Higgs, is a postulated quantum field, mediated by the Higgs boson, which is believed to permeate the entire universe. Its presence is said to be required in order to explain the large difference in mass between those particles which mediate weak interactions (the $W$ and $Z$ bosons) and that which mediates electromagnetic interactions (the photon).

This is a spin 0 field which signals the breaking of some symmetry in our theory. This means that when our system goes from a state of higher

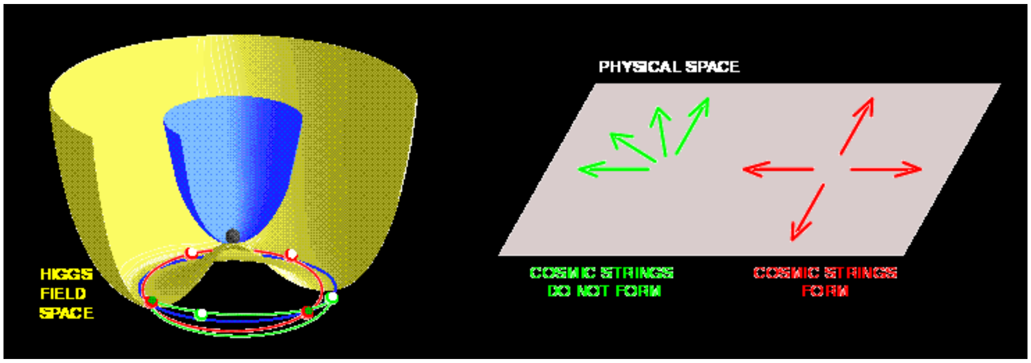

Figure 1.3: Higgs field space and physical space. Above $T_c$ the potential has a minimum at $\phi_1 = 0 = \phi_2$, but below $T_c$ the new form of the potential has its minima on a circle. If $m$ is an element of the coset space $G/H$ and $\Psi_1$ and $\Psi_2$ two different states at that circle, then $m\Psi_1 = \Psi_2$. Generally, every element of the coset space $G/H$ can produce all the other minimum energy states when acting on any of them. Thus, $G/H = \mathcal{M}$ where $\mathcal{M}$ stands for the vacuum manifold. On the right side of the figure one can have a picture of how a cosmic string forms when different regions of space met, having their Higgs field phases as above. Picture from astro-ph/0303504 (A.Gangui).

symmetry to a final state where it obeys a smaller group of symmetry rules, this field represents the symmetry breaking *order parameter* which acquires a non-zero vacuum expectation value. In the stages we described above, this field can settle into different ground states or to be more specific, the phase of the Higgs field can acquire different values. Topological defects are objects that locally restore the original symmetry. More details about spontaneous symmetry breaking will be given in the next chapter.

In the context of the standard Big Bang theory, the spontaneous breaking of fundamental symmetries is realized through phase transitions in the early universe. The time needed for such a transition is small compared to the expansion time. It is believed that all forces were united in the early stages of our cosmos and that these phase transitions play a significant role in order to end up to what we today know as four different natural forces. It is also believed that these transitions are the source of defect formation and if that's true, then there is an important link between particle physics and cosmology.

Kibble in 1976 [16] first noted that, in an expanding universe where are separated regions that have no "communication" amongst themselves, due to lack of causal contact, we can assume that they have different values of the phase of the Higgs field. As the universe expands and cools down, these regions expand and some of them come in contact with others. Thus, it is

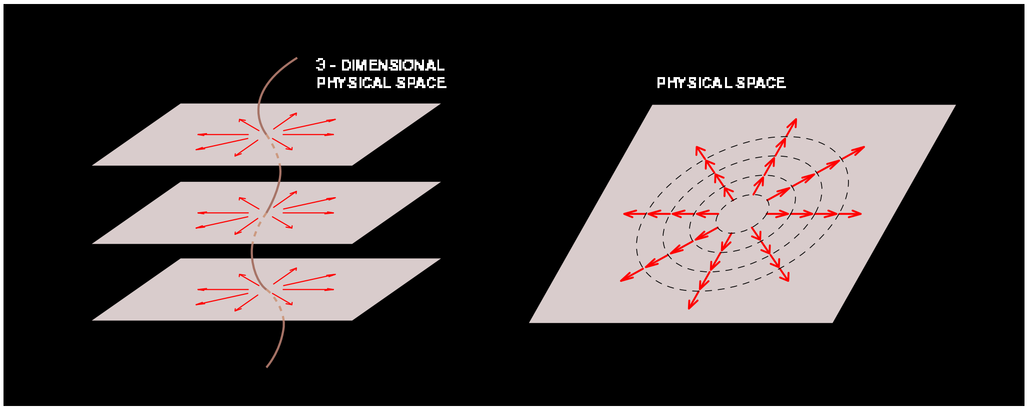

Figure 1.4: Cosmic string formation. Picture from astro-ph/0303504 (A.Gangui).

not impossible that by following a closed path through these regions that are in contact, their phases (orientation of the Higgs field) vary from 0 to $2n\pi$, where $n \neq 0$ is an integer and stands for the *winding number* of the field. Then, the "meeting point" between these "bubbles" is the core of a cosmic string (figs.1.3 and 1.4). In other words, a cosmic string forms when, for purely topological reasons, the orientation of the arrows cannot be adjusted in order to keep the Higgs field in the minimum energy state everywhere.

## 1.2 Classification of defects

The different kinds of defects are due to different symmetries of the Higgs field itself. For example, the Higgs field may have two possible states to fall into. Then, when regions that have taken opposite choices meet, their boundary is a *domain wall*. This narrow region of the defect is called *false vacuum* and should not exist but it does so, due to the geometry of the Higgs field. Now, if Higgs field has circular symmetry it can be represented by a "mexican-hat" analogy because ground state can lie anywhere within a circle in field space and its position can be denoted by an arrow. This is the case shown in the previous section and the defect involved there was a cosmic string.

Consider a temperature-dependent potential which at high temperatures has a single minimum at $\phi_c = 0$, while under a critical temperature $T_c$ it transforms into a potential which has a minimum for a non-trivial value of the field, $\phi_c \neq 0$ (fig.1.5). When $T < T_c$ the system will try to minimize its energy and will move at the new minimum. When this is done, and the

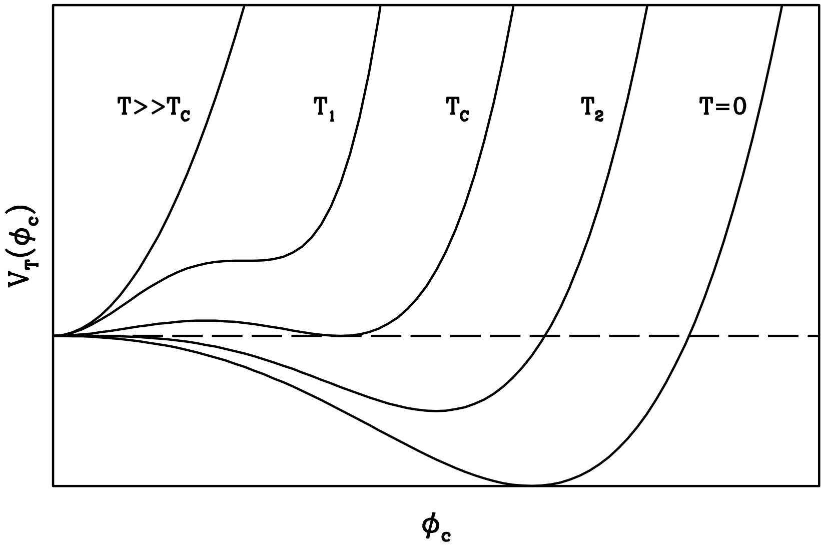

Figure 1.5: Temperature dependent potential. Here is an example of such potential and how it changes shape as temperature falls. It is clearly visible that above $T_c$ the system has one stable minimum at $\phi_c = 0$. As $T \rightarrow 0$ the potential develops a minimum at $\phi_c \neq 0$ and when the system settles there, we say that the initial symmetry of the system is broken. The ground state of the model does not respect the original symmetry of the Lagrangian. Picture from astro-ph/0303504 (A.Gangui).

phase transition has finished, our system is ruled by a smaller symmetry group, say $H$. Also name the previous, bigger symmetry group as $G$. Then the coset space $G/H$ produces the vacuum manifold $\mathcal{M}$ and the topology of the latter determines the type of defect that will finally arise. Homotopy theory helps us by telling us how to map $\mathcal{M}$ into physical space (fig.1.3). For example $\pi_1(\mathcal{M}) \neq \mathbf{1}$ indicates that the first homotopy group is not trivial and practically informs us for the existence of non contractible loops in $\mathcal{M}$, that is to say cosmic strings. Thus, in models where the symmetry of the ground state is associated with a non-trivial homotopy group, topological defects exist.

| | | |
|---|---|---|
| $\pi_0(\mathcal{M}) \neq \mathbf{1}$ | $\mathcal{M}$ disconnected | DOMAIN WALLS |
| $\pi_1(\mathcal{M}) \neq \mathbf{1}$ | non contractible loops in $\mathcal{M}$ | COSMIC STRINGS |
| $\pi_2(\mathcal{M}) \neq \mathbf{1}$ | non contractible 2-spheres in $\mathcal{M}$ | MONOPOLES |
| $\pi_3(\mathcal{M}) \neq \mathbf{1}$ | non contractible 3-spheres in $\mathcal{M}$ | TEXTURES |

## 1.3 Superconducting cosmic strings

*Cosmic strings* are linear vortex defects predicted to have formed at a cosmological phase transition during which the vacuum manifold was *not* simply connected. These strings have enormous energy per unit length, namely $\mu$. Roughly speaking, for a string created at a phase transition characterized by temperature $T_c$, then $\mu \sim T_c^2$. For GUT strings, $\mu \sim 10^{22} g/cm$. Their gravitational effects though, are negligible. The strength of their gravitational interaction is given in terms of the dimensionless quantity $G\mu \sim (T_c/M_P)^2$, with $G$ the Newton's constant and $M_P$ the Planck mass. There are other significant astrophysical effects when, for example, strings have supercurrent. The latter can make them transform into thin superconducting wires with critical current $\sim T_c$ thus, interacting strongly with magnetic fields.

It is useful to note here that the notion of *superconductivity* is also important in our research presented in Part II, where one can find details. This phenomenon was first discovered by Onnes in 1911 and exhibits many astonishing and interesting features, two very well known of which are:

- The superconducting material [1] while being below a critical temperature $T_c$, allows current flow in its interior with *zero* resistance.
- Magnetic fields generally can not penetrate in the interior of a superconducting material, the well known *Meißner effect.* [2]

There are two kinds of superconductors:

- *Type I:* Below a critical field $H_c(T)$ there is no penetration of flux inside the superconducting material, while above $H_c(T)$ the field penetrates perfectly in the material which has turned into its normal non-superconducting state.
- *Type II:* Below a critical field $H_a(T)$ again there is no penetration. The difference here is the existence of a second critical field $H_b(T)$ above which normal state is restored but for values of $H_c(T)$ where

---

[1] Not all elements or combinations of elements can be superconducting. In the years passed since its discovery, superconductivity appears in many other materials and the challenge for the years to come, is the construction of a material appearing superconducting properties below a $T_c$ which will be comparable to every day temperatures, say around 280 $^oK$. We are at $\sim 140$ $^oK$ for now.

[2] This effect is of crucial importance for the stability of vortex rings which will be studied later on.

$H_b(T) > H_c(T) > H_a(T)$ is valid, the applied field penetrates partially in the material which is in a *mixed* state where both normal and superconducting regions coexist.

## 1.4 Brief history of research on defects

- The beginning...

Skyrme in 1961 [17], presented the first three dimensional topological defect solution arising in a non-linear field theory and proposed that such solutions would have an important role in particle physics. Nambu in 1966, suggested the cosmological significance of defects. Before such proposals could be taken seriously, one had to establish the existence of stable topological defect solutions in realistic renormalizable theories. An important step towards that direction, was the discovery of defect solutions in Higgs and Yang-Mills theories, notably the Nielsen-Olesen vortex in 1973 [18], the 't Hooft-Polyakov monopole in 1974 [19] as well as GUT monopoles (i.e [20]).

The cosmological implications of symmetry breaking were pointed out by Kirzhnits in 1972 [21], who suggested that spontaneously broken symmetries in a field theory can be restored at high temperatures just as they are in condensed matter systems. Zel'dovich, Kozbarev and Okun in 1974 [22], argued that domain walls would form at phase transitions in which a discrete symmetry was broken. Weinberg in 1974 [23], noted that cosmic domains could form and Everett [24], in the same year studied possible interactions of domain walls with matter. It was then the pioneering paper of Kibble [16] in 1976, which showed that the existence of defects, depends on the topology of the vacuum manifold classifying them using homotory theory.

The circumstances above, led many researchers to start studying those defects and their role in cosmology. A new "golden" era for topological defects was starting.

- The "booming"...

The first interest in studying them comes from the fact that since a typical GUT predicts a few phase transitions and because the vacuum structure needed to form strings is generically realized, one can assume, also by following Vilenkin, that cosmic strings have a considerable existence probability. Cosmic strings appear in many papers especially in the 80's and early 90's as

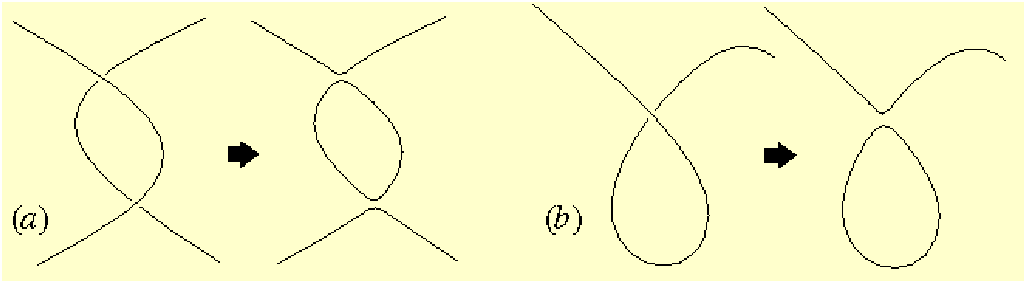

Figure 1.6: Apart from the intersection of two different strings (a), self-intersection of a cosmic string can be another mechanism of loop production (b). Picture from [135].

having important cosmological implications in structure formation by providing density fluctuations and thus, becoming the seed of galaxies [16]-[31]. Cosmic strings appear either as infinite straight strings or as rings. However, due to disagreement with the observations of the Cosmic Microwave Background, this theory was left aside until nowadays, as superstring theory discusses the possibility for the existence of cosmic superstrings in the framework of braneworld cosmologies. Such superstrings could play, under conditions, the role of cosmic strings. There was also an observational "adventure" as we will explain below.

There are numerous papers on the consequences of a possible existence of superconducting vortex rings [32]-[50]. String loops are predicted to have formed during phase transitions at the early universe. [15] refers to GUT mass scale $U(1)$ symmetry breaking occurence which gives rise to strings having important role in many popular cosmological scenarios seen mostly in the 80's. The cosmological role of loops has been analyzed in many papers such as [51]-[60], where the scenario is that galaxies condensate around oscillating loops of mass $\approx 10^9 M_\odot$. By the time those strings have radiated away their energy, the matter density fluctuations are large enough to grow independently. Additional loops can be produced by self-intersection of a string or by intersection of different strings (fig.1.6). Closed loops are doomed to extinction due to oscillation and gradual loss of energy through gravitational radiation [25, 26], unless perhaps they reintersect longer strings and become reconnected [32]. On the other hand, it's crucial for closed loops to have possibility more than 1/2 to intersect themselves and break up into smaller pieces in order not to dominate the energy density of a radiation-dominated universe [51]. Qualitative as well as quantitative details were revealed by simulations [61]-[67] of a cosmic string network consisting of infinite straight strings and a small percentage of loops.

- Today...

Until today, physicists search for a possible signal of a topological defect from the early universe through the ways the theories give them for detecting them [54], [68]-[72]. Especially for the case of a ring with supercurrent, when current saturates, such a string will emit particles copiously and may be seen as an X-ray or $\gamma$-ray source and it is believed to give contributions to X-ray background and high-energy ($10^{20}$ eV) cosmic rays [74]. In [76]-[78] one can find observations which were believed to involve, for the first time, a topological defect through gravitational lensing while in [79] the lensing from dark matter was excluded. Later observations and analysis though, showed that this is not in fact the case [80]. In fact, it is a very rare case of almost identical (up to 99.96% !) elliptical galaxies, separated by a misleadingly small, as it proved, distance. In [56] Kibble supports the cosmic string cosmological scenario using the above observations and predictions of fundamental string theory. Concerning the latter, in [81, 82] one can find details about the possibility of the existence of cosmic superstrings, that is to say superstrings of cosmic length, and observation of them as cosmic strings. As it concerns the observations, if we ever detect a topological defect, that would be a discovery of great importance. But even an observed absence of topological defects, is very useful too (i.e. [83]), since it imposes constraints on particle physics model building. For example, the non-abundance of magnetic monopoles inspired the inflationary revolution in cosmology and GUT's models are constrained to provide the requisite amount of inflation. Reviews on all these matters can be found in [129]-[134] and relevant books are [105, 136].

## 1.5 Solitons

Topological soliton in general, is a solution of a system of partial differential equations or of a quantum field theory that can be proven to exist because the boundary conditions entail the existence of homotopically distinct solutions. Typically, this occurs because the boundary on which the boundary conditions are specified, has a non-trivial homotopy group which is preserved by differential equations. The solutions to the differential equations are then topologically distinct, and are classified by their homotopy class. It is not easy to define precisely what a soliton is. Drazin and Johnson (1989) describe solitons as solutions of nonlinear differential equations which

- represent waves of *permanent* form

- are *localised*, so that they decay or approach a constant at infinity
- can interact strongly with other solitons, but they emerge from the collision *unchanged* apart from a phase shift.

There are many equations of mathematical physics which have solutions of the soliton type. Correspondingly, the phenomena which they describe, be it the motion of waves in shallow water or in an ionized plasma, exhibit solitons. The first observation of this kind of wave was made in 1834 by John Scott Russell, who followed on horseback a soliton propagating in the windings of a channel. In 1895, D. J. Korteweg and H. de Vries proposed an equation for the motion of waves in shallow waters which possesses soliton solutions, and thus established a mathematical basis for the study of the phenomenon. Interest in the subject, however, lay dormant for many years, and the major body of investigations began only in the 1950s. Researches done by analytical methods and by numerical methods made possible with the advent of computers gradually led to a complete understanding of solitons.

Eventually, the fact that solitons exhibit particle-like properties, because the energy is at any instant confined to a limited region of space, received attention, and solitons were proposed as models for elementary particles. However, it is difficult to account for all of the properties of known particles in terms of solitons. More recently it has been realized that some of the quantum fields which are used to describe particles and their interactions also have solutions of the soliton type. The solitons would then appear as additional particles, and may have escaped experimental detection because their masses are much larger than those of known particles. In this context the requirement that solitons emerge unchanged from a collision has been found too restrictive, and particle theorists have used the term soliton where traditionally the term solitary wave would be used.

We can classify solitons in three sectors, according to the origin of their stability:

- **Topological solitons:** They can be found in theories where the vacuum manifold is not simply connected and stability comes as a consequence of a topological conservation law.
- **Non-topological solitons:** These solitons are stabilized by the confinement of a conserved charge as a result of a Noether current arising from a symmetry of the theory and not from a topological conservation law as above [85].

- **Semi-topological solitons:** They are characterized by a winding number and are classically stable, being local minima of the energy functional, but in contrast to genuine topological defects, they can tunnel quantum mechanically and decay to the trivial vacuum. They were introduced for the first in [13, 14, 15, 88]. They are the only kind of defects that can exist in the SM of Particle Physics.

# PART I

## THEORETICAL FRAMEWORK

In this part, we present two well known models which provide the basis for our research. These are, the Nielsen-Olesen vortex [18] and the straight bosonic superconducting string [103]. These models also provide the theoretical framework on which we are based. The known solutions of these models help us to test our numerical algorithms and to reproduce the solutions. Before that, we explain the notion of spontaneous symmetry breaking of a global and a local symmetry as well as some other useful notions such as penetration depth and Meissner effect in superconductors and phase transitions.

# Chapter 2

# Cosmic string field theory

## 2.1 Spontaneous symmetry breaking

The purpose of this section is to introduce the notion of spontaneous symmetry breaking (SB) which is very important in our research part. *Goldstone theorem* as well as *Higgs mechanism* are presented.

### 2.1.1 Spontaneous breaking of a global symmetry

Consider the following Lagrangian density with a complex scalar $\phi$ field,

$$\mathcal{L} = \partial_\mu \phi \partial^\mu \phi^* - U(\phi, \phi^*) \tag{2.1}$$

with

$$U(\phi, \phi^*) = m^2 \phi^* \phi + \lambda (\phi^* \phi)^2 \tag{2.2}$$

This Lagrangian is invariant under the following $U(1)$ global transformation

$$\phi \to e^{ia} \phi \tag{2.3}$$

where $a$ a constant. The ground state of the theory is obtained by minimizing the potential $U$

$$\frac{\partial U}{\partial \phi} = m^2 \phi^* + 2\lambda \phi^* (\phi^* \phi) \tag{2.4}$$

- $m^2 > 0$: In this case we have a minimum at $\phi^* = \phi = 0$
- $m^2 < 0$: In this case, $\phi = 0$ is a maximum and the minimum is located at $|\phi|^2 = -m^2/2\lambda \equiv k^2$

In the second case, the minima lie along the circle $|\phi| = k$, which form a set of degenerate vacua related to each other by rotation. We can express the complex field $\phi$ as follows

$$\phi(x) = (r(x) + k) e^{i\theta(x)} \tag{2.5}$$

where $r$ and $\theta$ both have vanishing vacuum expectation values. We substitute in $\mathcal{L}$ and the potential term there becomes

$$U = \lambda r^4 + 4k\lambda r^3 + 4\lambda k^2 r^2 - \lambda k^4 \tag{2.6}$$

and we have a mass term for the field $r$, which means that $m_r^2 = 4\lambda k^2$, while $\theta$ is a massless field as there is no mass term for it. Thus, the two massive fields (real parts of $\phi$) became one massive and one massless field. In general there is the following theorem

- **Goldstone theorem**: The spontaneous breaking of a continuous global symmetry is always accompanied by the appearence of one or more massless scalar spin-0 particles known as the Goldstone bosons.

### 2.1.2 Spontaneous breaking of a gauge symmetry

Now we consider the Lagrangian density (2.1), which we demand to be invariant under the following $U(1)$ local (gauge) transformation

$$\phi \to e^{ia(x)}\phi \tag{2.7}$$

This results in the introduction of the electromagnetic field through a covariant derivative and the Lagrangian density becomes

$$\mathcal{L} = -\frac{1}{4}F_{\mu\nu}F^{\mu\nu} + |D_\mu\phi|^2 - U(\phi,\phi^*) \tag{2.8}$$

where $|D_\mu\phi|^2 = (\partial_\mu + ieA_\mu)\phi(\partial^\mu - ieA^\mu)\phi^*$, $F_{\mu\nu} = \partial_\mu A_\nu - \partial_\nu A_\mu$ while the potential is the same as above. Following the previous steps, in the case we consider $m^2 < 0$, the vacuum is at

$$|\phi| = k \equiv \left(\frac{-m^2}{2\lambda}\right)^{1/2} \tag{2.9}$$

We can set, as above,

$$\phi(x) = k + \frac{\phi_1(x) + i\phi_2(x)}{\sqrt{2}} \tag{2.10}$$

and substitute in the Lagrangian which becomes

$$\mathcal{L} = -\frac{1}{4}F_{\mu\nu}F^{\mu\nu} + \frac{1}{2}(\partial_\mu\phi_1)^2 + \frac{1}{2}(\partial_\mu\phi_2)^2 + e^2k^2A_\mu A^\mu - 2\lambda k^2\phi_1^2 + \cdots \tag{2.11}$$

where the dots represent cubic and quartic terms. There are two massive fields, the $\phi_1$ and $A_\mu$ which means that the photon became massive. The $\phi_2$ field is massless and can also be eliminated through an appropriate choice of the vacuum. The above phenomenon is summarized as follows

- **Higgs mechanism**: The spontaneous breaking of a gauge symmetry makes the massless field to disappear and we end up with a massive scalar field representing the Higgs particle, while the gauge field acquires mass.

The Higgs particle is believed to have large mass and this is the reason for not being discovered yet. LHC, a proton-proton collider will operate in the early 2008. It will work at energies until $7+7$ TeV, something which means that there are possibilities for finding that particle. To have answers in this subject is, maybe, the greatest challenge for the years to come. The following table summarizes the above cases.

| | **Goldstone mode** | **Higgs mode** |
|---|---|---|
| *Before* SB | 2 massive scalars | 2 massive scalars+1 photon |
| *After* SB | 1 massive+1 massless scalar | 1 massive scalar+1 massive photon |

Finally, if the ground state of the system, obeys the initial symmetry of the Lagrangian, the system is said to be in the *Wigner* mode.

## 2.2 Effective potential

The discussion of symmetry breaking is somewhat simplistic because we use classical potentials to determine the expectation value of the Higgs field $\phi$ in the models above. We have to keep in mind that, in reality $\phi$ is a quantum field interacting with itself and with other quantum fields and the classical potential $V(\phi)$, is modified by *radiative corrections*. The corrected potential for $\phi$, is called effective potential $V_{eff}$ and can be evaluated perturbatively as an expansion in powers of coupling constants

$$V_{eff}(\phi) = V(\phi) + V_1(\phi) + V_2(\phi) + \cdots \tag{2.12}$$

where $V(\phi)$ is the classical potential and $V_n(\phi)$ is the contribution of Feynman diagrams with $n$ closed loops. In some models, the radiative corrections are negligible, while in others they can alter the character of symmetry breaking. One example of the latter is the Higgs model

$$\mathcal{L} = -\frac{1}{4}F_{\mu\nu}F^{\mu\nu} + \overline{D_\mu\phi}D^\mu\phi - V(|\phi|) \tag{2.13}$$

with $V(|\phi|) = \mu_0^2|\phi|^2$, where $\mu_0$ a constant. The one-loop contribution to $V_{eff}(\phi)$ is given by [84] :

$$V_1(\phi) = \frac{3e^4}{16\pi^2}|\phi|^4 ln\left(\frac{|\phi|^2}{\sigma^2}\right) \tag{2.14}$$

where $\sigma$ the renormalization scale. If we introduce a dimensionless quantity

$$v \equiv \frac{16\pi^2\mu_0^2}{3e^4\sigma^2} \tag{2.15}$$

then, for $v > 0.45$ the $V_{eff}(\phi)$ has a single minimum at $\phi = 0$, but for $v < 0.45$ there is another minimum at a non-zero value of $\phi$, while for $v <$

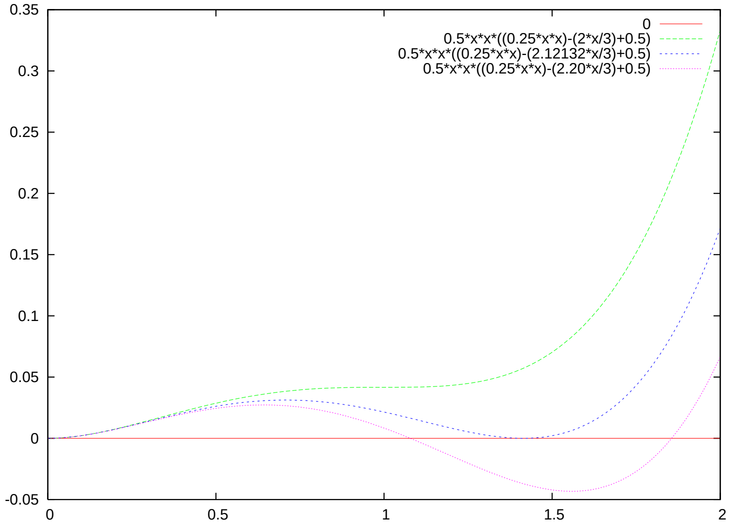

Figure 2.1: An example of a first order phase transition. The plots are for $\beta = 2 < \beta_{crit}$, $\beta = \beta_{crit}$, $\beta = 2.2 > \beta_{crit}$. Parameter is $a = 1$.

0.37 the latter minimum goes deeper than the one at $\phi = 0$. In the last case, the absolute minimum is at a non-zero value of $\phi$ and the symmetry is spontaneously broken.

In Chapter 4, we examine a modified Ginzburg-Landau potential. The modification has to do with the addition of a cubic term. Such term results from the 1-loop radiative corrections on the quartic potential [102].

## 2.3 Phase transitions

### 2.3.1 First order phase transition

In order to observe phase transitions and to find the distinguishing features we suppose appropriate effective potentials. For a first order phase transition, consider the following potential which we examine in detail in Chapter 4:

$$U(|\phi|) = \frac{a}{2}|\phi|^2\left(\frac{1}{4}|\phi|^2 - \frac{\beta}{3}|\phi| + \frac{1}{2}\right) \tag{2.16}$$

This potential has an obvious minimum at $|\phi| = 0$. This corresponds to the symmetric phase of the system. For $\beta \geq 2$, it develops a secondary minimum at $|\phi| = 1$. The critical value for this potential is $\beta = 3/\sqrt{2} \equiv \beta_{crit}$. This happens because for $\beta \geq \beta_{crit}$, the secondary minimum goes deeper than the

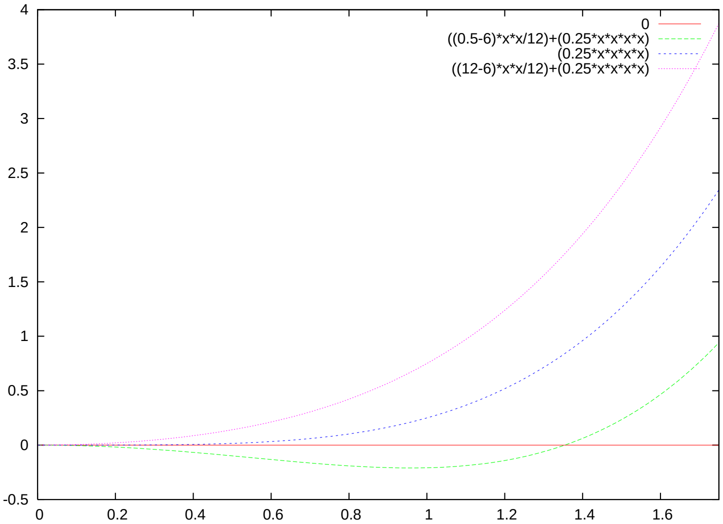

Figure 2.2: An example of a second order phase transition. The plots are for $T = \sqrt{0.5} < T_{crit}$, $T = T_{crit}$, $T = \sqrt{12} > T_{crit}$. Parameters are $\eta = 1,\ \lambda = 1$.

one at $|\phi| = 0$. When $\beta = \beta_{crit}$, the secondary minimum makes the potential zero, just like the original one at $|\phi| = 0$ (fig.2.1). The non-zero expectation value of $|\phi|$ is

$$|\phi| = \frac{\beta + \sqrt{\beta^2 - 4}}{2} \tag{2.17}$$

Generally, in a first-order phase transition, a new broken symmetry phase usually nucleates after the temperature falls some degrees below the critical temperature $T_c$. Separated areas of the new phase form independently and expand, resulting in a local selection of the broken symmetry vacuum. As a result of these independent selections, the final configuration may not be able to get rid of the locked-out fragments of the original vacuum (before transition).

### 2.3.2 Second order phase transition

In order to observe a second order phase transition, consider the following temperature-dependent potential:

$$U(|\phi|, T) = m^2(T)|\phi|^2 + \frac{\lambda}{4}|\phi|^4 \tag{2.18}$$

with

$$m^2(T) = \frac{\lambda}{12}\Big(T^2 - 6\eta^2\Big) \tag{2.19}$$

The critical value for this potential is $T_{crit} = \eta\sqrt{6}$. Above this temperature, the mass-squared term becomes positive, thus the potential is a sum of positive terms with a unique minimum at $|\phi| = 0$ which represents the symmetric phase (fig.2.2). When $T < T_{crit}$, then $m^2(T) < 0$ and the order parameter $|\phi|$ acquires a non-zero expectation value which is

$$|\phi| = \frac{1}{\sqrt{6}}\Big(T_{crit}^2 - T\Big)^{1/2} \tag{2.20}$$

In second-order phase transitions, the phase transformation occurs almost simultaneously throughout the volume. However, unless the critical temperature is traversed infinitesimally slowly, the resulting broken symmetry phase will contain many distinct regions with different choices of the local vacuum. This is because the selection of the new vacuum has to be, somehow, communicated if the same choice is to made elsewhere, and the speed at which this transformation can be propagated is finite.

The main difference between these phase transitions is that, at the first order phase transition the symmetric phase ($|\phi| = 0$) remains metastable when passing the critical value $\beta_{crit}$ and is often called “false vacuum”. A defining feature of the second order phase transition, is that the order parameter $|\phi|$ grows continuously from zero, as the temperature is decreased below $T_{crit}$.

## 2.4 Superconductivity and penetration depth

Ginzburg-Landau theory is used to model superconductivity. It examines the macroscopic properties of a superconductor with the aid of general thermodynamic arguments. Based on Landau’s previously-established theory of second-order phase transitions, Landau and Ginzburg argued that the free energy $F$ of a superconductor near the superconducting transition can be expressed in terms of a complex order parameter $\Psi$, which describes how deep into the superconducting phase the system is. The free energy has the form

$$F = F_n + a|\Psi|^2 + \frac{\beta}{2}|\Psi|^4 + \frac{1}{2m}|(-i\hbar\nabla - 2e\mathbf{A})\Psi|^2 + \frac{|\mathbf{B}|^2}{2\mu_0} \tag{2.21}$$

where $F_n$ is the free energy in the normal phase, $a$ and $\beta$ are phenomenological parameters, $\mathbf{A}$ is the electromagnetic vector potential, and $\mathbf{B}$ is the magnetic field. By minimizing the free energy with respect to fluctuations in the order parameter and the vector potential, one arrives at the Ginzburg-Landau equations. These equations produce many interesting and valid results. Perhaps the most important of these is its prediction of the existence of two characteristic lengths in a superconductor. The first is a coherence length $\xi$, given by

$$\xi = \sqrt{\frac{\hbar^2}{2m|a|}} \tag{2.22}$$

which describes the size of thermodynamic fluctuations in the superconducting phase. The second is the penetration depth $\lambda$, given by

$$\lambda = \sqrt{\frac{m}{4\mu_0 e^2 \Psi_0^2}} \tag{2.23}$$

where $\Psi_0$ is the equilibrium value of the order parameter in the absence of an electromagnetic field. The penetration depth describes the length to which an external magnetic field can penetrate the superconductor. In general, if one considers a superconducting semi-space at $x > 0$, and weak external magnetic field $B_0$ applied along $z$-direction in the empty space $x < 0$, then inside the superconductor the magnetic field is given by

$$B(x) = B_0 e^{-x/\lambda} \tag{2.24}$$

In atomic units, one can see that the penetration depth is, in fact,

$$\lambda \propto \frac{1}{e\Psi_0} \tag{2.25}$$

We will use this result in Chapter 5.

The formula (2.24), can be derived as follows. Suppose that an electric field $\mathbf{E}$ momentarily arises within a superconductor. The superconducting electrons will be freely accelerated without dissipation and their mean velocity will be

$$m\frac{d\mathbf{v}}{dt} = -e\mathbf{E} \tag{2.26}$$

The current density is

$$\mathbf{j} = -en\mathbf{v} \tag{2.27}$$

where $n$ the number of electrons per unit volume, and the above formula, with the help of (2.26) can be written as

$$\frac{d\mathbf{j}}{dt} = \frac{ne^2}{m}\mathbf{E} \tag{2.28}$$

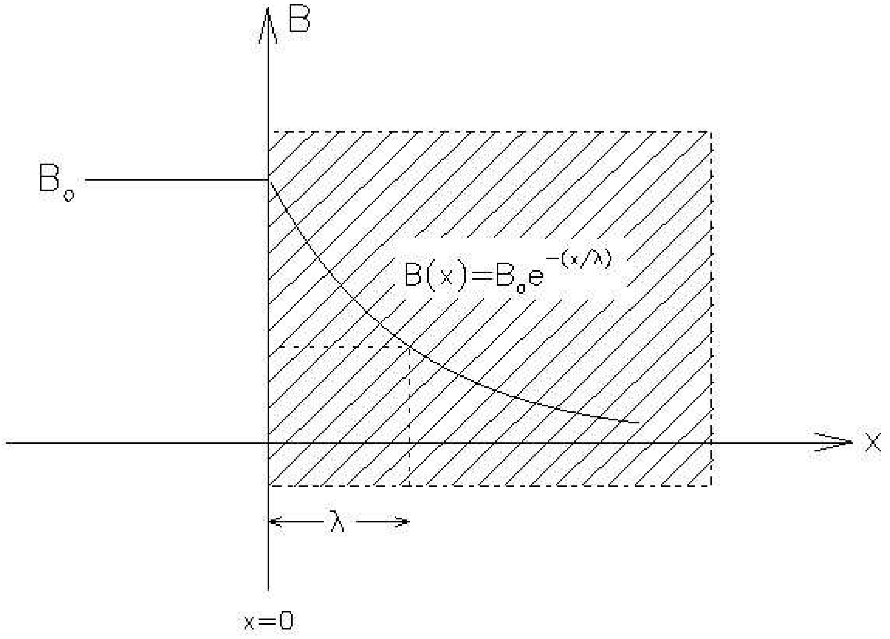

Figure 2.3: The magnetic field drops exponentially inside the superconductor.

If one substitutes into Faraday's law, this gives

$$\nabla \times \mathbf{E} = -\frac{1}{c}\frac{d\mathbf{B}}{dt} \Rightarrow \nabla \times \mathbf{j} = -\frac{ne^2}{mc}\mathbf{B} \tag{2.29}$$

Plug the result into Maxwell's equation and this results to

$$\nabla \times \mathbf{B} = \frac{4\pi}{c}\mathbf{j} \Rightarrow \nabla^2\mathbf{B} = \frac{4\pi ne^2}{mc^2}\mathbf{B} \tag{2.30}$$

Now, rename $mc^2/4\pi ne^2 \equiv \lambda^2$ and you get

$$\nabla^2\mathbf{B} = \frac{1}{\lambda^2}\mathbf{B} \tag{2.31}$$

where $\lambda$ is the London penetration depth. The last equation can be easily solved to give the result in (2.24).

## 2.5 Nielsen-Olesen vortex

### 2.5.1 Introduction

The simplest theory exhibiting string solutions is that of a complex scalar field $\phi(x)$, in a model described by the following Lagrangian density:

$$\mathcal{L} = \partial_\mu \phi^* \partial^\mu \phi - V(\phi), \quad V(\phi) = \frac{\lambda}{4}(|\phi|^2 - \eta^2)^2 \tag{2.32}$$

which has a global $U(1)$ symmetry under the transformation $\phi \longrightarrow \phi e^{ia}$ where $a$ a constant. The condensed matter analogue of global strings is the vortices in superfluid Helium-4 [86].

If we move a bid further and consider a gauge symmetry under the transformation $\phi \longrightarrow \phi e^{ia(\mathbf{x})}$ then we are led to the introduction of a vector field $A_\mu$ while the replacement of $\partial_\mu$ by the covariant derivative $D_\mu = \partial_\mu - ieA_\mu$ is required. Due to the existence of the vector field $A_\mu$, a relevant "magnetic" field exists as well. This theory describes the Nielsen-Olesen string [18].

### 2.5.2 The model

Consider an Abelian Higgs model in two dimensions with a charged complex scalar field $\phi$ and gauge field $A^\mu$. The **Lagrangian density** of the model under consideration is:

$$\mathcal{L} = \overline{D}_\mu \phi^* D^\mu \phi - \frac{1}{4} F_{\mu\nu} F^{\mu\nu} - \frac{\lambda}{4}(|\phi|^2 - \eta^2)^2 \tag{2.33}$$

where $D_\mu = \partial_\mu - ieA_\mu$, the covariant derivative and $F_{\mu\nu} = \partial_\mu A_\nu - \partial_\nu A_\mu$. The energy of a static vortex configuration in two dimensions follows:

$$E = \int d^2\rho \Bigg( |D\phi|^2 + \frac{1}{2}(\boldsymbol{E}^2 + \boldsymbol{B}^2) + V(|\phi|) \Bigg) \tag{2.34}$$

The vortex energy must be finite which means that field configuration must have a form that decreases to 0 fast enough, as $\rho \rightarrow \infty$. This requirement imposes some conditions on the asymptotic field configuration which are:

$$\begin{aligned} |\phi| &\rightarrow \eta \quad , \quad \rho \rightarrow \infty \\ A_\varphi &\rightarrow \frac{1}{e\rho}\frac{d\vartheta}{d\varphi} + \cdots \quad , \quad \rho \rightarrow \infty \end{aligned}$$

where $\vartheta$ is the phase of the Higgs field $\phi$[1]. The last condition on the gauge field, can be understood through the requirement that the covariant derivative must be zero as $\rho \to \infty$ and $\phi \neq 0$ there. When following a closed path around the vortex, the Higgs field must return to its original value $\phi(0) = \phi(2\pi)$ thus $1 = \exp 2i\pi n$, which means that the winding number $n$ must be an integer. Also, one expects somewhere in the vortex core to have $\phi(x) = 0$ for a non-trivial winding number. The fact that the winding number is an integer results to quantization of the magnetic flux.

$$n = \frac{1}{2\pi}\int_0^{2\pi}\frac{d\vartheta}{d\varphi}d\varphi = \frac{e}{2\pi}\oint_{S^1}\boldsymbol{A}\cdot\boldsymbol{dl} = \frac{e}{2\pi}\int \boldsymbol{B}\cdot\boldsymbol{dS} \Rightarrow \Phi_B = \frac{2\pi n}{e} \tag{2.35}$$

where $S^1$ is a circle of infinite radius centered on this string. This flux quantization is a result of the vanishing of the covariant derivative which determines $\mathbf{A}$ in terms of $\partial_i\phi$. The phase of $\phi$ must change by $2\pi n$ which forces the flux to be quantized. A rough estimation of the size and mass of our vortex can be done. These two characteristic features of the vortex are determined by the regions over which the scalar and gauge fields start to differ from their asymptotic values. These distance scales $\rho_s, \rho_v$ ($s$ for scalar, $v$ for vector), are related to the Higgs and vector particle masses off the string.

$$\rho_s \approx m_s^{-1} = (\sqrt{\lambda}e)^{-1} \tag{2.36}$$

$$\rho_v \approx m_v^{-1} = (\sqrt{2}e\eta)^{-1} \tag{2.37}$$

Written in terms of these lengths, and assuming $\rho_v > \rho_s$ (type II superconductor [2]), the energy reads:

$$E \approx 2\pi\eta^2\Big[ln\Big(\frac{\rho_v}{\rho_s}\Big) + \frac{1}{e^2\eta^2\rho_v^2} + \lambda\eta^2\rho_s^2\Big] \tag{2.38}$$

where the first term represents the gradient energy of the scalar field, the second is due to the fact that the magnetic flux does not wish to be confined and the last term is the cost of the difference of $|\phi|$ from its vacuum value $\eta$. Finally, this energy is minimized by replacing the characteristic lengths with their relative masses as above. Then we are led to the mass of the vortex configuration:

$$\mu \approx 2\pi\eta^2 ln\Big(\frac{m_s}{m_v}\Big) \tag{2.39}$$

---

[1] Suppose $\phi(\rho) = f(\rho)e^{in\theta}$, $\theta$ the phase of the Higgs field, $n$ the winding number.

[2] Our model can be compared with that of Ginzburg-Landau which has the same Lagrangian with ours and $\rho_s$ can be thought as the coherence length -having to do with the transition layer from superconducting to normal state- and $\rho_v$ the *London* penetration depth -referring to the exponential decay of the magnetic field at the surface of the superconductor- in terms of superconductivity.

a formula that in three dimensions gives the mass per unit length of the string.

The vortices in the Abelian Higgs model have condensed matter analogues like flux tubes in superconductors [124] but there are differences [125, 126] because Nielsen-Olesen vortices exist in a vacuum background while superconductor vortices are amongst charged bosons called Cooper pairs.

### 2.5.3 Ansatz and equations

The **Euler-Lagrange equations** of our model are:

$$\begin{aligned}(\partial_\mu - ieA_\mu)(\partial^\mu - ieA^\mu)\phi + \frac{\lambda}{2}\phi(\phi\overline{\phi} - \eta^2) &= 0 \quad (2.40)\\ \partial_\mu F^{\mu\nu} &= j^\nu \quad (2.41)\end{aligned}$$

where $j^\nu \equiv 2eIm[\overline{\phi}(\partial^\nu - ieA^\nu)\phi]$. We work in the Lorentz gauge ($\partial_\mu A^\mu = 0$) and we rescaled the fields ($\phi \to \eta^{-1}\phi$ , $A^\mu \to \eta^{-1}A^\mu$ and $x \to \eta x$), while we also set $\eta = 1$ for convenience. A proper **ansatz** for a string lying on the $z$-axis would be:

$$\begin{aligned}\phi(\rho) &= f(\rho)e^{in\varphi} \quad (2.42)\\ A(\rho) &= \frac{n}{e\rho}a(\rho)\hat{\varphi} \quad (2.43)\end{aligned}$$

where $\hat{\rho}$, $\hat{\varphi}$ are the cylindrical unit vectors. We use cylindrical coordinates $(\rho, \varphi, z)$. According to the above, the appropriate asymptotic conditions while $\rho \to \infty$ and boundary conditions at $\rho \to 0$ are:

$$f(\rho \to \infty) \to 1 \quad , \quad a(\rho \to \infty) \to 1 \quad (2.44)$$

$$f(\rho = 0) = 0 \quad , \quad a(\rho = 0) = 0 \quad (2.45)$$

With the above ansatz, we are led to the following system of non-linear differential equations:

$$\frac{d^2f}{d\rho^2} + \frac{1}{\rho}\frac{df}{d\rho} - \frac{n^2 f}{\rho^2}(a-1)^2 - \frac{\lambda}{2}f(f^2-1) = 0 \quad (2.46)$$

$$\frac{d^2a}{d\rho^2} - \frac{1}{\rho}\frac{da}{d\rho} - 2e^2f^2(a-1) = 0 \quad (2.47)$$

It is helpful to acquire an approximate asymptotic solution as $\rho \to \infty$. This is:

$$\begin{aligned}a(\rho) &\approx 1 - \mathcal{O}(\sqrt{\rho}\exp(-\sqrt{2}e\rho)) \quad (2.48)\\ f(\rho) &\approx 1 - \mathcal{O}(exp(-\sqrt{\lambda}\rho)) \quad (2.49)\end{aligned}$$

Finally, another way to acquire the solution of the system is through the minimization of the **energy functional** which is

$$E = 2\pi \int_{-\infty}^{\infty} \rho d\rho \left[ (\partial_\rho f)^2 + \frac{f^2}{\rho^2}(a-1)^2 + \frac{(\partial_\rho a)^2}{4\rho^2} + (f^2-1)^2 \right] \tag{2.50}$$

### 2.5.4 Virial theorem

Before the numerical results, it is important to have a way to check whether a final configuration of an algorithm can be accepted or not.

The energy density for a *static solution*, which is of interest here, reads:

$$T^{00} = \frac{1}{4} F_{ij} F_{ij} + |D_i \phi|^2 + V(|\phi|) \equiv \varepsilon \tag{2.51}$$

The solution of our physical problem, has to minimize the energy of the system:

$$\frac{\delta E}{\delta \phi} = \frac{\delta E}{\delta \phi^*} = \frac{\delta E}{\delta A_i} = 0 \tag{2.52}$$

Define

$$f_i \equiv \frac{\delta E}{\delta \phi} \partial_i \phi + \frac{\delta E}{\delta \phi^*} \partial_i \phi^* + \frac{\delta E}{\delta A_j} \partial_i A_j \tag{2.53}$$

which together with

$$\frac{\delta E}{\delta \Phi} = \frac{\partial T^{00}}{\partial \Phi} - \partial_k \frac{\partial T^{00}}{\partial(\partial_k \Phi)} \tag{2.54}$$

can be written in a shorter form $f_i = \partial_j G_{ij}$ where

$$G_{ij} = \varepsilon \delta_{ij} - \frac{\partial \varepsilon}{\partial(\partial_j \phi)} \partial_i \phi - \frac{\partial \varepsilon}{\partial(\partial_j \phi^*)} \partial_i \phi^* - \frac{\partial \varepsilon}{\partial(\partial_j A_k)} \partial_i A_k \tag{2.55}$$

This means that any static solution of the field equations satisfies

$$\partial_j G_{ij} = 0 \tag{2.56}$$

But, we have

$$\begin{aligned}
\frac{\partial \varepsilon}{\partial(\partial_j \phi)} &= (D_j \phi)^* \\
\frac{\partial \varepsilon}{\partial(\partial_j \phi^*)} &= D_j \phi \\
\frac{\partial \varepsilon}{\partial(\partial_j A_k)} &= \partial_j A_k - \partial_k A_j = F_{jk}
\end{aligned}$$

which leads to

$$\begin{aligned}
G_{ij} &= \varepsilon\delta_{ij} - (D_j\phi)^*\partial_i\phi - D_j\phi\partial_i\phi^* - F_{jk}\partial_i A_k \\
&= \varepsilon\delta_{ij} - (D_j\phi)^* D_i\phi - D_j\phi(D_i\phi)^* + ieA_i\phi(D_j\phi)^* \\
&- ieA_i\phi^* D_j\phi - F_{jk}F_{ik} - F_{jk}\partial_k A_i \\
&= \varepsilon\delta_{ij} - (D_i\phi)^* D_j\phi - (D_j\phi)^* D_i\phi - F_{ik}F_{jk} - \partial_k(F_{jk}A_i) \\
&+ A_i\Big(\partial_k F_{jk} - ie(\phi^* D_j\phi - (D_j\phi)^*\phi)\Big)
\end{aligned}$$

where on the second line we just add and subtract the necessary terms in order to derive the first four terms of the third line. Now, on the third line we have

$$\partial_j\partial_k(\partial_j A_k - \partial_k A_j)A_i = 0 \Rightarrow (\partial_j^2\partial_k A_k - \partial_k^2\partial_j A_j)A_i = 0 \tag{2.57}$$

and from the field equations, the last term of the third line is also zero as

$$\frac{\delta E}{\delta A_j} = 0 = \frac{\delta T^{00}}{\partial(\partial_k A_j)} = -ie(\phi^* D_j\phi - \phi(D_j\phi)^*) + \partial_k F_{jk} = 0 \tag{2.58}$$

thus

$$G_{ij} = \varepsilon\delta_{ij} - F_{ik}F_{jk} - (D_i\phi)^* D_j\phi - (D_j\phi)^* D_i\phi \tag{2.59}$$

but

$$F_{ik}F_{jk} = \epsilon_{nik}B_n\epsilon_{mjk}B_m = \mathbf{B}^2\delta_{ij} - B_iB_j \tag{2.60}$$

which means that

$$G_{ij} = \left(-\frac{\mathbf{B}^2}{2} + |D\phi|^2 + V\right)\delta_{ij} + B_iB_j - (D_i\phi)^* D_j\phi - (D_j\phi)^* D_i\phi \tag{2.61}$$

From (2.56) one obtains

$$\int d^3x G_{ik} = 0 = \int d^3x\partial_j(x_k G_{ij}) = \int dS_j x_k G_{ij} \tag{2.62}$$

The last equality follows from Gauss theorem, while the first is due to the fact that

$$\partial_j(x_k G_{ij}) = \frac{\partial x_k}{\partial x_i}G_{ij} + x_k(\partial_j G_{ij}) = \delta_{kj}G_{ij} = G_{ik} \tag{2.63}$$

where we also used (2.56).

- **Virial relation for Nielsen-Olesen string model**

The formulas above are general and can be applied to any model which is being examined for static solutions. For the model at hand, take the trace of equation (2.62)

$$\int d^3x TrG = \int dS_j x_i G_{ij} = 0 \tag{2.64}$$

while equation (2.61) leads to

$$TrG = -\frac{1}{2}\boldsymbol{B}^2 + |D\phi|^2 + 3V \tag{2.65}$$

Thus, by taking a cylindrical surface of integration around the infinite string with cylindrical symmetry we are led to a virial relation

$$\int d^2x \left(\frac{1}{2}B^2 - V\right) = 0 \tag{2.66}$$

Using $\nabla \times \boldsymbol{A} = \boldsymbol{B}$ and remembering that in our case

$$\boldsymbol{A} = \frac{a(\rho)}{e\rho}\hat{\varphi}, \quad V(|\phi|) = \frac{\lambda}{4}(|\phi|^2 - m_0^2)^2 \tag{2.67}$$

we acquire the formula for the magnetic field

$$\boldsymbol{B} = \frac{1}{e\rho}\frac{da(\rho)}{d\rho}\hat{z} \tag{2.68}$$

and rewrite in a more convenient way for our numerical purposes, the **virial** relation

$$2\pi \int \rho d\rho \left(\frac{1}{2e^2\rho^2}\left(\frac{da}{d\rho}\right)^2 - \frac{\lambda}{4}(f^2 - m_0^2)^2\right) = 0 \tag{2.69}$$

Numerically though, we “break” the integral into two parts. Consider for example

$$I_1 \equiv 2\pi \int \rho d\rho \left(\frac{1}{2e^2\rho^2}\left(\frac{da}{d\rho}\right)^2\right), \quad I_2 \equiv -2\pi \int \rho d\rho \left(\frac{\lambda}{4}(|\phi|^2 - m_0^2)^2\right) \tag{2.70}$$

Then we must have $I_1 + I_2 = 0$. We define the index $V = \frac{||I_1| - |I_2||}{|I_1| + |I_2|}$ and we want this index as small as possible.

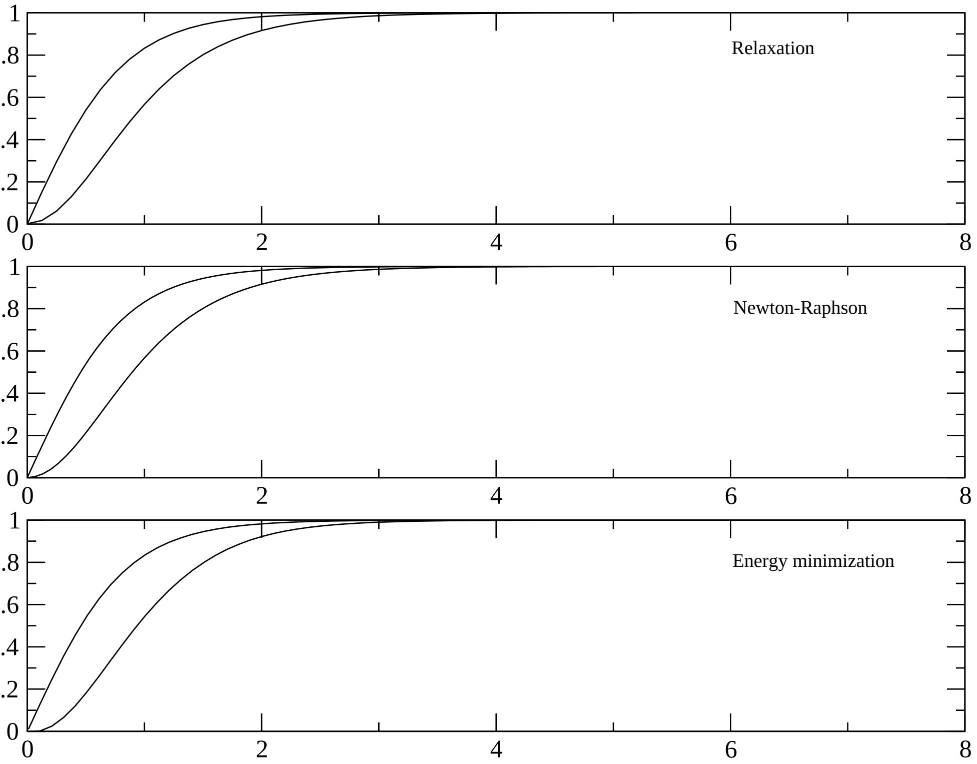

Figure 2.4: Nielsen-Olesen string. The graph on top is the output of a relaxation program. The graph in the middle is the result of a Newton-Raphson algorithm and the bottom graph is done through energy minimization. All graphs show $f(\rho)$ and $a(\rho)$, for $n = 1,\ \lambda = 2e^2 = 4$.

### 2.5.5 Numerical solution

There are many different numerical methods for solving the above system of equations. In figure 2.4 one can see the result of three different algorithms. Details concerning the Relaxation algorithm can be found on page 762 of [104] and a brief outline in chapter 7 (Part III). Details about the Newton-Raphson algorithm can also be found in chapter 7. Finally, as it concerns minimization algorithm, many details can be found in chapter 7, while we use minimization subroutines from page 425 of [104].

## 2.6 Straight bosonic superconducting string

### 2.6.1 Introduction

Superconductivity can be understood as a spontaneously broken electromagnetic gauge invariance. When the gauge invariance is broken, then any magnetic field applied at the boundary of a superconductor decays exponentially towards its interior. This happens due to the screening of the superconducting current which flows along the boundary. This is known as Mei$\beta$ner effect. Having this mechanism in mind, one can support the idea that cosmic strings can become superconductors and behave as thin superconducting wires with an enormous critical current. For this to happen, a charged scalar field must acquire a non-zero expectation value in the neighborhood of the string core. Practically, this points out the need of two complex scalar fields $\phi$ and $\sigma$ interacting with seperate $U_\phi(1)$ and $U_\sigma(1)$ gauge fields $R_\mu$ and $A_\mu$ respectively. The breaking of $U_\phi(1)$ is responsible for the existence of vortices, while if we identify $U_\sigma(1)$ with electromagnetism, then its breaking inside the string will result to supercurrents flowing along the string. If more fields are added to the Abelian Higgs model describing an Nielsen-Olesen vortex, then the appearence of currents in the core of the defect is possible. The notions involved in this case, which is one step further from the previous one, will be the basis for the case of vortex rings later on.

### 2.6.2 The model

The above description takes us to the following **Lagrangian density** for this model:

$$\mathcal{L} = |\tilde{D}_\mu\phi|^2 + |D_\mu\sigma|^2 - \frac{1}{4}B_{\mu\nu}B^{\mu\nu} - \frac{1}{4}F_{\mu\nu}F^{\mu\nu} - V(|\phi|, |\sigma|) \tag{2.71}$$

with potential of the following form:

$$V(|\phi|, |\sigma|) = \frac{\lambda_\phi}{8}(|\phi|^2 - \eta^2)^2 + \frac{\lambda_\sigma}{4}\left(|\sigma|^2 - \frac{m^2}{\lambda_\sigma}\right)^2 + \frac{v}{2}|\phi|^2|\sigma|^2 - \frac{m^4}{4\lambda_\sigma} \tag{2.72}$$

and $D_\mu\sigma = (\partial_\mu + ieA_\mu)\sigma$, $\tilde{D}_\mu\phi = (\partial_\mu + igR_\mu)\phi$, $F_{\mu\nu} = \partial_\mu A_\nu - \partial_\nu A_\mu$, $B_{\mu\nu} = \partial_\mu R_\nu - \partial_\nu R_\mu$.

Away from the string, we have the vacuum of the theory where $U_\phi(1)$ is broken. There, we have $< \phi >= \eta$ and the potential has the form:

$$V(|\phi| = \eta, |\sigma|) = \frac{\lambda_\sigma|\sigma|^2}{4}\Big(|\sigma|^2 + 2(v\eta^2 - m^2)\Big) \tag{2.73}$$

which takes us to the condition:

$$v\eta^2 - m^2 \geq 0 \Rightarrow v\eta^2 \geq m^2 \tag{2.74}$$

The latter ensures that away from the string: $<\sigma>=0$.

A topological defect, here a string, is a region where the original bigger symmetry of our system is restored, as mentioned in the introduction. There, we have $<\phi>=0$ and the potential becomes:

$$V(|\phi|=0,|\sigma|) = \frac{\lambda_\phi}{8}\eta^4 + \frac{\lambda_\sigma}{4}|\sigma|^4 - \frac{m^2}{2}|\sigma|^2 \tag{2.75}$$

Breaking of $U_\sigma(1)$ inside the string translates to [3] $<\sigma>=\frac{m}{\sqrt{\lambda_\sigma}}$ and the requirement of a non-zero potential means another condition:

$$\begin{aligned} \frac{\lambda_\phi}{8}\eta^4 - \frac{m^4}{4\lambda_\sigma} > 0 \Rightarrow & \\ & \frac{\lambda_\phi}{2}\eta^4 > \frac{m^4}{\lambda_\sigma} \end{aligned} \tag{2.76}$$

The **Euler-Lagrange** equations follow:

$$D_\mu D^\mu \phi + \frac{\lambda_\phi}{4}\Big(|\phi|^2 - \Big(\eta^2 - \frac{2v}{\lambda_\phi}|\sigma|^2\Big)\Big)\phi = 0 \tag{2.77}$$

$$D_\mu D^\mu \sigma + \frac{\lambda_\sigma}{2}\Big(|\sigma|^2 + \frac{v}{\lambda_\sigma}\Big(|\phi|^2 - \frac{m^2}{v}\Big)\Big)\sigma = 0 \tag{2.78}$$

$$\partial_\mu B^{\mu\nu} = \tilde{J}^\nu = -ig\Big(\overline{\phi}\tilde{D}^\nu\phi - \phi\overline{\tilde{D}}^\nu\overline{\phi}\Big) \tag{2.79}$$

$$\partial_\mu F^{\mu\nu} = J^\nu = -ie\Big(\overline{\sigma}D^\nu\sigma - \sigma\overline{D}^\nu\overline{\sigma}\Big) \tag{2.80}$$

Exploiting the equations with the currents above, useful and general relations can be extracted which can be helpful in order to write the differential equations for the gauge fields $A_\mu$ and $R_\mu$. Maxwell equation $\nabla \times \boldsymbol{B} = \boldsymbol{J}$ will be also used. Suppose a very general ansatz in three dimensions for $\phi$ and $\sigma$ such as

$$\phi = \phi_0(x,y,z)exp(i\varphi_\phi(x,y,z)) \tag{2.81}$$

$$\sigma = \sigma_0(x,y,z)exp(i\varphi_\sigma(x,y,z)) \tag{2.82}$$

---

[3] $<\sigma>\neq 0$ inside the string and $\frac{dV(\phi=0,\sigma)}{d\sigma} = 0 \rightarrow \sigma = \frac{m}{\sqrt{\lambda_\sigma}}$.

Then we get:

$$-\left(\frac{\partial^2 A_z}{\partial x^2}+\frac{\partial^2 A_z}{\partial y^2}\right)+\frac{\partial^2 A_x}{\partial z\partial x}+\frac{\partial^2 A_y}{\partial z\partial y}=J_z=-2e\sigma_0^2(eA_z-\partial_z\varphi_\sigma) \quad (2.83)$$

$$-\left(\frac{\partial^2 A_y}{\partial x^2}+\frac{\partial^2 A_y}{\partial z^2}\right)+\frac{\partial^2 A_x}{\partial y\partial x}+\frac{\partial^2 A_z}{\partial z\partial y}=J_y=-2e\sigma_0^2(eA_y-\partial_y\varphi_\sigma) \quad (2.84)$$

$$-\left(\frac{\partial^2 A_x}{\partial y^2}+\frac{\partial^2 A_x}{\partial z^2}\right)+\frac{\partial^2 A_y}{\partial x\partial y}+\frac{\partial^2 A_z}{\partial x\partial z}=J_x=-2e\sigma_0^2(eA_x-\partial_x\varphi_\sigma) \quad (2.85)$$

$$-\left(\frac{\partial^2 \tilde{A}_z}{\partial x^2}+\frac{\partial^2 \tilde{A}_z}{\partial y^2}\right)+\frac{\partial^2 \tilde{A}_x}{\partial z\partial x}+\frac{\partial^2 \tilde{A}_y}{\partial z\partial y}=\tilde{J}_z=-2g\phi_0^2(g\tilde{A}_z-\partial_z\varphi_\phi) \quad (2.86)$$

$$-\left(\frac{\partial^2 \tilde{A}_y}{\partial x^2}+\frac{\partial^2 \tilde{A}_y}{\partial z^2}\right)+\frac{\partial^2 \tilde{A}_x}{\partial y\partial x}+\frac{\partial^2 \tilde{A}_z}{\partial z\partial y}=\tilde{J}_y=-2g\phi_0^2(g\tilde{A}_y-\partial_y\varphi_\phi) \quad (2.87)$$

$$-\left(\frac{\partial^2 \tilde{A}_x}{\partial y^2}+\frac{\partial^2 \tilde{A}_x}{\partial z^2}\right)+\frac{\partial^2 \tilde{A}_y}{\partial x\partial y}+\frac{\partial^2 \tilde{A}_z}{\partial x\partial z}=\tilde{J}_x=-2g\phi_0^2(g\tilde{A}_x-\partial_x\varphi_\phi) \quad (2.88)$$

The first three equations lead to a differential equation for $A_\mu$ and the last three for $R_\mu$.

### 2.6.3 Ansatz and equations

The **ansatz** we use for the fields in the case of an infinite straight superconducting string lying along the $z$-axis, is the following:

$$\sigma = \sigma(\rho) \quad (2.89)$$

$$A_\mu = \frac{I(\rho)}{e}\partial_\mu z \quad (2.90)$$

$$\phi = f(\rho)e^{in\varphi} \quad (2.91)$$

$$R_\mu = \frac{P(\rho)}{g}\partial_\mu\varphi \quad (2.92)$$

where $\varphi$ is the polar angle and $n$ the winding number of the field $\phi$. We use cylindrical coordinates $(\rho,\varphi,z)$. These gauge fields have "magnetic" fields of the following form:

$$\boldsymbol{B} = -\frac{1}{e}\frac{dQ(\rho)}{d\rho}\hat{\boldsymbol{\varphi}} \quad (2.93)$$

$$\boldsymbol{B_R} = \frac{1}{g\rho}\frac{dP(\rho)}{d\rho}\hat{\boldsymbol{z}} \quad (2.94)$$

where $\hat{\rho}, \hat{\varphi}, \hat{z}$ are the cylindrical unit vectors. In order to have finite energy, the function $P(\rho)$ must vanish for large $\rho$ while the regularity condition at small $\rho$ demands that $P(0) = 1$ and $\phi(0) = 0$. The scalar field $\sigma$ does not have dependence on $\varphi$ at the origin or else we would have a singularity there. The vector potential $A_\mu$ describes the effects of any current present in the string. For large $\rho$ the function $I(\rho) \propto I_{tot} ln(\rho)$, where $I_{tot}$ is the total current inside the string.

The natural unit of length is the radius of the string $\delta = 1/\eta\sqrt{\lambda_\phi}$ so we choose to rescale our fields: $\sigma = Y\eta,\ \phi = X\eta,\ I = Q\eta$ and $\rho \rightarrow x = \sqrt{\lambda_\phi}\eta\rho$. Thus, the system of **field equations** to be solved becomes:

$$X^{''} + \frac{1}{x}X^{'} - \frac{(P-1)^2}{x}X - \frac{1}{2}X^3 + \frac{1}{2}X - \bar{v}XY^2 = 0 \tag{2.95}$$

$$Q^{''} + \frac{1}{x}Q^{'} - \bar{e}^2 Y^2 Q = 0 \tag{2.96}$$

$$Y^{''} + \frac{1}{x}Y^{'} - YQ^2 - \bar{\lambda}Y^3 + \bar{m}^2 Y - \bar{v}X^2 Y = 0 \tag{2.97}$$

$$P^{''} - \frac{1}{x}P^{'} - \bar{g}^2 X^2 (P-1) = 0 \tag{2.98}$$

where prime denotes differentiation with respect to $x$ and $\bar{\lambda} = \lambda_\sigma/\lambda_\phi$, $\bar{v} = v/\lambda_\phi$, $\bar{g}^2 = g^2/\lambda_\phi$, $\bar{e}^2 = e^2/\lambda_\phi$, $\bar{m}^2 = m^2/\lambda_\phi\eta^2$. According to these changes the conditions (2.74), (2.76) become:

$$\bar{v} \geq \bar{m}^2, \quad \bar{\lambda} \geq 2\bar{m}^4 \tag{2.99}$$

Notice that if we approximate $X(x)$ by $\tanh(x/2)$ for an ordinary cosmic string and search for a solution with vanishing electromagnetic current ($Q = 0$) then the $Y$-equation decouples from the others and becomes:

$$Y^{''} + \frac{1}{x}Y^{'} - \bar{\lambda}Y^2 - \bar{v}\tanh^2(x/2)Y + \bar{m}^2 Y = 0 \tag{2.100}$$

Finally, the **energy functional** which one has to minimize in order to get the final field configuration of this model, is:

$$E = 2\pi \int_0^\infty \rho d\rho \ \left[ (\partial_\rho X)^2 + (\partial_\rho Y)^2 + \frac{1}{2\eta\bar{e}^2}(\partial_\rho P)^2 + \frac{1}{2\bar{g}^2\rho^2}(\partial_\rho Q)^2 + \right.$$
$$\left. + \frac{1}{\rho^2}(Q-1)^2 X^2 + \frac{1}{\eta}Y^2 P^2 + \frac{\bar{\lambda}}{8}(X^2-1)^2 + \frac{\bar{\lambda}}{4}Y^4 + \frac{\bar{v}}{2}Y^2\left(Q^2 - \frac{\bar{m}^2}{v}\right)\right]$$

### 2.6.4 Numerical solution

We used Newton-Raphson algorithm (chapter 7) to solve the system of equations above with an initial guess that satisfies the boundary conditions and asymptotics of the fields. The virial relation for the problem at hand, changes slightly because of the existence of the scalar condensate $\sigma(x)$ and another "magnetic" term is added. Thus the virial relation we check, is:

$$\int d^2x \left( \frac{1}{2} B^2 + \frac{1}{2} B_R^2 - V \right) = 0 \tag{2.101}$$

We also found a solution to this model through minimization algorithm. The output of both algorithms is exhibited in figure 2.5 and the small differences one may observe are due to small changes in the parameters. A very helpful review and analysis concerning especially the $Y$ field, which is the charge condensate, can be found in [87].

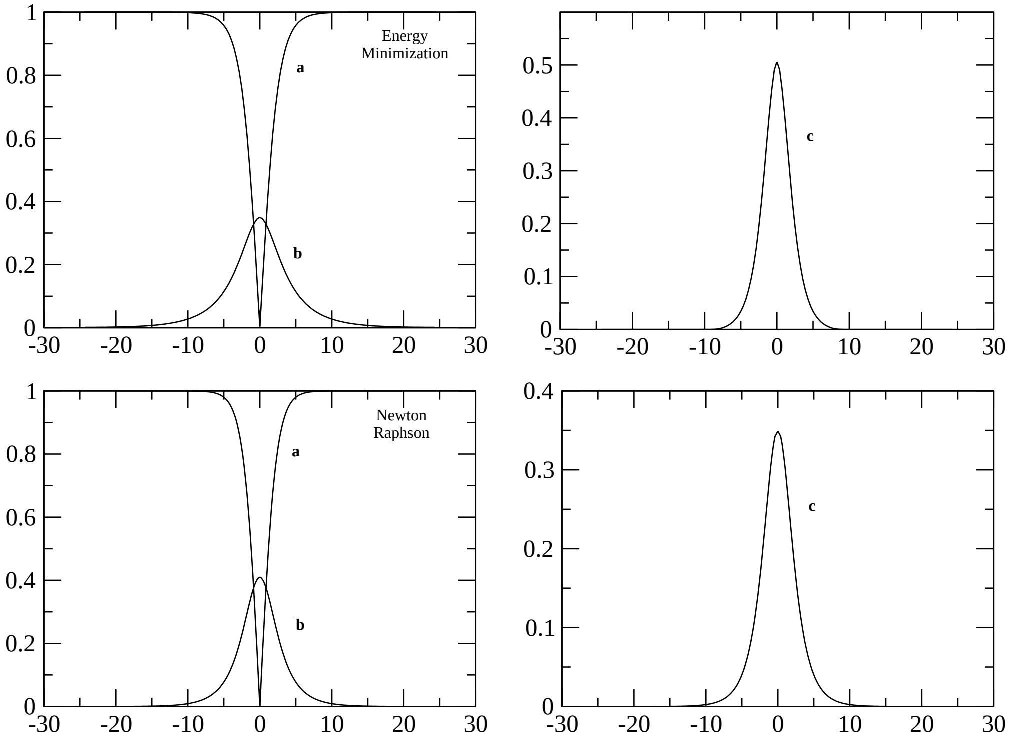

Figure 2.5: Straight bosonic superconducting string. Both graphs on top are the output of energy minimization algorithm. Parameters are $(\bar{\lambda}, \bar{m}^2, \bar{g}^2, \bar{v}, e)$ $=(1, 0.65, 0.25, 0.75, 1)$. Bottom graphs are the output of Newton-Raphson algorithm. Parameters are $(\bar{\lambda}, \bar{m}^2, \bar{g}^2, \bar{v}, e)$ $=(1, 0.62, 0.25, 0.75, 1)$. Letter $a$ denotes the scalar field, $b$ the charge condensate and $c$ the magnetic field associated with the $a$ field.

# PART II

## SEARCH FOR STRINGS AND SOLITONS

This part includes the research. Briefly, the first section involves a search on antiperiodic solitons on $S^1$ which is a based on [88]. The second section does a full numerical analysis of a straight string with a Ginzburg-Landau potential with a cubic term added to it. Such a potential is used in condensed matter physics as well [101]. The third section presents a numerical search on static bosonic superconducting vortex rings which is based on [13],[15] and can be seen as a continuation of [15], where spherically symmetric solutions were examined. The final section is based on the model of static vortex rings which is now extended by adding higher derivative terms. We analyze the behavior of the solutions of the model under these modifications.

# Chapter 3

# Antiperiodic solitons of the Goldstone model on $S^1$

## 3.1 Introduction

The purpose of this section is to present the complete list of static classical solutions of the Goldstone model on a circle $S^1$ of radius $L$ in 1+1 dimensions and the corresponding bifurcation tree together with a study of the stability of our solutions. It comes as a supplement to a previous note [88] which was searching for such solutions but with periodicity condition imposed there. Jacobi elliptic and standard trigonometric functions are used to express the solutions found and stability analysis of the latter is what follows. Classically stable quasi-topological solitons are identified. Many of the results have obvious similarities with those in [88]. We notice those and make comparisons with this reference. We also check the case of mixed boundary conditions and place a note with our conclusions in the end. The following analysis has both mathematical [108] and physical interest as it can be useful for the search of stable solitons in the two-Higgs standard model (2HSM) or the minimal supersymmetric standard model.

## 3.2 The classical solutions

The **Langrangian density** of our model is

$$\mathcal{L} = \frac{1}{2}(\partial_\mu \phi_1)^2 + \frac{1}{2}(\partial_\mu \phi_2)^2 - V(\phi_1, \phi_2)\,, \quad \mu = 0, 1 \tag{3.1}$$

with $\phi_1$ and $\phi_2$ real Higgs fields and potential of the following form:

$$V(\phi_1, \phi_2) = \frac{1}{4}(\phi_1^2 + \phi_2^2 - 1)^2 \tag{3.2}$$

We impose antiperiodic boundary conditions on the scalar fields with coordinates $x \in [0, 2\pi L]$.

$$\phi_i\,(x + 2\pi L) = -\phi_i\,(x)\ , \quad i = 1, 2 \tag{3.3}$$

The general static solution of model (3.1) can be expressed in terms of Jacobi elliptic functions:

$$\phi_1 = \sqrt{R}\,\cos\Omega, \quad \phi_2 = \sqrt{R}\,\sin\Omega \tag{3.4}$$

$$R(x) = a_1 + a_2 sn^2(\sqrt{2}\,\Lambda(x - x_0)\,, k) \tag{3.5}$$

$$\Omega(x) = C\int_{\xi}^{x} \frac{1}{R(y)}dy \tag{3.6}$$

where $C\left(a_1\left(k,\Lambda\right), a_2\left(k,\Lambda\right)\right)$ ,$x_0$,$\xi$ are constants while $sn$ denotes the Jacobi elliptic function; $sn(z,k)$, $sn^2(z,k)$ are periodic functions on the real axis with periods $4K(k)$ and $2K(k)$, respectively. $K(k)$ is the complete elliptic integral of the first kind. Inserting (3.4)-(3.6) into the equations corresponding to (3.1) leads to several conditions on the parameters and as a consequence to three different types of non-trivial solutions. We start with the simplest, the trivial solution.

## 3.3 The trivial solution

The energy functional for static configurations is given by

$$E = \int_0^{2\pi L} dx \left[\frac{1}{2}\left(\frac{\partial\phi_1}{\partial x}\right)^2 + \frac{1}{2}\left(\frac{\partial\phi_2}{\partial x}\right)^2 + V(\phi_1,\phi_2)\right] \tag{3.7}$$

and the field equations are

$$-\frac{d^2\phi_1}{dx^2} + \phi_1\Big(\phi_1^2+\phi_2^2-1\Big) = 0 \tag{3.8}$$

$$-\frac{d^2\phi_2}{dx^2} + \phi_2\Big(\phi_1^2+\phi_2^2-1\Big) = 0 \tag{3.9}$$

Apart from the vacuum solutions which have $E_{vac} = 0$, one can immediately think of the simplest solution, the trivial one

$$\phi_1 = \phi_2 = 0\ ,\ E_0 = \frac{L\pi}{2} \tag{3.10}$$

which exists for all values of $L$. The corresponding small oscillation eigenmodes, labeled by $j$, have

$$\tilde{\omega}^2(j) = \frac{1}{L^2}(\,(j+1/2)^2 - L^2\,)\ , \quad j = 0,1,2... \tag{3.11}$$

This solution is stable until $L = 1/2$ because $\tilde{\omega}^2(0) < 0$ for $L > 1/2$. Many additional solutions, some of which were discussed in [13] bifurcate from the solution $\phi_1 = \phi_2 = 0$ at critical values of $L$.

## 3.4 Three types of non-trivial solutions

Now, we present without many details the three non-trivial solutions and mention their similarities with those in [88]. The simplest case one can think, is to set $a_2 = 0$ so that from (3.5) we obtain $R(x) = a_1$ and the solution becomes

$$\phi_1 = \sqrt{1 - \frac{\left(N + \frac{1}{2}\right)^2}{L^2}}\ \cos\left(\frac{\left(N + \frac{1}{2}\right)x}{L}\right) \tag{3.12}$$

$$\phi_2 = \sqrt{1 - \frac{\left(N + \frac{1}{2}\right)^2}{L^2}}\ \sin\left(\frac{\left(N + \frac{1}{2}\right)x}{L}\right) \tag{3.13}$$

where $N$ is an integer. This solution is called type-I. One can observe that the above solution reduces to (3.10) when $L = N + 1/2$ i.e. when one of the $\tilde{\omega}$ of equation (3.11) crosses zero. The Higgs field winds $(2N+1)/2$ times around the top of the Mexican hat. It's energy is given by

$$E_I\left(L, N\right) = \frac{\pi}{L}\left(N + \frac{1}{2}\right)^2 - \frac{\pi}{2L^3}\left(N + \frac{1}{2}\right)^4 . \tag{3.14}$$

If we denote the above result which corresponds to the antisymmetric case we study here with $E_I^A$ and the result of [88] for the same type of solutions with $E_I^S$ where $S$ means "Symmetric" and $A$ "Antisymmetric", then we notice that

$$E_I^A\left(N\,, L\right) \ = \ E_I^S\left(N + \frac{1}{2}\,, L\right)$$

Another choice is to set $a_1 = 0$ on (3.5) so the solution now involves the Jacobi elliptic functions. $C$ becomes zero as well and the solution is

$$\phi_1 = 2k\Lambda sn\left(\sqrt{2}\Lambda x, k\right)\ , \qquad \phi_2 = 0\,, \qquad \Lambda^2 = \frac{1}{2\left(1 + k^2\right)} \tag{3.15}$$

This solution is called type-II. In fact, it corresponds to an oscillation of the Higgs field in the $\phi_2 = 0$ plane about the origin $\phi_1 = 0 = \phi_2$. If we take account of the antiperiodicity condition (3.3), then the argument $k$ of the Jacobi elliptic function is related to the radius $L$ of $S^1$ through the following formula

$$L = \frac{(2m+1)\,K(k)}{\pi}\sqrt{1 + k^2} \tag{3.16}$$

for some integer $m$. When we reach the limit of $k \to 0$ (i.e. $L \to m + \frac{1}{2}$) the solution (3.15) approaches (3.10). The energy of the solution above is given by the integral

$$E_{II} = \frac{4\,(2m+1)}{\sqrt{2}\Lambda\,(1+k^2)^2}\int_0^{K(k)} dy\left[\left(k^2 sn^2\,(y,k) - \frac{1+k^2}{2}\right)^2 + \frac{2k^2-1-k^4}{8}\right] \tag{3.17}$$

and by means of Elliptic integrals it becomes

$$E_{II} = \frac{4\,(2m+1)}{\sqrt{2}\Lambda\,(1+k^2)^2}\;\left[\frac{K(k)}{24}\;\left(3k^4+2k^2-5\right) + \frac{E(k)}{3}\;\left(k^2+1\right)\right] \tag{3.18}$$

Two specific values of $k$ with the corresponding results follow for $k=0$

$$E_{II}\,(L = m+1/2, m) = \frac{(2m+1)\,\pi}{4} \tag{3.19}$$

and for $k=1$

$$E_{II}\,(L=\infty, m) = \frac{4\,(2m+1)}{3\sqrt{2}} \tag{3.20}$$

The comparison of $E^A_{II}$ which represents our solutions, with $E^S_{II}$ which represents the symmetric case of the same type of solutions studied in [88], implies that

$$E^A_{II}(m) = E^S_{II}\left(m+\frac{1}{2}\right) \tag{3.21}$$

If none of $a_1, a_2$ are zero then we are led to type-III solutions where we have the following conditions for $a_1, a_2$ and $C^2$

$$a_1 = \frac{2}{3}\left(1 - 2\Lambda^2\left(1+k^2\right)\right), \qquad a_2 = 4k^2\Lambda^2 \tag{3.22}$$

$$\begin{aligned} C^2 &= \frac{4}{27}\left(1+\left(4k^2-2\right)\Lambda^2\right)\left(1+\left(4-2k^2\right)\Lambda^2\right)\left(1-2\Lambda^2\left(1+k^2\right)\right) = \\ &= \frac{2}{9}\left(1+\left(4k^2-2\right)\Lambda^2\right)\left(1+\left(4-2k^2\right)\Lambda^2\right)a_1 \end{aligned} \tag{3.23}$$

Here, one can explicitly observe the fact that when $a_1 = 0$ then $C^2 = 0$ as well. In addition, $R$ and $C^2$ must not be negative. This means another condition

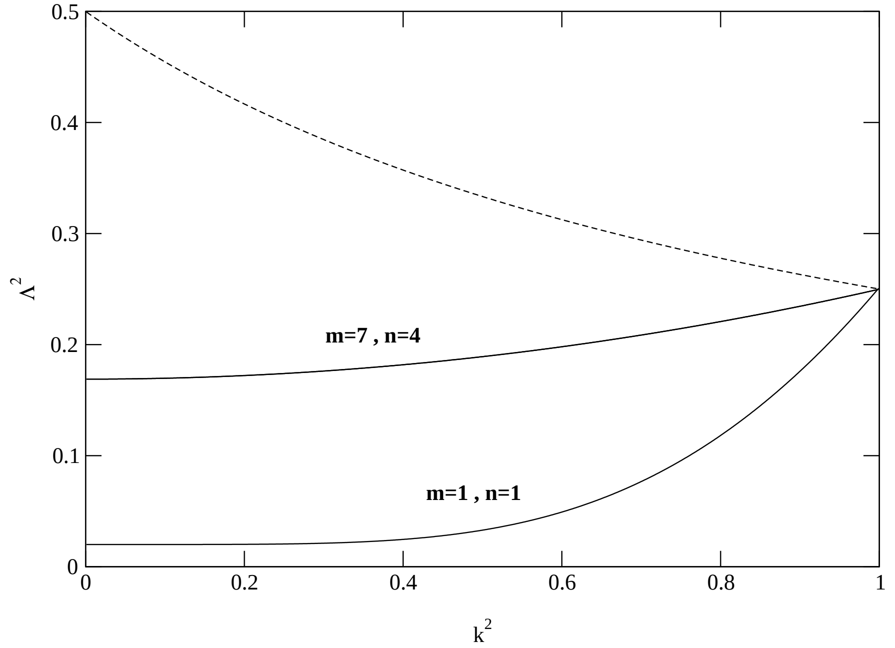

Figure 3.1: **Goldstone model:** The solutions of equations (3.25) and (3.26) are plotted as functions of $k^2$ for two values of $(n, m)$. The dashed curve indicates the limit (3.24).

$$\Lambda^2 \leq \frac{1}{2\left(1+k^2\right)} \tag{3.24}$$

with the equality leading to type-II solutions.

In order for $\Omega$ to satisfy $\Omega\left(x+2\pi L\right) = \Omega\left(x\right) + \pi$ and $R$ to be periodic (so for the solution to be antiperiodic as we want) on $[0, 2\pi L]$ the following equations must hold:

$$C \int_0^{2\pi L} \frac{1}{R(y)} dy = \left(2n+1\right)\pi \tag{3.25}$$

$$L = \frac{\left(2m+1\right) K(k)}{\sqrt{2}\pi\Lambda} \tag{3.26}$$

where $m, n$ are positive integers which respectively determine the number of oscillations of the modulus of the Higgs field and the number of the Higgs field windings around the origin $\phi_1 = 0 = \phi_2$ in a period $2\pi L$.

Now we return to (3.22) and (3.23) and analyze further type-III solutions. Solving these equations for $k = 0$, remembering that $K(0) = \pi/2$, we find the critical values of $L$ where these solutions start to exist:

$$\Lambda^2 = \frac{m^2}{6\left(2n+1\right)^2 - 4m^2} \quad \Rightarrow \quad L^2 = \frac{3}{4}\left(2n+1\right)^2 - \frac{m^2}{2} \tag{3.27}$$

The expression for $\Lambda^2$ together with (3.24) leads to the condition $2n+1 > m$ on the integers $m$ and $n$ ($m$ and $n \neq 0$). For any $n$ and $m \neq 2n+1$ the coefficient of $sn^2$ in the integral (3.6) is proportional to $k^2$ and if one expands the solution in powers of $k^2$ is led to the following formulae

$$\Lambda^2 = \frac{m^2}{6\left(2n+1\right)^2 - 4m^2}\left(1 + \frac{k^2}{2}\right) + \mathcal{O}\left(k^4\right) \tag{3.28}$$

$$L^2 = \frac{3}{4}\left(2n+1\right)^2 - \frac{m^2}{2} + \mathcal{O}\left(k^4\right) \tag{3.29}$$

$$C^2 = \frac{4}{3}\frac{\left(\left(2n+1\right)^2 - m^2\right)^2\left(2n+1\right)^2}{\left(3\left(2n+1\right)^2 - 2m^2\right)^3} + \mathcal{O}\left(k^4\right). \tag{3.30}$$

This expansion is necessary as there is no closed form for integral (3.25). In the limit $k = 0$ we observe that the $2n$ solutions of type-III yield the type-I solution with $N = n + 1/2$ at $L^2 = (3/4)\left(2n+1\right)^2 - m^2/2$ , where $m = 1, 2, ..., 2n$. For fixed values of $k$, $n$, $m$ we find a single solution $\Lambda^2\left(k,\ \left(2n+1\right)/m\right)$ obeying the following properties

$$\begin{aligned} \Lambda^2\left(k=0,\ \left(2n+1\right)/m\right) &= \frac{m^2}{6\left(2n+1\right)^2 - 4m^2} \\ \Lambda^2\left(k=1,\ \left(2n+1\right)/m\right) &= 1/4 \end{aligned} \tag{3.31}$$

This is illustrated in figure 3.1 for two different values of the pair $(n, m)$ by the solid curves, the dashed curve representing the limit (3.24).

The energy of the general type-III solution is given by the integral

$$E_{III} = \frac{2m+1}{\sqrt{2}\,\Lambda}\cdot\int_0^{K(k)} dy\left[\left(a_1 - 1 + a_2 sn^2(y,k)\right)^2 + \frac{1}{6}\ \left(1 + 16\Lambda^4\left(k^2 - 1 - k^4\right)\right)\right] \tag{3.32}$$

which, by means of $K(k)$, $E(k)$ becomes

$$
\begin{aligned}
E_{III} &= \frac{2m+1}{\sqrt{2}\,\Lambda}\left[K(k)\,\left(\frac{8}{9}\Lambda^2 k^2\left(1+\Lambda^2-\Lambda^2 k^2\right)-\frac{8}{9}\Lambda^2\left(2+\Lambda^2\right)+\frac{5}{18}\right)+\right. \\
&+ \left.\frac{8}{3}\Lambda^2 E(k)\right] \qquad (3.33)
\end{aligned}
$$

For $k = 1$ one obtains

$$
E_{III}\left(1,m,n\right) = \frac{4\left(2m+1\right)}{3\sqrt{2}} = E_{II}\left(1,m\right). \qquad (3.34)
$$

This shows that solution III approaches solution II in the limit $k \to 1$, a fact which also appears in [88].

The energies of the solutions of some low-lying branches are presented in figure 3.2 as functions of $L$ . For $L > 5/2$ all four types of solutions coexist and satisfy

$$
E_I\left(L,N=0\right) < E_I\left(L,N=1\right) < E_{III}\left(L,m=1,n=1\right) < E_{II}\left(L,m=1\right) < E_0\left(L\right). \qquad (3.35)
$$

The four stars on the upper part of the figure show the position of the four bifurcation points $L = 3.279,\ 3.775, 4.093, 4.272$ of the $n = 2,\ m = 3, 2, 1, 0$ solutions respectively from the $N = 2$ type-I solution. The two lower stars show the bifurcation values ($L = 2.179,\ 2.5$) of the $n = 1,\ m = 2, 1$ solutions respectively from the $N = 1$ type-I solution.

## 3.5 Stability Analysis

### 3.5.1 Type-I solutions

In order to analyze the stability of type-I solutions we follow the steps done in [88] which uses notions that can be found in [110] and [115]. Thus perturbing the fields $\phi_a$, $a = 1, 2$ around the classical solution (3.12)-(3.13), denoted here by $\phi_a^{cl}$,

$$
\phi_a\left(x\right) = \phi_a^{cl}\left(x\right) + \eta_a\left(x\right)\exp\left(-i\omega t\right) \qquad (3.36)
$$

we are led to the following equation for the normal modes:

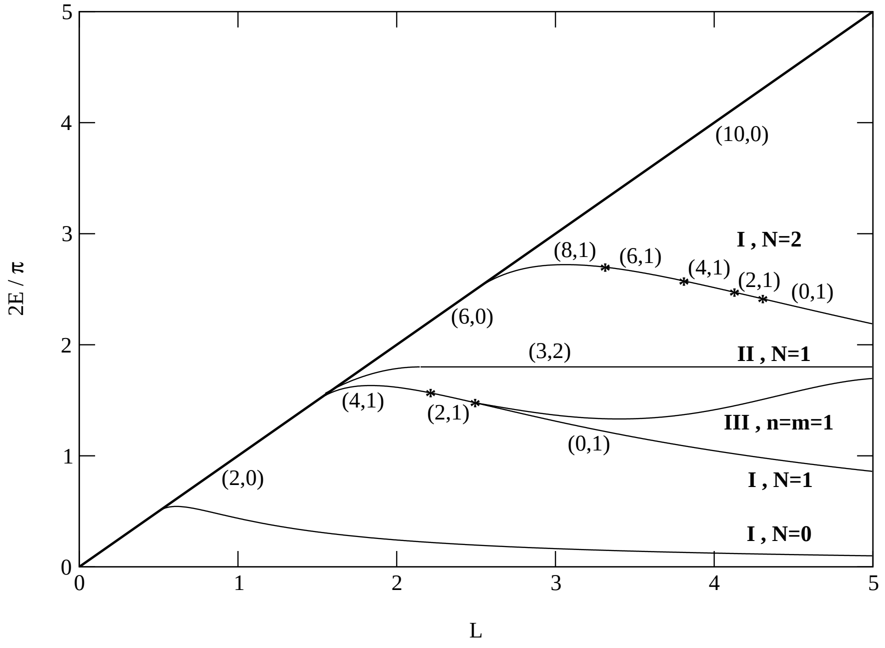

Figure 3.2: **Goldstone model:** The energies of some of the solutions are plotted as functions of the parameter $L$. The four stars on the upper branch indicate the four bifurcation points on the $N = 2$ type-I solution. The two lower stars indicate the two bifurcation points on the $N = 1$ type-I solution. The two numbers in parentheses refer to the number of negative and zero modes of the corresponding solution.

$$A\left(\tilde{N}, L\right)\begin{pmatrix} \eta_1 \\ \eta_2 \end{pmatrix} = \omega^2 \begin{pmatrix} \eta_1 \\ \eta_2 \end{pmatrix} \tag{3.37}$$

$$A\left(\tilde{N}, L\right) \equiv -\frac{d^2}{dx^2} + 2\left(1 - \left(\frac{\tilde{N}}{L}\right)^2\right)\begin{pmatrix} c^2 & sc \\ sc & s^2 \end{pmatrix} - \left(\frac{\tilde{N}}{L}\right)^2 \tag{3.38}$$

where $\omega^2$ is the eigenvalue and

$$c \equiv \cos\left(\tilde{N}x/L\right), \quad s \equiv \sin\left(\tilde{N}x/L\right), \quad N + 1/2 \equiv \tilde{N} \tag{3.39}$$

We derived the above formula by substituting (3.36) into the field equations (3.8). Terms $\mathcal{O}(\eta_a^s)$ with $s \geq 2$ are considered small.

The complete list of eigenvalues of the operator $A\left(\tilde{N}, L\right)$ for $\tilde{N} \geq 1$ can be obtained by classifying its invariant subspaces. This can be done by using the Fourier decomposition. Type-I solution has a twisted translational invariance and one can check that for an integer $n \geq \tilde{N}$ the following finite-dimensional vector spaces[1] are preserved by $A\left(\tilde{N}, L\right)$

$$V_n = Span\left\{a_p \cos\frac{px}{L}\ ,\ \beta_p \sin\frac{px}{L}\ ,\ p-n=0\left(mod 2\tilde{N}\right)\ ,\ |p|\leq n\right\}, \quad (3.40)$$

$$\tilde{V_n} = Span\left\{a_p \cos\frac{px}{L}\ ,\ -\beta_p \sin\frac{px}{L}\ ,\ p-n=0\left(mod 2\tilde{N}\right)\ ,\ |p|\leq n\right\} \quad (3.41)$$

under the following condition

$$a_p = \beta_p \qquad \text{if} \qquad p-n+2\tilde{N} > 0 \quad (3.42)$$

where $a_p$ , $\beta_p$ are arbitrary constants. The operator $A\left(\tilde{N}, L\right)$ can then be diagonalized on each of the finite-dimensional vector spaces above, leading to a set of algebraic equations.

To be more specific, define $\lambda_1 \equiv 2\left(1-\lambda_2\right)$, $\lambda_2 \equiv \left(\tilde{N}/L\right)^2$. Also, consider the vector

$$\begin{pmatrix} V_{\tilde{N}+k} \\ V_{\tilde{N}-k} \end{pmatrix} \text{ with } \quad V_{\tilde{N}+k} \equiv \begin{pmatrix} \cos\left(\frac{\tilde{N}+k}{L}\right)x \\ \sin\left(\frac{\tilde{N}+k}{L}\right)x \end{pmatrix}\ ,\ V_{\tilde{N}-k} \equiv \begin{pmatrix} \cos\left(\frac{\tilde{N}-k}{L}\right)x \\ \sin\left(\frac{\tilde{N}-k}{L}\right)x \end{pmatrix} \quad (3.43)$$

Acting with the operator $A\left(\tilde{N}, L\right)$ on one of the above vectors (say $V_{\tilde{N}+k}$) we have the following steps:

$$\left\{-\frac{d^2}{dx^2} + \frac{\lambda_1}{2}\begin{pmatrix} 2c^2 & 2sc \\ 2sc & 2s^2 \end{pmatrix} - \lambda_2 - \omega^2\right\} V_{\tilde{N}+k} = 0 \quad \Rightarrow$$

$$\Rightarrow \left\{-\frac{d^2}{dx^2} + \frac{\lambda_1}{2}\mathbf{1} - \lambda_2 - \omega^2 + \frac{\lambda_1}{2}\mathbf{M}\right\} V_{\tilde{N}+k} = 0 \quad (3.44)$$

---

[1] These vector spaces should have been the same as in (34) of [88] (with $N \rightarrow \tilde{N}$) but they are not, due to a misprint in [88]. Here we correct this by writing these spaces explicitly in equations (3.40) and (3.41).

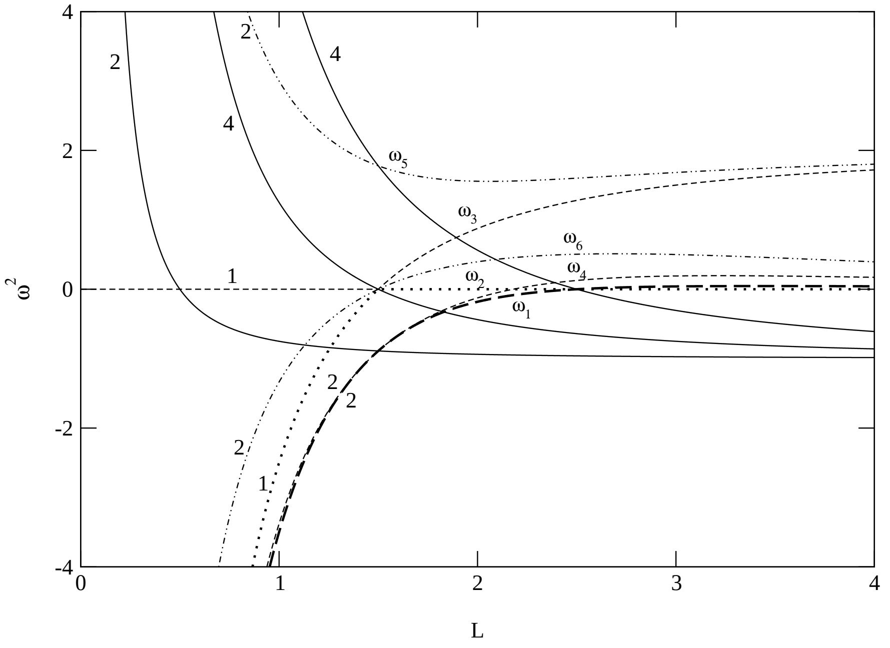

Figure 3.3: **Goldstone model:** The values (3.11) are plotted as functions of $L$ for $j = 0, 1, 2$ (solid curves), together with the values $\omega_1^2(1,1,-1)$, $\omega_2^2(1,0,-1)$, $\omega_3^2(1,0,1)$, $\omega_4^2(1,2,-1)$, $\omega_5^2(1,1,1)$, $\omega_6^2(1,3,-1)$ of (3.46) (dashed and dotted curves). The numbers indicate the multiplicity of the eigenvalues.

where $\mathbf{1}$ is the $2 \times 2$ unit matrix and

$$\mathbf{M} \equiv \begin{pmatrix} \cos\left(\frac{2\tilde{N}x}{L}\right) & \sin\left(\frac{2\tilde{N}x}{L}\right) \\ \sin\left(\frac{2\tilde{N}x}{L}\right) & -\cos\left(\frac{2\tilde{N}x}{L}\right) \end{pmatrix}$$

which has the action

$$\mathbf{M}V_{\tilde{N}+k} = V_{\tilde{N}-k} \tag{3.45}$$

The same happens if we choose $V_{\tilde{N}-k}$ instead. In that case, the equation above is $\mathbf{M}V_{\tilde{N}-k} = V_{\tilde{N}+k}$ as expected. A matrix which has exactly the same action as above can be found easily and this is $\begin{pmatrix} 0 & \lambda_1/2 \\ \lambda_1/2 & 0 \end{pmatrix}$.

Finally, we observe that

$$\begin{pmatrix} \left(\frac{\tilde{N}+k}{L}\right)^2 + \frac{\lambda_1}{2} - \lambda_2 - \omega^2 & \frac{\lambda_1}{2} \\ \frac{\lambda_1}{2} & \left(\frac{\tilde{N}-k}{L}\right)^2 + \frac{\lambda_1}{2} - \lambda_2 - \omega^2 \end{pmatrix} V_{\tilde{N}+k} = 0$$

which implies the condition that the determinant of the above matrix must be zero in order to acquire the non-zero eigenvalues.

The eigenvalues of $A\left(\tilde{N}, L\right)$ on $V_n$ are

$$\begin{aligned}\omega^2\left(N,k,\pm1\right) &= \frac{1}{L^2}\left[L^2-\left(N+\frac{1}{2}\right)^2+k^2\right]\pm\\ &\pm \frac{1}{L^2}\sqrt{\left(L^2-\left(N+\frac{1}{2}\right)^2\right)^2+4k^2\left(N+\frac{1}{2}\right)^2}\end{aligned} \quad (3.46)$$

for $k=0,1,2,...$ and similarly on $\tilde{V_n}$ for $k=1,2,3,....$ Notice that if we replace $N+1/2$ by $\tilde{N}$ then the above result is the same with eq.(36) of [88].

For $N$ having a specific value and $L$ slightly greater than $N$, the solution (3.12)-(3.13) possess $4N$ negative modes corresponding to $k=1,2,3,...,2N$ in (3.46) (minus sign). When $L$ increases, the number of positive eigenmodes increases as well

$$L^2=\frac{3}{4}\left(2N+1\right)^2-\frac{m^2}{2}, \qquad m=1,2,...,2N, \quad (3.47)$$

i.e. (cf(3.27)) at those values of $L$ where the solutions of type-III with $n=N$ bifurcate from the solution of type-I. For

$$L^2\geq L^2_{cr}\left(N\right)\equiv\frac{3}{4}\left(2N+1\right)^2-\frac{1}{2} \quad (3.48)$$

all the modes are positive and (3.12)-(3.13) are classically stable solitons. These results are illustrated in figure 3.2 for $N=1$ and $N=2$. The numbers in parentheses represent the number of negative and zero modes of the corresponding branch.

### 3.5.2 Type-II and Type-III solutions

The equations for the fluctuations about the solution (3.15) decouple to take the form of Lame equations:

$$\left\{-\frac{d^2}{dy^2}+6k^2sn^2\left(y,k\right)\right\}\eta_1=\Omega_1^2\eta_1 \quad (3.49)$$

$$\left\{-\frac{d^2}{dy^2}+2k^2sn^2\left(y,k\right)\right\}\eta_2=\Omega_2^2\eta_2 \quad (3.50)$$

where

$$x = \sqrt{1+k^2}\, y\,, \qquad \Omega_a^2 \equiv \left(\omega_a^2 + 1\right)\left(k^2+1\right), \qquad a = 1,2 \tag{3.51}$$

and $\omega_a^2$ is the effective eigenvalue of the relevant operator. Equations (3.49) and (3.50) admit two and one algebraic modes, respectively, with corresponding eigenvalues

$$\Omega_1^2 :\ 4+k^2\ ,\ 1+4k^2 \qquad\quad \textit{and} \qquad\quad \Omega_2^2 :\ 1+k^2 \tag{3.52}$$

The corresponding values of $\omega^2$ follow immediately from (3.51); they have signature $(+,+)$ and $(0)$, respectively.

It's a property of the Lame equation that the solutions determined algebraically correspond to the solutions of the lowest eigenvalues. The remaining part of the spectrum therefore consists of positive eigenvalues. The spectrum of the equation (3.49) was studied perturbatively in [109], while the relation between the Lame equation and the Manton-Samols sphalerons was first pointed out in [111]-[113].

Concerning the stability equation of type-III solution, it seems to be more difficult to deal with as the presence of the Jacobi Elliptic functions prevent us from having an analytic expression for $\Omega(x)$ in (3.4). Thus, we are not able to follow the steps done in the case of type-I solutions (i.e. find the $\mathbf{M}$ matrix) where trigonometric functions are easier to handle. Detailed analysis especially for the case of Lame equations can be found in [112] and [115].

## 3.6 Conclusions

A detailed analytical study of the static solutions of the Goldstone model on a circle has been given in [88] and we followed the same path here for our boundary conditions. Many results of [88] are connected with ours by a simple change on variables used. We write them explicitly above whenever is necessary. We also note our effort to impose mixed boundary conditions as well. Specifically, we enforced $\phi_1$ to be antiperiodic and $\phi_2$ periodic but there was no solution to satisfy this choice so it's needless to extend beyond this small remark here.

Many details were presented on the stability analysis for the solutions found. Classically stable solitons were identified, together with the range of the parameter $L$ for which they are stable.

This simpler model we present here and many others can be connected and can also give us the experience to deal with realistic $(3+1)$-dimensional particle physics models in our search for possible metastable localized solitons. Ref. [88] on which this note was based, has connections with [109] and [110] as it concerns the branches of their solutions, also with [13], while there are also interesting physical applications [114] as it is already mentioned in [88]. Soliton solutions in $(3+1)$-dimensional models with antiperiodic boundary condition imposed on one spatial dimension, which is compactified on $S^1$, are analyzed in [115]-[117] where supersymmetry breaking is examined.

# 3.7 APPENDIX

## 3.7.1 Part I: Jacobi elliptic functions

The following serves as a small and helpful supplement on the mathematical functions we used above, as well as some of their basic properties, which were useful.

Consider the following elliptic integral of first kind

$$u = \int_0^{\varphi} \frac{d\theta}{\sqrt{1 - k\sin^2\theta}} \tag{3.53}$$

Then we have the following definitions of the Jacobi elliptic functions

$$\begin{aligned} sn\ u &= \sin\varphi && (3.54)\\ cn\ u &= \cos\varphi && (3.55)\\ dn\ u &= \sqrt{1 - k\sin^2\varphi} && (3.56) \end{aligned}$$

There are other nine Jacobi elliptic functions which are constructed from the above three but we don't use them here. The parameter $k$ is called elliptic modulus and $0 \leq k \leq 1$, so the elliptic functions can be thought of as being given by two variables, the amplitude $\varphi$ and the parameter $k$.

From the above definition, it is easy to see that

$$cn^2 + sn^2 = 1 \tag{3.57}$$

is valid. Also,

$$dn^2 + k^2 sn^2 = 1 \tag{3.58}$$

The derivatives of these functions are

$$\begin{aligned} \frac{d}{dz}\,sn(z,k) &= cn(z,k)dn(z,k) && (3.59)\\ \frac{d}{dz}\,cn(z,k) &= -sn(z,k)dn(z,k) && (3.60)\\ \frac{d}{dz}\,dn(z,k) &= -k^2 sn(z,k)cn(z,k) && (3.61) \end{aligned}$$

where $z$, in fact, depends on $u$.

Practically, $sn(x,k)$ is the solution of the following differential equations

$$\frac{d^2y}{dx^2} + (1+k^2)y - 2k^2y^3 = 0, \quad \left(\frac{dy}{dx}\right)^2 = (1-y^2)(1-k^2y^2) \tag{3.62}$$

and $cn(x,k)$ is the solution of the following equations

$$\frac{d^2y}{dx^2} + (1-2k^2)y + 2k^2y^3 = 0, \quad \left(\frac{dy}{dx}\right)^2 = (1-y^2)(1-k^2+k^2y^2) \tag{3.63}$$

while $dn(x,k)$ is the solution of the following equations

$$\frac{d^2y}{dx^2} - 2k^2y + 2y^3 = 0, \quad \left(\frac{dy}{dx}\right)^2 = -(1-y^2)(1-k^2-y^2) \tag{3.64}$$

# Chapter 4

# $U(1)$ model for straight strings

## 4.1 Introduction

The evolution of the Universe is believed to involve several symmetry breaking phase transitions, out of which, topological defects, such as strings, are created [16, 100, 106]. These transitions can be examined in the framework of condensed matter systems. Although there are differences from the cosmological case where, relativistic dynamics must be used and gravity is important, the formation of such defects in the laboratory [99], can provide helpful hints for cosmology. Topologically stable knots and vortex-like structures in general, are of wide interest in condensed matter physics. For example, one can think of Bose-Einstein condensates (BEC) (i.e. see [8]), vortices in superfluid Helium-3 and Helium-4 [9] , or nematic liquid crystals [11, 12].

Also, in the framework of high energy physics, future experiments in LHC could answer whether metastable particle-like solitons exist in minimal supersymmetric Standard Model or two-Higgs Standard Model (2HSM) or not. In [15, 13], work on classically stable, metastable quasi-topological domain walls and strings in simple topologically trivial models, as well as in the 2HSM has been done. These solutions are local minima of the energy functional and can quantum mechanically tunnel to the vacuum, not being protected by an absolutely conserved quantum number. One can also find other interesting subjects involving superconducting vortex rings such as, rotating superconducting rings [40], electroweak strings [92, 93] or work on such rings in $SU(2)$ non-Abelian Yang-Mills-Higgs model [94]. Finally, twisted semilocal vortices examined in [95] can be connected to the models we present below while one can also search if stable rings can be made out of these strings.

In this chapter, we consider a $U(1)_A$ model with a modified Ginzburg-Landau (GL) potential. The modification has to do with the addition of a cubic term. In Thermal Field Theory, such term comes from the 1-loop radiative corrections to the GL potential [102]. We search whether this model can admit stable strings or not. The features of such strings, if they exist, are the supercurrent which flows on the surface of the defect within a certain finite width, as well as, a magnetic flux in the interior of the defect (fig.4.1). This magnetic flux is a consequence of the existence of the supercurrent. One has to keep in mind that the magnetic field can penetrate in a certain depth inside the superconducting regions where the supercurrent flows. If the penetration depth is greater than the width of the superconducting surface, then the defect becomes unstable and can be destroyed. The GL potential we use here, is used in condensed matter physics as well (see [101] and references therein).

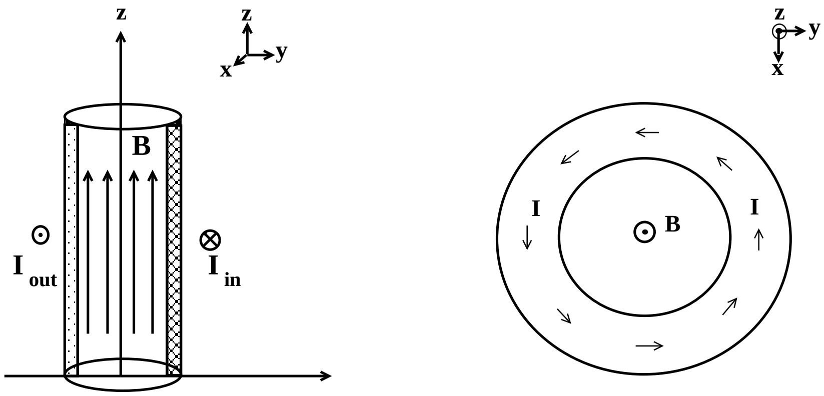

Figure 4.1: $U(1)_A$ **model:** The relative position of the supercurrent as well as of the magnetic field on a $xy$-profile of the system on the right. The left picture is strongly reminiscent of an infinite solenoid.

Stable defects of this $U(1)_A$ model, can also be used to form torus-like strings and study their stability. This can happen by taking a piece of such straight string and periodically connect its ends together. These string loops are examined in [90] (chapter 5) but in the frame of a $U(1) \times U(1)$ model, where the existence of the defect is ensured for topological reasons. That model, is a continuation of previous work [15, 13]. In chapter 6, we will examine an extended version of the model in [90] (chapter 5).

## 4.2 The $U(1)_A$ model

This model consists of a complex scalar field $\psi$ and a gauge field $A_\mu$. The **Lagrangian density** describing our system is:

$$\mathcal{L} = -\frac{1}{4}F_{\mu\nu}^2 + |D_\mu\psi|^2 - U(|\psi|) \tag{4.1}$$

where the covariant derivative is $D_\mu \equiv \partial_\mu + ieA_\mu$, the strength of the field is $F_{\mu\nu} = \partial_\mu A_\nu - \partial_\nu A_\mu$, while $e$ is the $U(1)_A$ charge. The Lagrangian (4.1), is invariant under the following $U(1)$ gauge transformation

$$\psi \rightarrow e^{ib(\mathbf{x})}\psi, \quad A_\mu \rightarrow A_\mu - \frac{1}{e}\partial_\mu b(\mathbf{x}) \tag{4.2}$$

.

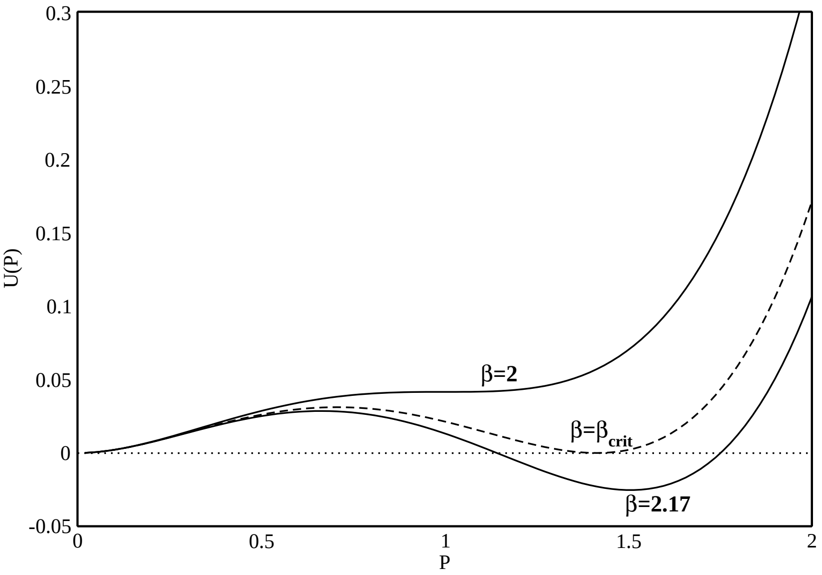

Figure 4.2: $U(1)_A$ **model:** The potential for $a = 1$ and $\beta = 2$, $\beta = \beta_{crit} = \frac{3}{\sqrt{2}}$ (dashed line) and $\beta = 2.17$ (bottom line). The plot is $U$ vs. $P$.

where $b(\mathbf{x})$ is a position-dependent phase. We choose the potential

$$U(|\psi|) = \frac{a}{2}|\psi|^2\left(\frac{1}{4}|\psi|^2 - \frac{\beta}{3}|\psi| + \frac{\gamma}{2}\right) \tag{4.3}$$

where $a, \beta, \gamma$ constants. We can set $\gamma = 1$. Since $\sqrt{\gamma}$ has dimensions of mass, we count the energy of the system in units of $\sqrt{\gamma}$. The vacuum is $|\psi| = 0$. This vacuum leaves unbroken the gauge symmetry $U(1)_A$. When

$$|\psi| = |\psi_0| \equiv \frac{\beta + \sqrt{\beta^2 - 4}}{2} \tag{4.4}$$

(for $\beta > 2$), we have $U(1)_A \to \mathbf{1}$ giving non-zero mass to $A$. Thus, one may generate an electric current flowing along regions where $|\psi| \neq 0$. In fig.4.2 one can see the shape of the potential. The equation (4.4) gives the position of the minimum of interest for every $\beta > 2$. When $\beta = 2$, the secondary (non-trivial) minimum of the potential disappears, at $|\psi| = 1$ position. When $2 < \beta < \frac{3}{\sqrt{2}} \equiv \beta_{crit}$, it becomes zero only at $|\psi| = 0$, while another minimum with non-zero $|\psi|$ forms. When $\beta = \beta_{crit}$, the potential has another zero at $|\psi| = \sqrt{2}$ which is also a local minimum. Finally, when $\beta > \beta_{crit}$ it has two more zeros at

$$P_{\pm} = \frac{2\beta}{3} \pm \sqrt{\frac{4\beta^2}{9} - 2} \tag{4.5}$$

between which, it becomes negative (fig.4.6). The mass spectrum is

$$m_A = 0, \quad m_\psi^2 = \frac{a}{2} \tag{4.6}$$

## 4.3 The $U(1)_A$ model: Search for stable vortices

We are interested in configurations having cylindrical symmetry, that is, infinite straight strings. The field $\psi$ can be non-vanishing on a cylindrical surface of specific radius. At infinity ($\rho \to \infty$), we have the vacuum of the theory $|\psi| = 0$. The **ansatz** for the fields is:

$$\psi(\rho, \varphi, z) = P(\rho) e^{iM\varphi}, \quad \mathbf{A}(\rho, \varphi, z) = \frac{A_\varphi(\rho)}{\rho} \hat{\varphi} \tag{4.7}$$

where $M$ the winding number of the field $\psi$ and $\hat{\rho}$, $\hat{\varphi}$, $\hat{z}$ are the cylindrical unit vectors. We use cylindrical coordinates $(t, \rho, \varphi, z)$, with space-time metric $g_{\mu\nu} = diag(1, -1, -\rho^2, -1)$. We work in the $A^0 = 0$ gauge. For the gauge field we suppose the above form based on the following thought: The $\mathbf{A}$ field is the one produced by the supercurrent flowing on the cylindrical surface. The current is in the $\hat{\varphi}$ direction thus, we expect the non-vanishing component to be $A_\varphi$ and the amplitude $P$ of $\psi$ to be independent of $\varphi$. As it concerns the scalar field $\psi$, since it follows the geometry of the cylindrical defect, we expect that its amplitude is independent of $z$ as well.

With the above ansatz, the **energy functional** for minimization takes the form

$$E = 2\pi \int_0^\infty \rho d\rho \left[ \frac{1}{2\rho^2} (\partial_\rho A_\varphi)^2 + (\partial_\rho P)^2 + \frac{P^2}{\rho^2} (eA_\varphi + M)^2 + U(P) \right] \tag{4.8}$$

and the potential is

$$U(P) = \frac{a}{2} P^2 \left( \frac{1}{4} P^2 - \frac{\beta}{3} P + \frac{1}{2} \right) \tag{4.9}$$

The gauge field $\mathbf{A}$ has a magnetic field of the form

$$\mathbf{B} = \frac{1}{\rho} \frac{\partial A_\varphi}{\partial \rho} \hat{z} \tag{4.10}$$

while, the **field equations** are

$$\partial_\rho^2 P + \frac{1}{\rho}\partial_\rho P - \frac{P}{\rho^2}(eA_\varphi + M)^2 - \frac{aP}{4}\Big(P^2 - \beta P + 1\Big) = 0 \tag{4.11}$$

$$\partial_\rho^2 A_\varphi - \frac{1}{\rho}\partial_\rho A_\varphi - 2eP^2(eA_\varphi + M) = 0 \tag{4.12}$$

The usual rescaling arguments lead to the **virial** relation:

$$2\pi\int_0^\infty \rho d\rho\left(\frac{B^2}{2} - U\right) = 2\pi\int_0^\infty \rho d\rho\left(\frac{(\partial_\rho A_\varphi)^2}{2\rho^2} - \frac{aP^2}{2}\left(\frac{P^2}{4} - \frac{\beta P}{3} + \frac{1}{2}\right)\right) = 0 \tag{4.13}$$

Define

$$\begin{aligned} I_1 &\equiv 2\pi\int_0^\infty \rho d\rho\,\frac{1}{2\rho^2}\left(\frac{\partial A_\varphi}{\partial\rho}\right)^2 \\ I_2 &\equiv -2\pi\int_0^\infty \rho d\rho\,\frac{aP^2}{2}\left(\frac{P^2}{4} - \frac{\beta P}{3} + \frac{1}{2}\right) \end{aligned}$$

For a solution of the model, we theoretically must have $I_1 + I_2 = 0$. In fact, we define the index $V \equiv \frac{||I_1| - |I_2||}{|I_1| + |I_2|}$. We want this index as small as possible. Other virial relations can be derived as follows. For example, one can consider the double rescaling of $\rho \to \lambda\rho$ and either $P \to \mu P$ or $A_\varphi \to \mu A_\varphi$ or even both of the fields and then demand $\partial_\lambda E|_{\lambda=1=\mu} = 0 = \partial_\mu E|_{\lambda=1=\mu}$.

## 4.4 The $U(1)_A$ model: Numerical results

We use a standard minimization algorithm to minimize the energy functional (4.8). The algorithm is written in C. One can find details about the algorithm used, on page 425 of [104] but, briefly, the basic idea is this: Given an appropriate initial guess, there are several corrections to it, having as a criterion the minimization of the energy in every step. When the corrections at the value of the energy are smaller than $\approx 10^{-8}$ the program stops and we get the final results. We are interested in final configurations having nontrivial energy. This signals the existence of a stable vortex with that energy. We check our results through virial relation (4.13). Finally, our results must also satisfy the field equations (4.11), (4.12).

The **initial guess** we use for our computation is:

$$\begin{aligned} P(\rho) &= \xi_1\rho^M(1 - \tanh(0.2\rho^2)) \\ A_\varphi &= -\tanh(\xi_2\rho^2) \end{aligned}$$

.

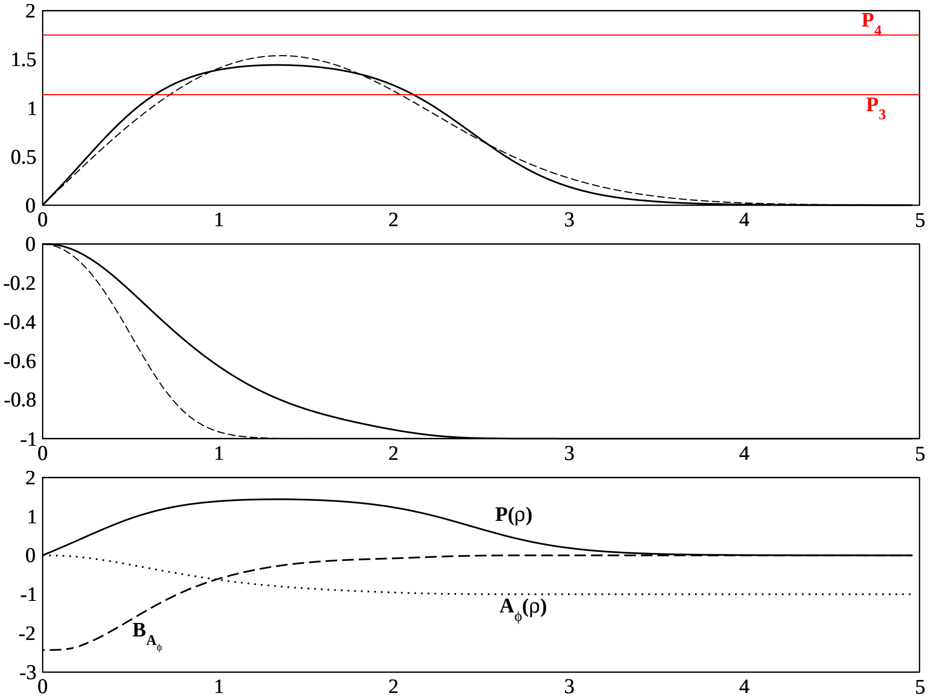

Figure 4.3: $U(1)_A$ **model:** In the first two graphs we have the initial guess (dashed lines - - - ) as well as the final configuration of fields (solid lines — ) $P(\rho)$, $A_\varphi(\rho)$. We chose $M = 1$, $e = 1$, $\beta = 2.17$, $a = 43.7$. The energy $E = 35.3$ and virial is $10^{-4}$. The bottom graph gathers all the fields. For the field $P$, the area between the horizontal lines $P_3$ and $P_4$ is energetically favorable (see also fig.4.6).

where $\xi_1, \xi_2$ are constants, the value of which, depends also on the location of the minimum (say $|\psi| = |\psi_0|$) of the potential. For the final configurations we present in the figures 4.3, 4.4, we chose $\xi_1 = 1.75,\ \xi_2 = 2$.

The initial guess also satisfies the appropriate asymptotics

- near $\rho = 0$: $P \sim \rho^M, \quad A_\varphi \sim \rho^2$
- at infinity: $P \to 0$, exponentially

while $P$ must be non-zero somewhere between $\rho = 0$ and $\rho \to \infty$. One must make a careful choice of the initial guess. That is to say, the maximum value of $P$ in the initial guess (dashed lines) must be inside the favorable area denoted by the horizontal lines in figs.4.3-4.4. This area is dictated by the form of the potential and especially by its negative sectors (see fig.4.6).

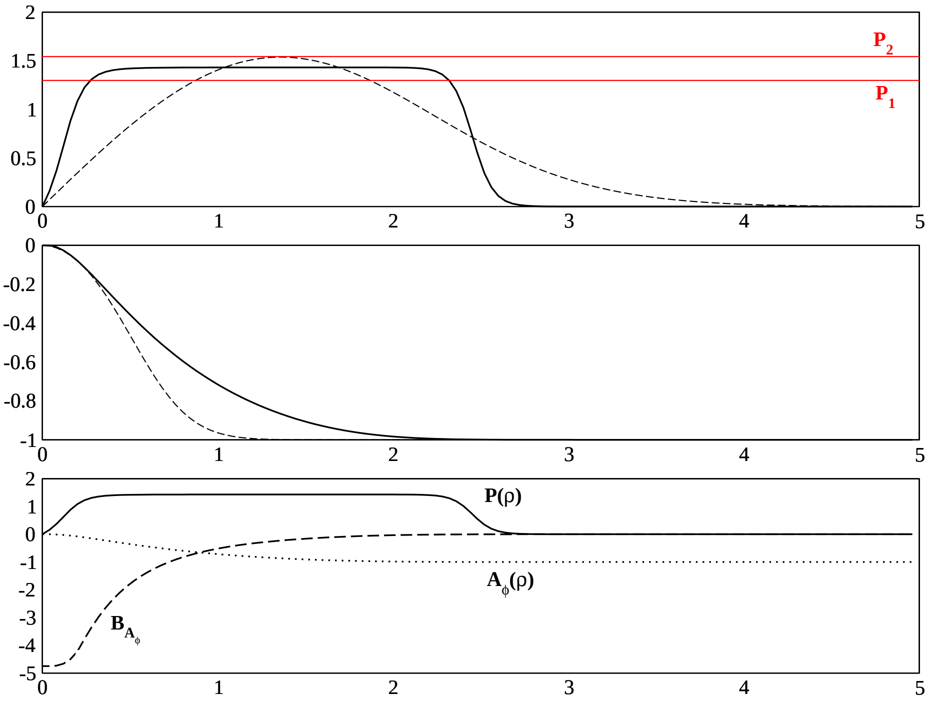

Figure 4.4: $U(1)_A$ **model:** In the first two graphs we have the initial guess (dashed lines - - - ) as well as the final configuration of fields (solid lines — ) $P(\rho)$, $A_\varphi(\rho)$. We chose $M = 1$, $e = 1$, $\beta = 2.13$, $a = 1104$. The energy $E = 115.2$ and virial is $2 \cdot 10^{-3}$. The bottom graph gathers all the fields. For the field $P$, the area between the horizontal lines $P_1$ and $P_2$ is energetically favorable (see also fig.4.6).

Since, for values of $\beta$ where $2 \leq \beta \leq \beta_{crit}$ is valid, we find no non-trivial solution, we searched and tried to find out what happens when we make the minimum of interest deeper. For that reason we searched in the region where $\beta > \beta_{crit}$. It is possible to find solutions to this model until $\beta$ reaches 2.13 (from above). Under this value, this is difficult if not impossible. Even at $\beta = 2.13$ (fig.4.4) we use great values of $a$ in order to find the solution exhibited. The relation between $a$ and $\beta$ can be found in fig.4.7. The solutions of the model for two different values of $\beta > \beta_{crit}$, are shown in figs.4.3-4.4 and a comparison between them in fig.4.5 in order to observe their different features.

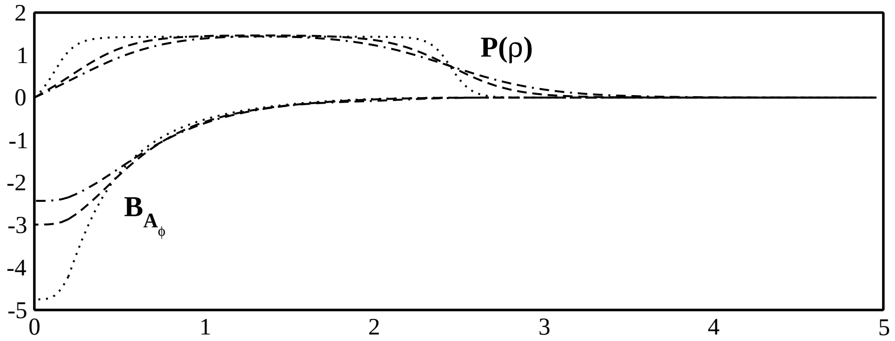

Figure 4.5: $U(1)_A$ **model:** Here we have a plot in order to compare the changes of $P(\rho)$ and $B_A(\rho)$ as $a$ goes from 2.17 (dashed and dotted - · - ), to 2.15 (dashed - - - ) and 2.13 (dotted · · ·).

### 4.4.1 Analysis for $2.13 \leq \beta \leq 2.2$

We observe that for a specific $\beta$, there is a small range for the parameter $a$ of the potential, where the model exhibits the solution presented in the figures. Out of this small range and for greater $a$, we end up to a final configuration of negative energy. This happens because, the bigger the parameter $a$ becomes, the stronger the potential is, thus the field $P$ strongly prefers to acquire the value where the non-trivial minimum of the potential is (see fig.4.2), in order to decrease further the energy. But, for $\beta > \beta_{crit}$ we have $U < 0$ at the position of that minimum, which also enforces the total energy $E$ to be negative in this case. We have to note that, virial relation of such a final configuration is *not* satisfied due to the great values the term $(\partial_\rho P)^2$ acquires around $\rho = 0$ and $\rho \to \infty$. This is clear if one directly observes (4.13), which can not be satisfied for $U < 0$.

On the other hand, for smaller values of $a$, we get the trivial configuration ($P = 0, A_\varphi = 0$), as the benefit from the potential term is no longer satisfactory in order to have a non-trivial $P$.

### 4.4.2 Reasons for instability when $\beta > 2.2$

Now, for high values of $\beta$ (i.e. $\beta > 2.2$) we faced difficulties in finding a solution. We believe that this has the following explanation: as $\beta$ grows, the area of values where the potential $U$ is negative, increases as well.

If the parameter $a$ is large, then the potential becomes a strong factor in reducing the energy, as it is highly negative. Thus, for large $a$ it is energetically favorable to decrease further the potential value. The latter happens by converting $P$ function in such a way, so as to be, as much of it as possible, inside the energetically favorable area (it is denoted by the horizontal lines in the figs.4.3-4.4). Thus, we end up to a final configuration with potential $U << 0$ and virial relations can not be satisfied (see for example eq.4.13) as we have a sum of positive terms.

On the other hand, for lower $a$ the potential is no longer a strong factor for reducing the energy. In this case, it is energetically favorable to reduce the value of the $(\partial_\rho P)^2$ and $(\partial_\rho A_\varphi)^2$ terms as the system can gain more from these. The consequence is that $P$ leaves the area of stability as its peak lowers in order to reduce the two terms above and there is only one possibility: to end up to zero energy, that is to say, the trivial configuration.

The difference in the stable solutions we have found above, is that the values of $\beta$ are such, that the potential is negative but not strongly negative while the changes on the terms $(\partial_\rho P)^2$ and $(\partial_\rho A_\varphi)^2$ can deform the field $P$ in such a way, so that it can still be inside the favorable area. Then, the potential term has the possibility to change in such a way, so it can satisfy virial as well.

### 4.4.3 Reasons for instability when $\beta \leq \beta_{crit}$

In the following explanation we will use fig.4.5 & 4.6. In fig.4.5 one can observe that as we get closer to the critical value $\beta = 3/\sqrt{2} \equiv \beta_{crit}$, the $P$ field tends to acquire everywhere the value $P = P_0$ (location of the non-trivial minimum of the potential). This leads to greater values of $\partial_\rho P$.

The above has a reasonable explanation which can be found in fig.4.6. As we get closer to $\beta_{crit}$, the space within the lines, where the potential can get negative values, becomes smaller. Under $\beta_{crit}$ the potential can be either positive or zero (the latter for $P = 0$ only).

Observe the energy functional to be minimized:

$$E = 2\pi \int_0^\infty \rho d\rho \left[ \frac{1}{2\rho^2}(\partial_\rho A_\varphi)^2 + (\partial_\rho P)^2 + \frac{P^2}{\rho^2}(eA_\varphi + M)^2 + U(P) \right] \quad (4.14)$$

The main target of minimization is to "fix" all the above terms in order to have the minimum possible value for the energy. Below, we analyze the possible cases.

- $\beta \to \beta_{crit}^+$:

.

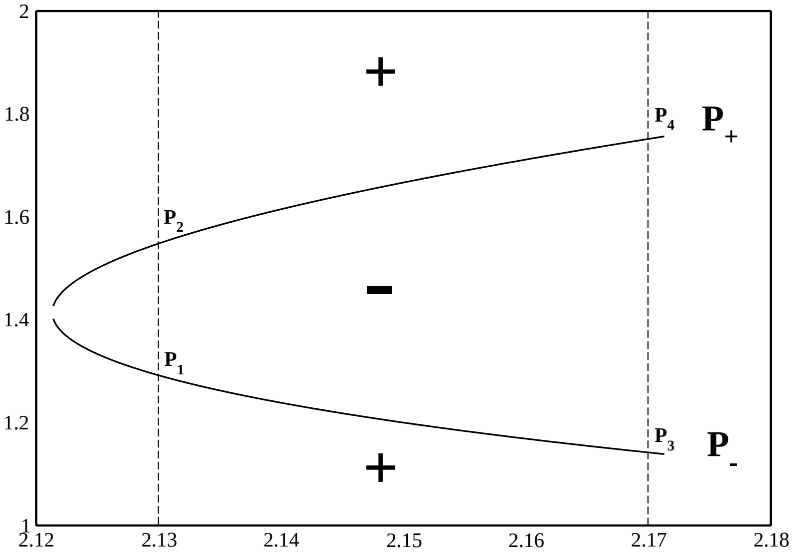

Figure 4.6: $U(1)_A$ **model:** The $P_+$ and $P_-$ solution of eq.(4.5), for which the potential becomes zero. Between these lines the potential gets negative values (see also fig.4.2). The plot is $P$ vs. $\beta$ for $\beta > \beta_{crit.} = \frac{3}{\sqrt{2}}$.

In that case, all terms except for the potential term, can be either positive or zero. The potential term (as we saw in fig.4.6) can become negative for a range of values of $P$. But, as $\beta$ decreases, this range becomes narrower (as we see in fig.4.6 as well as in figs.4.3-4.4 where this range is represented by the space between the two horizontal lines) and $(\partial_\rho P)^2$ increases. This happens because the energy functional tends to decrease its value through the negative values of the potential term. We believe that this can *not* continue for $\beta$ very close to $\beta_{crit}$ due to the fact that the range we described above, becomes so small, that $P$ tends to get everywhere a constant value (the value $P_0$, which makes the potential negative). But $P$ must be zero at $\rho = 0$ and $\rho \to \infty$, thus there will be a considerable increase in the $(\partial_\rho P)^2$ term of the functional, and that makes the benefits of the negative value of the potential to go away, while the trivial solution $P = 0$ becomes energetically favorable.

- $\beta \leq \beta_{crit}$: In that case, the potential term can no longer become negative. It can be either positive or zero and because of the fact that the energy functional is a sum of five positive terms, it's reasonable to prefer the zero value which, at the same time, minimizes all the terms

.

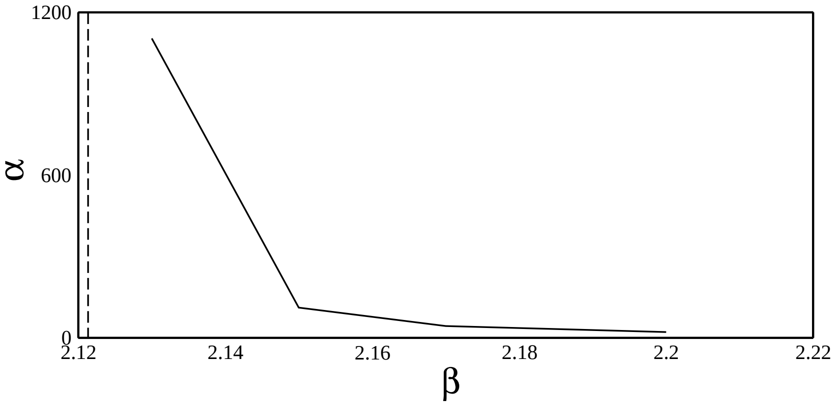

Figure 4.7: $U(1)_A$ **model:** The plot exhibits the relation of the parameter $a$ with respect to $\beta$. We observe that as we approach the limit $\beta_{crit}$, we need an increasingly deeper minimum of the potential which is expressed through the fastly increasing value of $a$. The dashed vertical line signals the position of $\beta_{crit} = \frac{3}{\sqrt{2}}$.

of the functional.

From all the above, one can observe that the crucial difference between the above two cases of $\beta$, is that in the $\beta > \beta_{crit}$ case, the energy can have a minimum value (through the potential term) which corresponds to a non-trivial solution for $P$. The existence of negative values of the potential are the "way-through" that make this possible.

## 4.5 Conclusions

We studied a $U(1)_A$ model with a GL potential with a cubic term added to it. After the numerical analysis we did, we came to the conclusion that for $\beta \leq \beta_{crit}$ we find no non-trivial solution. For $2.13 \leq \beta \leq 2.20$ we get non-trivial solutions which have the profiles we present in figs.4.3-4.4. Over $\beta = 2.20$ we have no non-trivial solutions. We analyze and explain our results in these cases.

The form of the potential we have in this search, can be found in condensed matter physics as well. On the other hand, one could try to make a loop out of the straight string studied above. We did this, but it was difficult to study mainly due to the fact that there are two instability modes, one having to do with the defect itself and another which has to do with the loop that tends to shrink due to its tension. The former instability is excluded in [90] for topological reasons. More details about the latter, can be found in the next chapter.

# Chapter 5

# On axially symmetric solitons in Abelian-Higgs models

## 5.1 Introduction

In a series of papers [13, 15] classically stable, metastable quasi-topological domain walls and strings in simple topologically trivial models, as well as in the two-Higgs Standard Model (2HSM) were studied. They are local minima of the energy functional and can quantum mechanically tunnel to the vacuum, not being protected by an absolutely conserved quantum number. In [15] a search for spherically symmetric particle-like solitons in the 2HSM with a simplified Higgs potential was performed without success. Although the existence of spherically symmetric particle-like solitons in the 2HSM has not been ruled out, we shall here look, instead, for axially symmetric solutions in a similar system.

Consider a model with superconducting strings [15, 103]. Take a piece of such string, close it to form a donut-shaped loop and let current in it. A magnetic field due to the supercurrent will be passing through the hole of the donut (fig.5.2). The energy of the loop has, a term proportional to the length of the string and will tend to shrink the radius of the donut to zero and the ring to extinction. However, another force opposes this tendency. Namely, as the loop shrinks, the magnetic field lines are squeezed in the hole, since, due to the Meissner effect, they cannot leave the loop. They are trapped inside the hole of the donut, oppose further shrinking and might even stabilize the string. A brief plan of what we are searching, can be seen in fig.5.1.

This, as well as other arguments [41]-[50] are inspiring but not conclusive. The magnetic field will not be trapped inside the loop if the penetration depth of the superconductor is larger than the thickness of the ring. Also, once the magnetic field gets strong it can destroy superconductivity and penetrate [105]. Further, there is a maximum current a superconductor can support (current quenching). This sets a limit on the magnetic field one can have through the loop, and this may not be enough to stabilize it. Thus, the above approach may work at best in a certain region of the parameter space, depending also on the defect characteristics [15]. The purpose of this work is to apply the above straightforward idea to search for string loops in a $U(1) \times U(1)$ gauge model and to determine the parameter space, if any, for their existence and stability.

Another interesting subject is to have a rotating ring. The rotation is another extra factor which could help the ring to stabilize. This work was done with success both analytically and numerically in [40] where vortons are exhibited. Another recent example of rotating superconducting electroweak strings can be found in [92], while for a review on electroweak strings, the reader should also check [93]. Finally, a work on static classical vortex rings

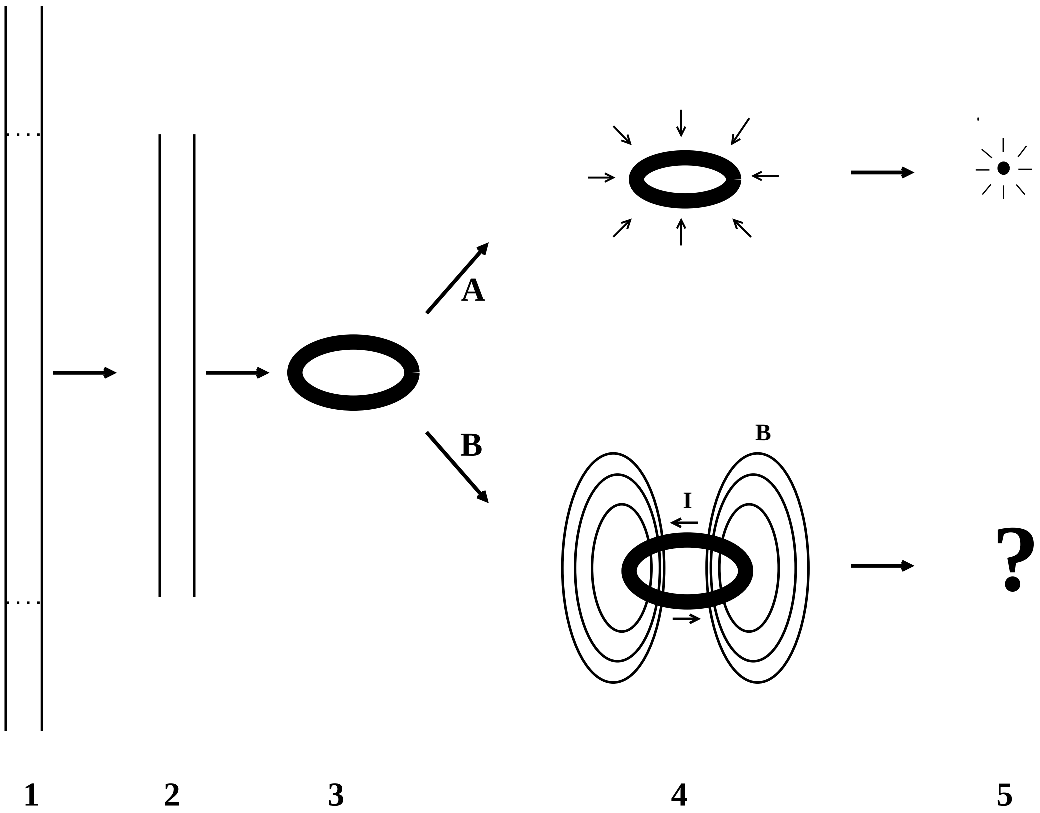

Figure 5.1: $U(1)_A \times U(1)_W$ **model:** Step 1: Infinite straight string. Step 2: Cut a piece of it. Step 3: Periodically connect its ends together to form a loop. Step 4A: Rings without current shrink due to their tension... Step 5A: ...and finally collapse. Step 4B: Superconducting vortex rings can be stabilized?... Step 5B: ... or not?

in $SU(2)$ non-Abelian Yang-Mills-Higgs model can be found in [94].

## 5.2 The $U(1)_A \times U(1)_W$ model

The **Lagrangian density** of our model is:

$$\mathcal{L} = -\frac{1}{4}F_{\mu\nu}^2 - \frac{1}{4}W_{\mu\nu}^2 + |D_\mu\psi|^2 + |\tilde{D}_\mu\phi|^2 - U(|\phi|, |\psi|) \tag{5.1}$$

where the covariant derivatives are $D_\mu\psi \equiv \partial_\mu\psi + ieA_\mu\psi$, $\tilde{D}_\mu\phi \equiv \partial_\mu\phi + iqW_\mu\phi$, the strength of the fields are $F_{\mu\nu} = \partial_\mu A_\nu - \partial_\nu A_\mu$, $W_{\mu\nu} = \partial_\mu W_\nu - \partial_\nu W_\mu$, while

$e$ and $q$ stand as the relevant $U(1)$ charges. The above Lagrangian (5.1), is invariant under the following $U(1)$ gauge transformations

$$\begin{aligned} \phi &\to e^{ip(\mathbf{x})}\phi \quad , \qquad W_\mu \to W_\mu - \frac{1}{q}\partial_\mu p(\mathbf{x}) \\ \psi &\to e^{ib(\mathbf{x})}\psi \quad , \qquad A_\mu \to A_\mu - \frac{1}{e}\partial_\mu b(\mathbf{x}) \end{aligned}$$

where $b(\mathbf{x})$, $p(\mathbf{x})$ are position dependent phases. We choose the potential $U$

$$U(|\phi|,|\psi|) = \frac{g_1}{4}\left(|\phi|^2 - v_1^2\right)^2 + \frac{g_2}{4}\left(|\psi|^2 - v_2^2\right)^2 + \frac{g_3}{2}|\phi|^2|\psi|^2 - \frac{g_2}{4}v_2^4 \qquad (5.2)$$

The vacuum $|\phi| = v_1 \neq 0$, $|\psi| = 0$, breaks $U(1)_W \times U(1)_A \to U(1)_A$, giving non-zero mass to $W$. The photon field stays massless. There, $U(v_1, 0) = 0$. The vacuum manifold $\mathcal{M}$ in this theory is a circle $S^1$ and the first homotopy group of $\mathcal{M}$ is $\pi_1(\mathcal{M}) = \pi_1(S^1) = \mathbf{Z} \neq \mathbf{1}$ which signals the existence of strings. In regions where $|\phi| = 0$, the field $|\psi|$ is arranged to be non-vanishing and $U(1)_W \times U(1)_A \to U(1)_W$. Thus, $U(1)_A \to \mathbf{1}$ and one may generate an electric current flowing along regions with vanishing $|\phi|$. Hence, this theory has superconducting strings [103].

In fact, with $|\phi| = F$ and $|\psi| = P$, the extrema of the potential are four:

- $F = 0 = P$ with $U(0,0) = \frac{1}{4}g_1 v_1^4$.
- $F = 0$, $P = v_2$ with $U(0, v_2) = \frac{1}{4}g_1 v_1^4 - \frac{1}{4}g_2 v_2^4$.
- $F = v_1, P = 0$ with $U(v_1, 0) = 0$.
- $F = a_1, P = a_2$ with $U(a_1, a_2) = a_3 - \frac{1}{4}g_2 v_2^4$

with

$$a_1 = \left(\frac{g_2(g_1 v_1^2 - g_3 v_2^2)}{g_1 g_2 - g_3^2}\right)^{1/2}, \quad a_2 = \left(\frac{g_1(g_2 v_2^2 - g_3 v_1^2)}{g_1 g_2 - g_3^2}\right)^{1/2},$$

$$a_3 = \frac{g_3(g_1 g_3(g_3 - g_1 g_2)v_1^4 + g_2 g_3(g_3 - g_1 g_2)v_2^4 - 2g_1 g_2(g_3^2 - g_1 g_2)v_1^2 v_2^2)}{4(g_1 g_2 - g_3^2)^2}$$

The vacuum that is of interest to us is: $|\phi| = v_1, \;\; |\psi| = 0$ and leaves unbroken the electromagnetic $U(1)_A$.

We can choose $\phi = (f_1(\mathbf{x}) + v_1)e^{i\theta_1(\mathbf{x})}$ and $\psi = f_2(\mathbf{x})e^{i\theta_2(\mathbf{x})}$ with $< 0|f_1(\mathbf{x})|0 >= 0 =< 0|f_2(\mathbf{x})|0 >$. Plugging these in the Lagrangian, we have the masses of the fields:

$$m_A = 0, \;\; m_W = qv_1, \;\; m_\phi^2 = g_1 v_1^2, \;\; m_\psi^2 = \frac{1}{2}\big(g_3 v_1^2 - g_2 v_2^2\big) \tag{5.3}$$

When $|\phi| = v_1$, the potential becomes:

$$U(v_1, |\psi|) = |\psi|^2 \left( \frac{g_2}{4}|\psi|^2 + k^2 \right) \tag{5.4}$$

where $k^2 = \frac{1}{2}(g_3 v_1^2 - g_2 v_2^2)$. Searching for the minimum we find:

$$\frac{dU}{d|\psi|} = 0 \to |\psi| \left( 2k^2 + g_2|\psi|^2 \right) = 0 \tag{5.5}$$

When $k^2 > 0$, we have only one minimum at $|\psi| = 0$. Otherwise ($k^2 < 0$) we have a minimum at $|\psi|^2 = -\frac{2k^2}{g_2}$ which means that the photon acquires mass. Thus, we choose the condition $k^2 > 0$ which reads as the right equation that follows:

$$g_1 > g_2 \frac{v_2^4}{v_1^4}, \quad g_3 > g_2 \frac{v_2^2}{v_1^2} \tag{5.6}$$

The left equation is another condition which comes from the fact that when $|\phi| = 0$ and $|\psi| = v_2$ the potential has value

$$U(0, v_2) = \frac{g_1 v_1^4}{4} - \frac{g_2 v_2^4}{4} \tag{5.7}$$

and in order to ensure that this is greater from the value of the potential at the vacuum, which is 0, we arrive at the condition above. This makes the value of the vacuum of interest, lower than the other extremum values as well since

$$U(0,0) \; > \; U(0,v_2) \; > \; 0 = U(0,0) \tag{5.8}$$

## 5.3 The $U(1)_A \times U(1)_W$ model: Search for superconducting vortex rings

Configurations with torus-like shape, representing a piece of a $U(1)_W \to \mathbf{1}$ Nielsen-Olesen string [18], closed to form a loop, are of interest in this search.

Thus, we will require $\phi$ to vanish on a circle of radius $a$ (the torus radius) $\phi(\rho = a, z = 0) = 0$. At infinity ($\rho \to \infty, z \to \infty$), we have the vacuum of the theory. This translates to $|\phi| \to v_1$, $|\psi| \to 0$. The **ansatz** for the fields is:

$$\begin{aligned}
\phi(\rho, \varphi, z) &= F(\rho, z) e^{iM\Theta(\rho,z)} \\
\psi(\rho, \varphi, z) &= P(\rho, z) e^{iN\varphi} \\
\mathbf{A}(\rho, \varphi, z) &= \frac{A_\varphi(\rho, z)}{\rho}\, \hat{\varphi} \\
\mathbf{W}(\rho, \varphi, z) &= W_\rho(\rho, z)\, \hat{\rho} + W_z(\rho, z)\, \hat{z}
\end{aligned}$$

where $M$, $N$ are the winding numbers of the relevant fields, $\hat{\rho}$, $\hat{\varphi}$, $\hat{z}$ are the cylindrical unit vectors and we define

$$\Theta(\rho, z) = \arctan\left(\frac{z}{\rho - a}\right) \tag{5.9}$$

We use cylindrical coordinates $(t, \rho, \varphi, z)$, with space-time metric $g_{\mu\nu} = diag(1, -1, -\rho^2, -1)$. We work in the $A^0 = 0 = W^0$ gauge. Especially for the gauge fields, we suppose the above form based on the following reasonable thoughts: The **W**-field is the one related to the formation of the string thus, it exists in the constant-$\varphi$ plane. This means that in general its non-vanishing components will be $W_\rho$ and $W_z$. The **A**-field is the one produced by the supercurrent flowing inside the toroidal object. The current is in the $\hat{\varphi}$ direction thus, we in general expect the non-vanishing component to be $A_\varphi$. Finally, as it concerns the scalar fields $\phi, \psi$, they follow the geometry of the toroidal defect which has axial symmetry thus, we expect that their amplitude is independent of $\varphi$.

A more general choice for $\phi$ would be

$$\phi(\rho, \varphi, z) = F(\rho, z) e^{iM\Theta(\rho,z) + i\chi(\rho,z)} \tag{5.10}$$

where $\chi(\rho, z)$, an arbitrary function. But gauge invariance allows us to change $\phi \to \phi e^{ib(\mathbf{x})}$, where $b(\mathbf{x})$ an arbitrary space-dependent phase. We can choose $b(\mathbf{x}) = -\chi(\rho, z)$ thus, gauge fixing removes the arbitrary function $\chi$.

We proceed by extracting the energy-momentum tensor and by considering the above ansatz we will derive the energy functional. Couple the system to an external gravitational field $g_{\mu\nu}$ and define

$$T^{\mu\nu} = -\frac{2}{\sqrt{-g}} \frac{\delta S}{\delta g_{\mu\nu}} \tag{5.11}$$

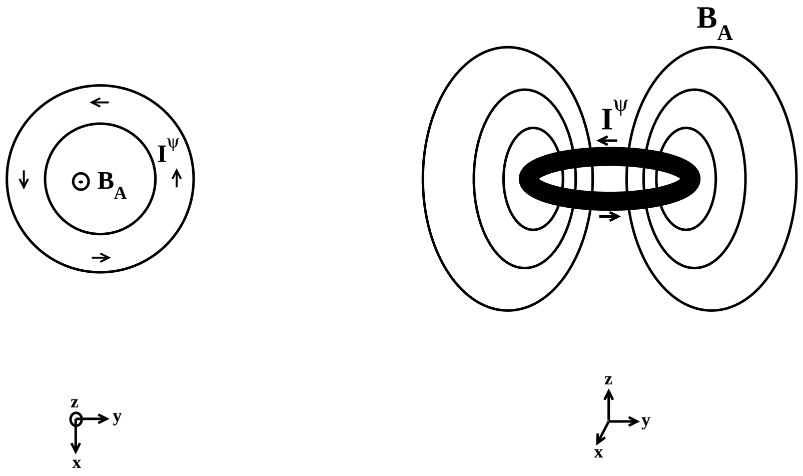

Figure 5.2: $U(1)_A \times U(1)_W$ **model:** A $x-y$ profile of the superconducting ring (left) as well as a $y-z$ profile (right) where one can view how the mechanism we propose, against shrinking, works.

The model coupled to the background gravitational field is

$$\mathcal{L} = \sqrt{-g}\Bigg( -\frac{1}{4}g^{\mu\lambda}g^{\nu\rho}F_{\mu\nu}F_{\lambda\rho} + g^{\mu\nu}(D_\mu\psi)^* D_\nu\psi - \frac{1}{4}g^{\mu\lambda}g^{\nu\rho}W_{\mu\nu}W_{\lambda\rho} + g^{\mu\nu}(\tilde{D}_\mu\phi)^*\tilde{D}_\nu\phi - U\Bigg)$$

and by using

$$\delta g^{\mu\nu} = -g^{\mu a}g^{\beta\nu}\delta g_{a\beta}, \quad \delta\sqrt{-g} = \frac{1}{2}\sqrt{-g}g^{a\beta}\delta g_{a\beta}$$

we get

$$T^{a\beta} = -F^a_\mu F^\beta_\nu g^{\mu\nu} + 2(D^a\psi)^* D^\beta\psi - W^a_\mu W^\beta_\nu g^{\mu\nu} + 2(\tilde{D}^a\phi)^*\tilde{D}^\beta\phi - \frac{g^{a\beta}\mathcal{L}}{\sqrt{-g}} \tag{5.12}$$

We are interested in the energy of the system which is the integral of the 00 component of the energy-momentum tensor

$$E = \int d^n x \sqrt{g}\, T^{00} \tag{5.13}$$

where $\sqrt{g}$ is the determinant of the spatial part of the metric. The energy density for the static ansatz above is

$$T^{00} = \frac{1}{4}g^{ik}g^{jl}F_{ij}F_{kl} - g^{ij}(D_i\psi)^* D_j\psi + \frac{1}{4}g^{ik}g^{jl}W_{ij}W_{kl} - g^{ij}(\tilde{D}_i\phi)^*\tilde{D}_j\phi + U \tag{5.14}$$

The terms of the energy density are

$$\begin{aligned}
\frac{1}{4}g^{ik}g^{jl}F_{ij}F_{kl} &= \frac{1}{2}\left(\frac{(\partial_\rho A_\varphi)^2}{\rho^2} + \frac{(\partial_z A_\varphi)^2}{\rho^2}\right)\\
\frac{1}{4}g^{ik}g^{jl}W_{ij}W_{kl} &= \frac{1}{2}(\partial_\rho W_z - \partial_z W_\rho)^2\\
-g^{ij}(D_i\psi)^* D_j\psi &= (\partial_\rho P)^2 + (\partial_z P)^2 + \frac{P^2}{\rho^2}(eA_\varphi + N)^2\\
-g^{ij}(\tilde{D}_i\phi)^*\tilde{D}_j\phi &= (\partial_\rho F)^2 + (\partial_z F)^2 + ((qW_\rho + M\partial_\rho\Theta)^2 + (qW_z + M\partial_z\Theta)^2)F^2
\end{aligned}$$

Thus, with the above ansatz, the **energy functional** takes the form:

$$\begin{aligned}
E &= 2\pi v_1 \int_0^\infty \rho d\rho \int_{-\infty}^\infty dz \Bigg[\frac{1}{2\rho^2}\Big((\partial_\rho A_\varphi)^2 + (\partial_z A_\varphi)^2\Big) + \\
&+ (\partial_\rho P)^2 + (\partial_z P)^2 + \frac{P^2}{\rho^2}(eA_\varphi + N)^2 + \\
&+ (\partial_\rho F)^2 + (\partial_z F)^2 + \frac{1}{2}(\partial_\rho W_z - \partial_z W_\rho)^2 + \\
&+ \Big((qW_\rho + M\partial_\rho\Theta)^2 + (qW_z + M\partial_z\Theta)^2\Big)F^2 + U(F,P)\Bigg]
\end{aligned} \tag{5.15}$$

and the potential $U$ (fig.5.3) can be written as follows:

$$U(F,P) = \frac{g_1}{4}\big(F^2 - 1\big)^2 + \frac{g_2}{4}\big(P^2 - u^2\big)^2 + \frac{g_3}{2}F^2P^2 - \frac{g_2}{4}u^4 \tag{5.16}$$

where $u \equiv v_2/v_1$. This is the energy functional we use in our numerical work. The **conditions** (5.6) to be satisfied by the parameters become:

$$g_1 > g_2 u^4 \quad , \quad g_3 > g_2 u^2 \tag{5.17}$$

The gauge fields $\mathbf{A}$, $\mathbf{W}$ have magnetic fields of the following form:

$$\nabla \times \mathbf{A} = \mathbf{B_A} = \frac{1}{\rho}\left(\frac{\partial A_\varphi}{\partial \rho}\,\hat{z} - \frac{\partial A_\varphi}{\partial z}\,\hat{\rho}\right)$$

$$\nabla \times \mathbf{W} = \mathbf{B_W} = -\left(\frac{\partial W_z}{\partial \rho} - \frac{\partial W_\rho}{\partial z}\right)\hat{\varphi}$$

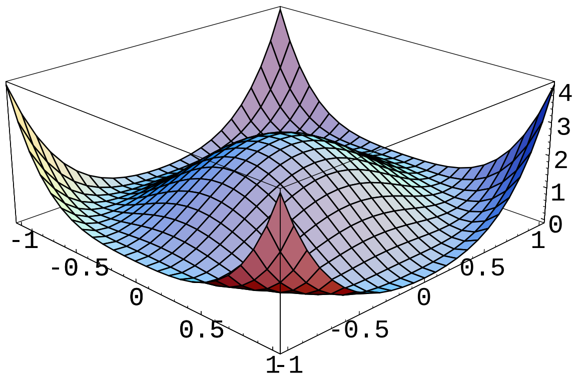

Figure 5.3: $U(1)_A \times U(1)_W$ **model:** A wider view of the "Mexican hat" potential (eq.5.16) for $(g_1, g_2, u) = (10, 8, 1)$.

The **field equations** follow:

$$\partial_\rho^2 F + \partial_z^2 F + \frac{\partial_\rho F}{\rho} - \frac{g_1}{2}\Big(F^2 - 1\Big)F - \frac{g_3}{2}P^2 F -$$

$$\left[\left(qW_\rho - M\frac{zcos^2\Theta}{(\rho-a)^2}\right)^2 + \left(qW_z + M\frac{cos^2\Theta}{(\rho-a)}\right)^2\right]F = 0$$

$$\partial_\rho^2 P + \partial_z^2 P + \frac{\partial_\rho P}{\rho} - \Big(eA_\varphi + N\Big)^2\frac{P}{\rho^2} - \frac{g_2}{2}\Big(P^2 - u^2\Big)P - \frac{g_3}{2}F^2 P = 0$$

$$\partial_\rho^2 A_\varphi + \partial_z^2 A_\varphi - \frac{\partial_\rho A_\varphi}{\rho} - 2eP^2\Big(eA_\varphi + N\Big) = 0$$

$$\partial_z^2 W_\rho - \partial_z\partial_\rho W_z - 2qF^2\left(qW_\rho - M\frac{zcos^2\Theta}{(\rho-a)^2}\right) = 0$$

$$\partial_\rho^2 W_z + \frac{1}{\rho}\Big(\partial_\rho W_z - \partial_z W_\rho\Big) - \partial_\rho\partial_z W_\rho - 2qF^2\left(qW_z + M\frac{cos^2\Theta}{(\rho-a)}\right) = 0$$

We can also write down the currents associated with $\phi$ field, namely $j_\rho^\phi$ and $j_z^\phi$ and the total current $\mathcal{I}^\phi$ out of these as well as the supercurrent $\mathcal{I}^\psi$ associated with the $\psi$ field. These are

$$\mathcal{I}^\phi = \sqrt{(j_\rho^\phi)^2 + (j_z^\phi)^2}\ , \quad \mathcal{I}^\psi = -\frac{2eP^2}{\rho}(eA_\varphi + N) \tag{5.18}$$

where

$$j_\rho^\phi = -2qF^2(qW_\rho + M\partial_\rho\Theta), \quad j_z^\phi = -2qF^2(qW_z + M\partial_z\Theta) \tag{5.19}$$

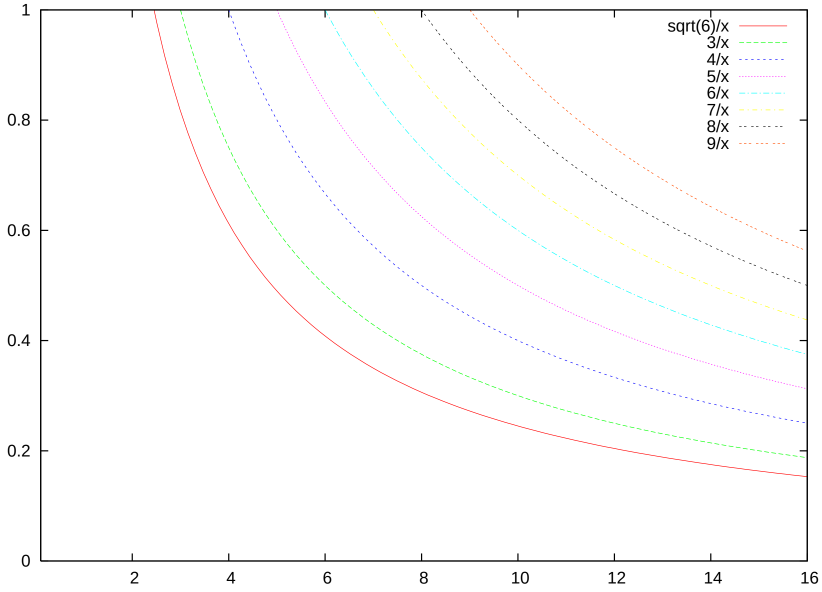

Figure 5.4: $U(1)_A \times U(1)_W$ **model:** For different values of $\sqrt{g_1}$, we plot the lower bound over which the condition (5.20) is satisfied. The plot is $P_{max}$ vs. $e$ and we plot the function $P_{max} = \frac{\sqrt{g_1}}{e}$.

As explained in the Introduction, Meissner effect is of crucial importance for the stability of the torus-like object. The magnetic fields produced by the supercurrent $\mathcal{I}^{\psi}$ penetrate into the toroidal defect in a distance dictated by the penetration depth. In this theory, the $U(1)_{\mathbf{A}}$ symmetry breaks inside the string and the photon acquires mass $m_{\mathbf{A}}^2 = e^2 < P >^2$ where $< P >$ is the expectation value of the charge condensate in the vicinity of the string core. There is the superconducting sector of the defect. The penetration depth is $\lambda = \frac{1}{m_{\mathbf{A}}} = \frac{1}{e<P>}$. But $< P >= P_{max} \leq u$ thus, one can have an estimate for $\lambda$, with a lower bound for its value. This is $\lambda \geq \frac{1}{eu}$ where the equality holds when $P_{max} = u$. On the other hand, one can also compute an upper bound for the thickness of the defect. We know that $r_\phi = \frac{1}{m_\phi} = \frac{1}{\sqrt{g_1}}$. If our concern is to search for stable rings, a reasonable step is to demand the penetration depth to be smaller than the string thickness which means

$$\lambda < r_\phi \Rightarrow \frac{1}{eP_{max}} < \frac{1}{\sqrt{g_1}} \Rightarrow e^2 P_{max}^2 > g_1 \tag{5.20}$$

This is the condition needed in this case. From the above condition, we get the diagram shown in fig.5.4 where one can see the area where it's more possible to find stable solutions if they exist. The numerical results we present later, are what we found while searching inside this region.

Below, we analyze a way to derive some virial relations in order to check our results. The energy density for a *static solution*, which is of interest here, reads:

$$T^{00} = \frac{1}{4}F_{ij}F_{ij} + |\tilde{D}_i\phi|^2 + \frac{1}{4}W_{ij}W_{ij} + |D_i\psi|^2 + U(|\phi|, |\psi|) \equiv \varepsilon \tag{5.21}$$

where $F_{ij} = \partial_i A_j - \partial_j A_i$ and $W_{ij} = \partial_i W_j - \partial_j W_i$. For the solution of the system, we can write:

$$\frac{\delta E}{\delta \phi} = \frac{\delta E}{\delta \phi^*} = \frac{\delta E}{\delta W_i} = \frac{\delta E}{\delta \psi} = \frac{\delta E}{\delta \psi^*} = \frac{\delta E}{\delta A_i} = 0 \tag{5.22}$$

Define

$$f_i \equiv \frac{\delta E}{\delta \phi}\partial_i\phi + \frac{\delta E}{\delta \phi^*}\partial_i\phi^* + \frac{\delta E}{\delta W_l}\partial_i W_l + \frac{\delta E}{\delta \psi}\partial_i\psi + \frac{\delta E}{\delta \psi^*}\partial_i\psi^* + \frac{\delta E}{\delta A_j}\partial_i A_j = 0 \tag{5.23}$$

which together with

$$\frac{\delta E}{\delta \Phi} = \frac{\partial T^{00}}{\partial \Phi} - \partial_k \frac{\partial T^{00}}{\partial(\partial_k \Phi)} \tag{5.24}$$

can be written in a shorter form $f_i = \partial_j G_{ij}$ where

$$\begin{aligned} G_{ij} &= \varepsilon\delta_{ij} - \frac{\partial\varepsilon}{\partial(\partial_j\phi)}\partial_i\phi - \frac{\partial\varepsilon}{\partial(\partial_j\phi^*)}\partial_i\phi^* - \frac{\partial\varepsilon}{\partial(\partial_j A_k)}\partial_i A_k \\ &- \frac{\partial\varepsilon}{\partial(\partial_j\psi)}\partial_i\psi - \frac{\partial\varepsilon}{\partial(\partial_j\psi^*)}\partial_i\psi^* - \frac{\partial\varepsilon}{\partial(\partial_j W_l)}\partial_i W_l \end{aligned}$$

This means that any static solution of the field equations satisfies

$$\partial_j G_{ij} = 0 \tag{5.25}$$

But, we have

$$\begin{aligned} \frac{\partial\varepsilon}{\partial(\partial_j\phi)} &= (\tilde{D}_j\phi)^* \\ \frac{\partial\varepsilon}{\partial(\partial_j\phi^*)} &= \tilde{D}_j\phi \\ \frac{\partial\varepsilon}{\partial(\partial_j A_k)} &= \partial_j A_k - \partial_k A_j = F_{jk} = \epsilon_{ijk}B_{A_i} \\ \frac{\partial\varepsilon}{\partial(\partial_j\psi)} &= (D_j\psi)^* \\ \frac{\partial\varepsilon}{\partial(\partial_j\psi^*)} &= D_j\psi \\ \frac{\partial\varepsilon}{\partial(\partial_j W_l)} &= \partial_j W_l - \partial_l W_j = W_{jl} = \epsilon_{ijl}B_{W_i} \end{aligned}$$

which leads to

$$\begin{aligned}
G_{ij} &= \varepsilon\delta_{ij} - (\tilde{D}_j\phi)^*\partial_i\phi - \tilde{D}_j\phi\partial_i\phi^* - W_{jl}\partial_i W_l - \\
&- (D_j\psi)^*\partial_i\psi - D_j\psi\partial_i\psi^* - F_{jk}\partial_i A_k = \\
&= \varepsilon\delta_{ij} - (\tilde{D}_j\phi)^*\tilde{D}_i\phi - \tilde{D}_j\phi(\tilde{D}_i\phi)^* + iqW_i\phi(\tilde{D}_j\phi)^* - \\
&- iqW_i\phi^*\tilde{D}_j\phi - W_{jl}W_{il} - W_{jl}\partial_l W_i - \\
&- (D_j\psi)^*D_i\psi - D_j\psi(D_i\psi)^* + ieA_i\psi(D_j\psi)^* - \\
&- ieA_i\psi^*D_j\psi - F_{jk}F_{ik} - F_{jk}\partial_k A_i = \\
&= \varepsilon\delta_{ij} - (\tilde{D}_i\phi)^*\tilde{D}_j\phi - (\tilde{D}_j\phi)^*\tilde{D}_i\phi - W_{il}W_{jl} - \partial_l(W_{jl}W_i) \\
&+ W_i\Big(\partial_l W_{jl} - iq(\phi^*\tilde{D}_j\phi - (\tilde{D}_j\phi)^*\phi)\Big) - \\
&- (D_i\psi)^*D_j\psi - (D_j\psi)^*D_i\psi - F_{jk}F_{ik} - \partial_k(F_{jk}A_i) + \\
&+ A_i\Big(\partial_k F_{jk} - ie(\psi^*D_j\psi - (D_j\psi)^*\psi)\Big)
\end{aligned}$$

where in the second equality we just add and subtract the necessary terms in order to have the terms only with covariant derivatives. The latter happens because all the other terms are gone as we see below:

$$\begin{aligned}
\partial_j\partial_k(\partial_j A_k - \partial_k A_j)A_i = 0 \;\;&\Rightarrow\;\; (\partial_j^2\partial_k A_k - \partial_k^2\partial_j A_j)A_i = 0 \\
\partial_j\partial_l(\partial_j W_l - \partial_l W_j)W_i = 0 \;\;&\Rightarrow\;\; (\partial_j^2\partial_l W_l - \partial_l^2\partial_j W_j)W_i = 0
\end{aligned}$$

and from the field equations, the following terms are also zero

$$\begin{aligned}
\frac{\delta E}{\delta W_j} = 0 = \frac{\delta T^{00}}{\partial(\partial_l W_j)} &= -iq(\phi^*\tilde{D}_j\phi - \phi(\tilde{D}_j\phi)^*) + \partial_l W_{jl} = 0 \\
\frac{\delta E}{\delta A_j} = 0 = \frac{\delta T^{00}}{\partial(\partial_k A_j)} &= -ie(\psi^*D_j\psi - \psi(D_j\phi)^*) + \partial_k F_{jk} = 0
\end{aligned}$$

thus

$$G_{ij} = \varepsilon\delta_{ij} - W_{il}W_{jl} - (\tilde{D}_i\phi)^*\tilde{D}_j\phi - (\tilde{D}_j\phi)^*\tilde{D}_i\phi - F_{jk}F_{ik} - (D_i\psi)^*D_j\psi - (D_j\psi)^*D_i\psi \tag{5.26}$$

but

$$\begin{aligned}
F_{ik}F_{jk} &= \epsilon_{nik}B_{A_n}\epsilon_{mjk}B_{A_m} = \mathbf{B}_A^2\delta_{ij} - B_{A_i}B_{A_j} \\
W_{il}W_{jl} &= \epsilon_{pil}B_{W_p}\epsilon_{qjl}B_{W_q} = \mathbf{B}_W^2\delta_{ij} - B_{W_i}B_{W_j}
\end{aligned}$$

which means that

$$\begin{aligned} G_{ij} \;\; &= \;\; \Bigg( -\frac{\mathbf{B}_A^2}{2} - \frac{\mathbf{B}_W^2}{2} + |\tilde{D}\phi|^2 + |D\psi|^2 + U \Bigg)\delta_{ij} + B_{W_i}B_{W_j} + B_{A_i}B_{A_j} - \\ &- \;\; (D_i\psi)^* D_j\psi - (D_j\psi)^* D_i\psi - (\tilde{D}_i\phi)^*\tilde{D}_j\phi - (\tilde{D}_j\phi)^*\tilde{D}_i\phi \end{aligned}$$

From (5.25) one obtains

$$\int d^3x G_{ik} = 0 = \int d^3x \partial_j (x_k G_{ij}) = \int dS_j x_k G_{ij} \tag{5.27}$$

The last equality follows from Gauss theorem, while the first is due to the fact that

$$\partial_j (x_k G_{ij}) = \frac{\partial x_k}{\partial x_j} G_{ij} + x_k (\partial_j G_{ij}) = \delta_{kj} G_{ij} = G_{ik} \tag{5.28}$$

where we also used (5.25). Take the trace of (5.27). We have

$$\int d^3x Tr G_{ik} = 2\pi \int \rho d\rho dz \Bigg( -\frac{\mathbf{B}_A^2}{2} - \frac{\mathbf{B}_W^2}{2} + |\tilde{D}\phi|^2 + |D\psi|^2 + 3U \Bigg) \tag{5.29}$$

while the left hand side of (5.27) in the $\hat{\varphi}$ direction of integration of the toroidal object gives

$$2\pi \int dS_\varphi G_{\varphi\varphi} = 0 \tag{5.30}$$

and (5.27) finally ends up to the following:

$$2\pi \int \rho d\rho dz \Bigg( \frac{1}{2}\Big( B_W^2 + B_A^2 \Big) - U \Bigg) = 0 \tag{5.31}$$

Another way to derive **virial** relations is through Derrick's scaling argument. The virial relation for the field $\phi$ of our model, must have the constraint $\phi_\kappa(\rho = a, z) = \phi(\rho = a, \kappa z) = 0$. Consider the rescalings $\rho \to \rho$, $z \to \kappa z$, $F_\kappa \to F$, $P_\kappa \to P$, $A_{\varphi_\kappa} \to A_\varphi$, $W_{\rho,z_\kappa} \to \kappa W_{\rho,z}$. Then, we find the minimum through the relation $\frac{\partial E}{\partial \kappa} = 0$ when $\kappa = 1$. The virial relation for our model, which is a way to check our numerical results is:

$$\begin{aligned}
I_1 &= 2\pi v_1 \int_0^\infty \rho d\rho \int_{-\infty}^\infty dz \Bigg[\frac{1}{2}(\partial_\rho W_z - \partial_z W_\rho)^2 + \frac{1}{2\rho^2}(\partial_z A_\varphi)^2 + (\partial_z P)^2 + \\
&+ (\partial_z F)^2 + 2F^2\Bigg(qW_\rho(qW_\rho + M\partial_\rho\Theta) + (qW_z + M\partial_z\Theta)^2\Bigg)\Bigg] \\
I_2 &= -2\pi v_1 \int_0^\infty \rho d\rho \int_{-\infty}^\infty dz \Bigg[\frac{1}{2\rho^2}(\partial_\rho A_\varphi)^2 + (\partial_\rho F)^2 + (\partial_\rho P)^2 + \\
&+ \frac{P^2}{\rho^2}(eA_\varphi + N)^2 + (\partial_z W_\rho)(\partial_\rho W_z - \partial_z W_\rho) + \\
&+ F^2\Bigg((qW_\rho + M\partial_\rho\Theta)^2 + (qW_z + M\partial_z\Theta)^2\Bigg) + \\
&+ \frac{g_1}{4}(F^2-1)^2 + \frac{g_2}{4}(P^2-u^2)^2 + \frac{g_3}{2}F^2P^2 - \frac{g_2}{4}u^4\Bigg]
\end{aligned}$$

and we must have $I_1 + I_2 = 0$. We define the index $V = \frac{||I_1|-|I_2||}{|I_1|+|I_2|}$ and we want its value to be as small as possible. We can derive many other virial relations by assuming generally for a field $\phi$, the "double" rescaling $\phi(\vec{x}) \rightarrow \kappa\phi(\mu\vec{x})$ and then demanding $\frac{\partial E}{\partial \kappa}|_{\kappa=1=\mu} = 0 = \frac{\partial E}{\partial \mu}|_{\kappa=1=\mu}$. For example, consider the following rescalings $\rho \rightarrow \rho$, $z \rightarrow \mu z$, $F_\kappa \rightarrow F$, $P_\kappa \rightarrow \kappa P$, $A_{\varphi_\kappa} \rightarrow A_\varphi$, $W_{\rho,z_\kappa} \rightarrow W_{\rho,z}$. We have

$$\begin{aligned}
I_3 &= 2\pi v_1 \int_0^\infty \rho d\rho \int_{-\infty}^\infty dz \Bigg[\frac{1}{2\rho^2}(\partial_z A_\varphi)^2 + (\partial_z P)^2 + (\partial_z F)^2 + \\
&+ 2F^2\Bigg(M\partial_z\Theta(qW_z + M\partial_z\Theta)\Bigg) + \frac{1}{2}(\partial_\rho W_z - \partial_z W_\rho)^2\Bigg] \\
I_4 &= -2\pi v_1 \int_0^\infty \rho d\rho \int_{-\infty}^\infty dz \Bigg[\frac{1}{2\rho^2}(\partial_\rho A_\varphi)^2 + (\partial_\rho P)^2 + (\partial_\rho F)^2 + \\
&+ \frac{P^2}{\rho^2}(eA_\varphi + N)^2 + \partial_\rho W_z(\partial_\rho W_z - \partial_z W_\rho) + \\
&+ F^2\Bigg((qW_\rho + M\partial_\rho\Theta)^2 + (qW_z + M\partial_z\Theta)^2\Bigg) + \\
&+ \frac{g_1}{4}(F^2-1)^2 + \frac{g_2}{4}(P^2-u^2)^2 + \frac{g_3}{2}F^2P^2 - \frac{g_2}{4}u^4\Bigg]
\end{aligned}$$

together with

$$\begin{aligned} I_5 &= 4\pi v_1 \int_0^\infty \rho d\rho \int_{-\infty}^{\infty} dz \left[ (\partial_\rho P)^2 + (\partial_z P)^2 + \frac{P^2}{\rho^2}(eA_\varphi + N)^2 \right] \\ I_6 &= 2\pi v_1 \int_0^\infty \rho d\rho \int_{-\infty}^{\infty} dz \left[ g_2 \Big( P^2 - u^2 \Big) P^2 + g_3 F^2 P^2 \right] \end{aligned}$$

where, as above, we must have $I_3 + I_4 = 0 = I_5 + I_6$.

## 5.4 The $U(1)_A \times U(1)_W$ model: Numerical results

A standard minimization algorithm is used to minimize the energy functional of (5.15). The algorithm is written in C. One can find details about the algorithm on page 425 of [104] but, briefly, the basic idea is this: Given an appropriate initial guess, there are several corrections to it, having as a criterion the minimization of the energy in every step. When the corrections on the value of the energy are smaller than $\sim 10^{-8}$ the program stops and we get the final results. A 90×20 grid for every of the five functions is used, that is, 90 points on $\rho$-axis and 20 on $z$. Here, we begin with fixed torus radius $a$. Then, the configuration with minimum energy for this $a$ is found. Other values of $a$ are chosen as well and the same process goes on until we plot the energy vs. the torus radius $E(a)$. It would be very interesting to find a non-trivial minimum of the energy (in $a_{min} \neq 0$), which would correspond to stable toroidal defects with radius $a_{min}$.

The **initial guess** (figure 5.5) we use for our computation is:

$$\begin{aligned} F(\rho, z) &= \tanh((\rho - a)^2 + z^2)^{M/2} \\ P(\rho, z) &= \tanh(\rho^N)(1 - \tanh((\rho - a)^2 + z^2) \\ A_\varphi(\rho, z) &= -\frac{N}{e} \tanh\left( \frac{\xi \rho^2}{((\rho - a)^2 + z^2)^2} \right) \\ W_\rho(\rho, z) &= \frac{Mz \cos^2 \Theta}{q(\rho - a)^2} \left( \frac{(\rho - a)^2 + z^2}{(\rho - a)^2 + z^2 + (a^2/4)} \right)^2 \\ W_z(\rho, z) &= -\frac{M \cos^2 \Theta}{q(\rho - a)} \left( \frac{(\rho - a)^2 + z^2}{(\rho - a)^2 + z^2 + (a^2/4)} \right) \end{aligned}$$

where $\xi$ a constant. Figures 5.6, 5.7 indicate what exactly we plot in fig.5.5 and where. This initial guess also satisfies the appropriate asymptotics

.

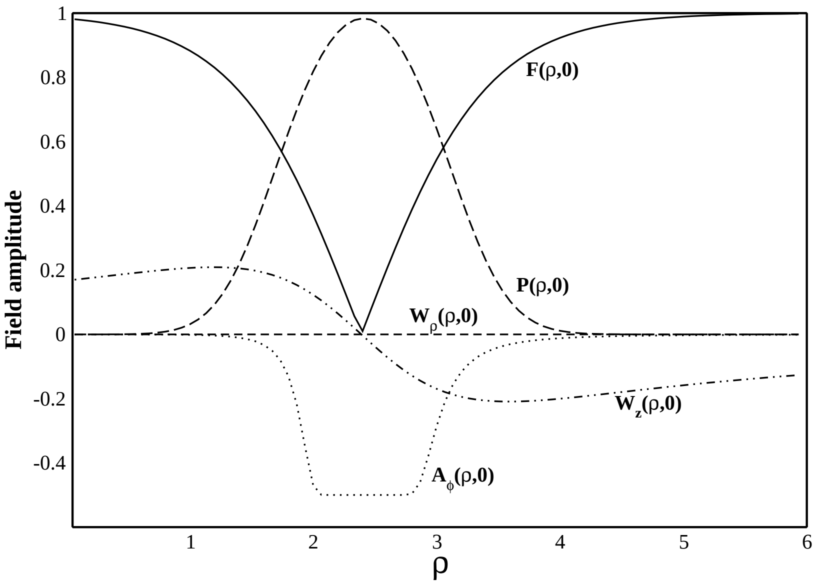

Figure 5.5: $U(1)_A \times U(1)_W$ **model:** A typical plot of the initial guess we use for the five fields, for the lowest winding state $M = 1, N = 1$ on $z = 0$ plane.

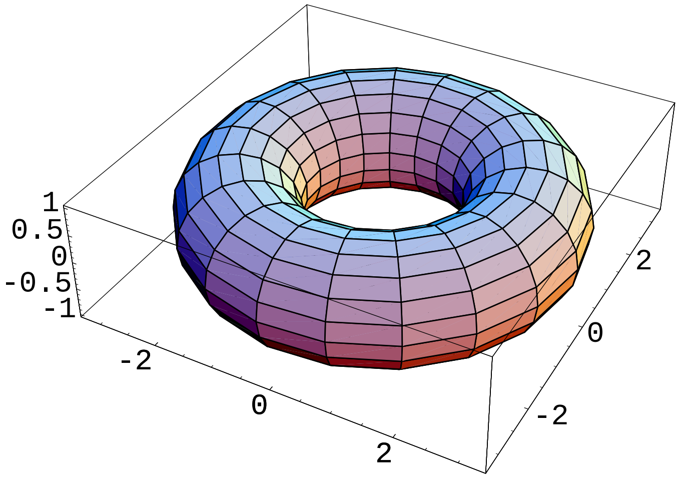

Figure 5.6: $U(1)_A \times U(1)_W$ **model:** This is a typical picture of the toroidal soliton we are after.

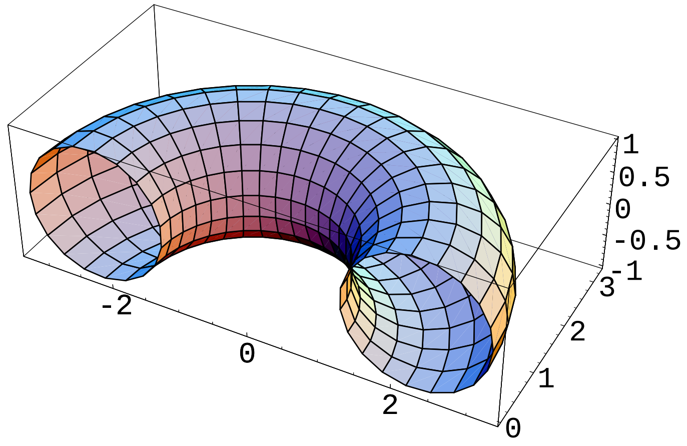

Figure 5.7: $U(1)_A \times U(1)_W$ **model:** The profile of the torus has two identical cycles. The initial configuration of fields (plotted in fig.5.5) is the same in both of them thus, we choose to plot only the right side.

- near $\rho = 0$:

$$F \neq 0, \;\; P \sim \rho^N, \;\; A_\varphi \sim \rho^2 f(z) \tag{5.32}$$

- near $(\rho = a, z = 0)$:

$$F \sim \tilde{\rho}^{M/2}, \;\; W_\rho = 0 = W_z \tag{5.33}$$

- at infinity:

$$\begin{aligned} F &\sim 1 - \mathcal{O}(e^{-\sqrt{\tilde{\rho}}}), \quad P \sim \mathcal{O}(e^{-\sqrt{\rho^2+z^2}}) \\ W_\rho &\sim -\frac{M}{q}\partial_\rho\Theta|_\infty + \mathcal{O}(e^{-\sqrt{\tilde{\rho}}}), \quad W_z \sim -\frac{M}{q}\partial_z\Theta|_\infty + \mathcal{O}(e^{-\sqrt{\tilde{\rho}}}) \end{aligned}$$

where $\tilde{\rho} \equiv (\rho - a)^2 + z^2$.

For fixed torus radius (i.e. here $a \approx 2.2$) we present a typical graph of the final configuration of the lowest energy (see fig.5.8). We also present the plot of the energy of the system vs. the radius of the toroidal object which reveals the instability of the system as there is no non-trivial minimum (see fig.5.11).

From the results, we can point out a few things. Firstly, the greater the value of $e$ we use, the stronger the supercurrent becomes. Secondly, the greater the value of $e$ we use, the lower the radius $a$ where the supercurrent quenches (fig.5.9). These are expected as the increase of $e$ makes the condition of equation (5.20) stronger, something which means that the mass of

.

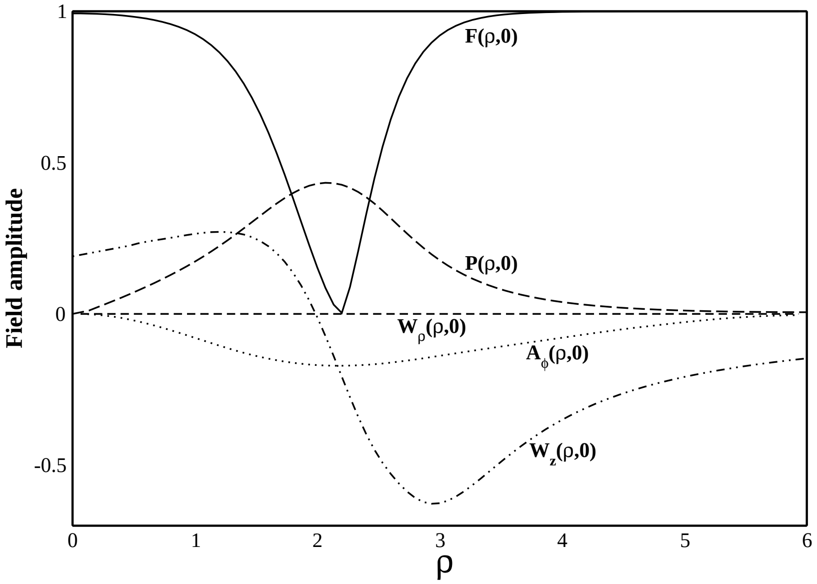

Figure 5.8: $U(1)_A \times U(1)_W$ **model:** Typical plot of the final configuration of fields. Parameters are $M = 1$, $N = 1$, $e = 5$, $q = m_W = 2$, $g_1 = 14$, $m_\phi = \sqrt{g_1} = 3.74$, $g_2 = 12$, $g_3 = 14$, $u = 1$, $m_\psi = \sqrt{(g_3 - g_2 u^2)/2} = 1$, $v_1 = 7.5 \cdot 10^{-3}$. Energy $E = 0.72$ and virial is $1.5 \cdot 10^{-3}$.

the photon increases and the penetration depth decreases at the same time. It is also reasonable that a stronger current can “defend” the defect, against the magnetic field, a little longer.

Another observation is that as $g_2$ increases and becomes close to $g_1$, we see that the maximum current increases and the quenching takes place again at lower $a$ (fig.5.10). This is expected as one can see from the potential in equation (5.16) of the energy functional, because the stronger the coupling $g_2$ is, the more important the relevant term $g_2(P^2 - u^2)^2/4$ becomes. The latter has as a consequence, the increase of $P_{max}$ which counteracts the effects from the increasing $g_2$ coupling.

The parameter space where we searched, starts from $g_1 = 4$ ($m_\phi = 2$). In order to search the model, we reached values around $g_1 = 30$ ($m_\phi \approx 5.48$) over which, $e$ has to be very large in order to respect the condition (5.20). There is also the fact that great values of $e$ in general is an unwanted feature since we use a semiclassical approach. As it concerns the other couplings we have $g_3 = g_1$ and $g_2 = g_1 - k$ with $0.5 \leq k \leq 8$, ($u = 1$).

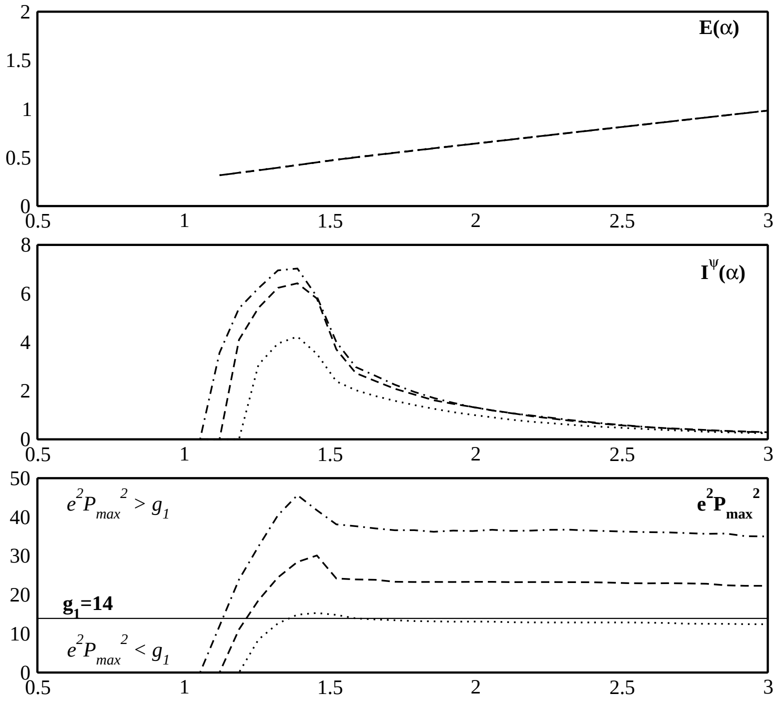

Figure 5.9: $U(1)_A \times U(1)_W$ **model:** The top graph is the energy vs. the torus radius $E(a)$. The middle graph is the supercurrent $I^{\psi}$ vs. $a$. In that graph one can clearly see current quenching. The bottom graph is the quantity $e^2 P_{max}^2$ vs. $a$ (or $m_{\mathbf{A}}$ vs. $a$) where one can see the area in which the condition of eq.5.20 holds (lines over the $g_1$-limit line). The resistance from the magnetic field can be seen as a sharp increase on the supercurrent. Dotted lines are for $e = 6$, dashed for $e = 8$ while dashed and dotted for $e = 10$. All plots are for $(M, N, u, g_1, g_2, g_3)$=(1, 1, 1, 14, 12.5, 14).

## 5.5 Explanation concerning the instability of the vortex ring

From the condition of equation (5.20), it is understood that we are enforced to lower $g_1$ as much as possible and/or increase $e$. But these steps are not as easy as they might seem. There are some limitations. The lower bound on the value of $g_1$ has a reasonable explanation. For low values of $g_1$, the coupling $g_2$ is also low (because $g_1 > g_2 u^4$). Now, when $g_2$ is small enough, the changes on the term $g_2(P^2 - u^2)^2/4$ are unimportant for the energy, in comparison to the term $(\partial_\rho P)^2$. In that case, the lowering of the last term minimizes the energy, something which means that $P \rightarrow 0$. Indeed, this is numerically observed. There is also a lower limit on $e$ which is reasonable because the lowering of $e$ results to an increasing penetration depth.

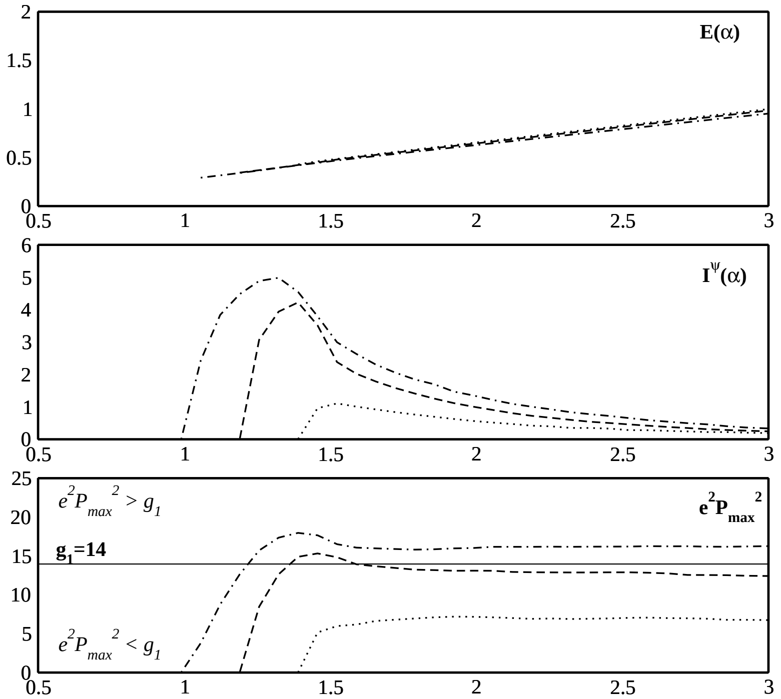

Figure 5.10: $U(1)_A \times U(1)_W$ **model:** The top graph is the energy vs. the torus radius $E(a)$. The middle graph is the supercurrent $I^{\psi}$ vs. $a$. In that graph one can clearly see current quenching. The bottom graph is the quantity $e^2P^2_{max}$ vs. $a$ (or $m_{\mathbf{A}}$ vs. $a$) where one can see the area in which the condition of eq.5.20 holds (lines over the $g_1$-limit line). The resistance from the magnetic field can be seen as a sharp increase on the supercurrent. Dotted lines are for $g_2 = 12$, dashed for $g_2 = 12.5$ while dashed and dotted for $g_2 = 13$. All plots are for $(M, N, u, e, g_1, g_3)$=$(1, 1, 1, 6, 14, 14)$.

We searched for stable objects for values over these limits described above. The numerical results are exhibited in figs.5.9-5.11 and as we see, these objects are unstable. We argue that the explanation for the instability is **current quenching** and that, only for high values of $e$. For lower values of $e$, that is, of the order of 1, we have, according to equation (5.20), that the penetration depth is much bigger than the string thickness thus, stability is out of the question. The latter is also numerically observed.

Now, we base our aspect about quenching on qualitative as well as quantitative arguments. We observe that as the torus shrinks, the supercurrent suddenly drops to zero which signals the destruction of the defect. Just before the sharp drop, we notice that the supercurrent rises with increasing rate. This must be due to the resistance the torus meets from the magnetic

.

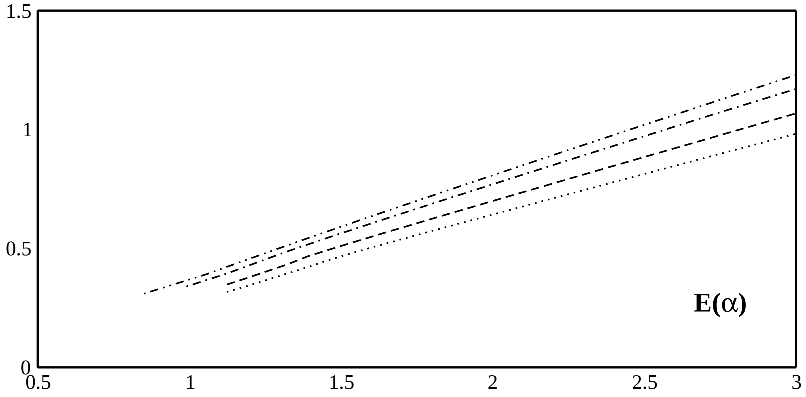

Figure 5.11: $U(1)_A \times U(1)_W$ **model:** The plot of the energy of the system vs. the radius of the torus for four different sets of parameters. Dotted is for $(g_1, g_2, g_3)$= $(14, 12.5, 14)$, dashed is for $(18, 15, 18)$, dashed and dotted is for $(25, 20, 25)$ while dashed with two dots is for $(30, 24, 30)$. For all data sets we have $(e, M, N, u)$=$(10, 1, 1, 1)$. As one can observe, there exists no minimum.

lines as it shrinks. One can observe that as the supercurrent increases and the condition of equation (5.20) is satisfied at the same time (i.e. see dashed and dotted line of fig.5.9), suddendly the current is lost. This can be explained only through current quenching. The above phenomenon is not observed when equation (5.20) is not satisfied (i.e. see dotted line of fig.5.10). There, as the magnetic lines penetrate the ring, they meet almost no resistance since $\lambda$ is much greater than $r_\phi$.

Another observation which supports our quenching argument is that, rough estimations on the maximum current a string can sustain, lead us to the following formula (see page 129 of [105] or Appendix I at the end of the chapter) which makes a small overestimation in order to have an upper limit:

$$\mathcal{I}^{\psi}_{max} < \sqrt{\sigma} e u \tag{5.34}$$

where $\sigma \equiv \int\int d\rho dz \ P^2$. In figs.5.9-5.10, the maximum value of the supercurrent is close to the limit of the estimation of equation (5.34). The table below gathers the estimated $\mathcal{I}^{\psi}_{est.}$ (according to equation (5.34)) and the computed maximum supercurrent ($\mathcal{I}^{\psi}_{com.}$) for the parameters of these figures.

| $e$ | $g_1$ | $g_2$ | $g_3$ | $\mathcal{I}^{\psi}_{est.}$ | $\mathcal{I}^{\psi}_{com.}$ |
|---|---|---|---|---|---|
| 6 | 14 | 12.5 | 14 | 4.6 | 4.3 |
| 6 | 14 | 13 | 14 | 5.2 | 5.0 |
| 8 | 14 | 12.5 | 14 | 6.7 | 6.4 |
| 10 | 14 | 12.5 | 14 | 8.0 | 7.2 |

.

Finally, one can make an estimation of the value of the supercurrent which would stabilize the ring, namely $\mathcal{I}^{\psi}_{stab.}$. This can be done as follows. As explained in the introduction, there is the tension of the string which shrinks the loop and the magnetic field which opposes this tendency. When the ring is stabilized we have $E_{tension} = E_{magnetic}$. Here, $E_{tension} \sim 1$ and $E_{magnetic} = 2\pi v_1 \int \rho d\rho \int dz(B_A^2/2)$. Without any calculation, one can point out that, since the *total* energy in the quenching radius is below $E_{tension} = 1$, then the $E_{magnetic}$ which is a fraction of it, would be even smaller. Recall that $B_A \propto \mathcal{I}^{\psi}$, which means that we need a $\mathcal{I}^{\psi}_{stab.}$ which is well above the maximum current we can have inside the defect. Calculations of the magnetic energy are in agreement with the above observation and place its value around $E_{magnetic} \sim 5 \cdot 10^{-3} << E_{tension} \sim 1$. This translates to the following conclusion: $\mathcal{I}^{\psi}_{stab.} \gtrsim 10 \cdot \mathcal{I}^{\psi}_{est.}$.

Thus, we find out that the current needed for stabilization, is at least ten times bigger than the value of the maximum current our string can sustain. We also observe that our numerical maximum current values are close to the theoretical estimations about quenching. This means, that we will have current quenching as an “obstacle” towards stabilization, since the supercurrent will not be enough in order to create the magnetic field needed.

.

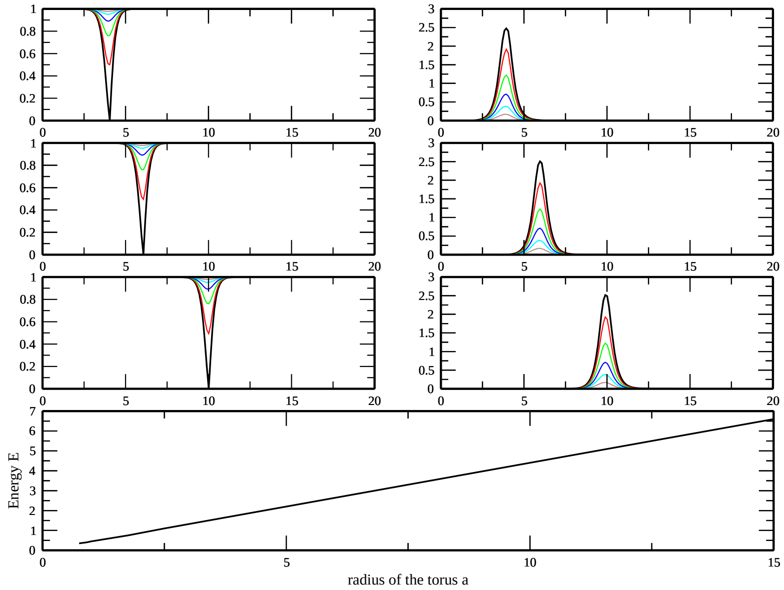

Figure 5.12: $U(1)_W$ **model:** Profiles for the scalar field $F(\rho, z)$ on the left and for the magnetic field $B_W$ on the right side, for three random values of $a$. On the bottom graph there is the energy vs. radius of the torus $a$. Parameters are $(M, m_\phi, m_W, v_1)$=$(1, 4.47, 2, 0.01)$. Black solid line is for $z = 0$.

## 5.6 $U(1)_W$ model: Vortex ring without supercurrent

Here, we present a simpler model of a string of toroidal geometry but without the $\psi$ scalar field responsible for the existence of supercurrent. In this model, we only have the scalar field $\phi(\rho, z)$ together with its gauge field $W(\rho, z)$. The presence of the latter gives us the freedom to choose $\Theta(\rho, z) = \arctan(z/(\rho - a))$, as we did before. The **initial guess** we use for the fields is the following:

$$\begin{aligned}
F(\rho, z) &= \tanh((\rho - a)^2 + z^2)^{M/2} \\
W_\rho(\rho, z) &= \frac{Mz\cos^2\Theta}{q(\rho - a)^2}\left(\frac{(\rho - a)^2 + z^2}{(\rho - a)^2 + z^2 + (a^2/4)}\right)^2 \\
W_z(\rho, z) &= -\frac{M\cos^2\Theta}{q(\rho - a)}\left(\frac{(\rho - a)^2 + z^2}{(\rho - a)^2 + z^2 + (a^2/4)}\right)
\end{aligned}$$

As there is no current flowing inside the string there will be no Meissner effect which means that there is no reason to prevent the vortex ring from collapsing. Thus, we expect to find no non-trivial minimum on the energy of the system, something which signals the instability of that object (fig.5.12).

## 5.7 Conclusions

Future experiments in LHC could answer whether metastable particle-like solitons exist in MSSM or 2HSM *or* not. In [15] there is a search for spherically symmetric solitons in the frame of the 2HSM with a simplified potential. Here we search for axially symmetric solitons which, if stable, will have a mass of the order of TeV [15]. We considered the $U(1)_A \times U(1)_W$ model, where the existence of the vortex is ensured, for topological reasons. There, we searched for stable toroidal strings. We present and analyze our observations. This chapter tries to answer to expectations having to do with observations of stable axially symmetric solitons which would be possible to detect in later experiments of LHC. For relatively small values of $e$ ($\sim 1$), which are of interest in that case, the system seems to have no stable vortex rings. In fact, this instability is present even in other parameter areas where we searched (i.e. $e \geq 6$ see figs.5.9,5.10). We explain why we believe that the main reason of instability is current quenching.

## 5.8 APPENDIX

### 5.8.1 Part I: Derivation of the formula $\mathcal{I}^{\psi}_{max} \leq \sqrt{\sigma} e u$

To derive the above formula, we follow the steps of [105] (pages 129-130). The current density is given by

$$j^{\mu} = ie(\overline{\psi} D^{\mu} \psi - \psi \overline{D^{\mu} \psi}) \tag{5.35}$$

where $\psi = P(\rho) e^{i\Phi(\varphi)}$ and the covariant derivative $D^{\mu} = \partial^{\mu} + ieA^{\mu}$. Substituting above, the absolute value of the current density is $j^{\varphi} = 2eP^2 D^{\varphi}\Phi$ and the total supercurrent is the integral of the cross section of the current density

$$\mathcal{I} = \int_0^{\infty} d\rho \int_{-\infty}^{\infty} dz \;\; j^{\varphi} \tag{5.36}$$

from which we get $\mathcal{I} = 2\sigma e D^{\varphi}\Phi$, where we denote $\int\int d\rho dz P^2$ by $\sigma$.

The term $g_2(P^2 - u^2)^2/4$ of the potential, enforces the expectation value of $P$ to reach $u$. On the other hand, in the energy functional there is the term $P^2(D^{\varphi}\Phi)^2$ which tries to "counteract" the above potential term. The latter means that $(D^{\varphi}\Phi)^2$ acts as a "negative mass" squared. Because of that term, the expectation value of $P$, say $P_0$, is not $u$ but

$$P_0^2 \approx u^2 - \frac{2}{g_2}(D^{\varphi}\Phi)^2 \tag{5.37}$$

The above decrease has an effect on the supercurrent as well. It decreases its value thus,

$$\mathcal{I} = 2\sigma e(D^{\varphi}\Phi)\left[1 - 2\sigma \frac{(D^{\varphi}\Phi)^2}{u^2}\right] \tag{5.38}$$

In the above equation, only $D^{\varphi}\Phi$ has dimensions (of mass) and we rename it as $X$. We want to find the maximum value of the current:

$$\frac{d\mathcal{I}}{dX} = 0 \rightarrow X \approx \frac{u}{\sqrt{\sigma}} \tag{5.39}$$

and by substituting, we find out that the maximum value of the supercurrent is

$$\mathcal{I}_{max} \leq \sqrt{\sigma} e u \tag{5.40}$$

### 5.8.2 Part II: Toroidal coordinate system

The toroidal coordinates $(\eta, \xi, \varphi)$ are related to the cartesian $(x, y, z)$ through the following definition:

$$x = \frac{a}{D}\sinh\eta\cos\varphi,\ y = \frac{a}{D}\sinh\eta\sin\varphi,\ z = \frac{a}{D}\sin\xi \tag{5.41}$$

with $a$ a scale factor of the torus, $D = \cosh\eta - \cos\xi$ and $0 \leq \eta < \infty$, $0 \leq \xi \leq 2\pi$, $0 \leq \varphi \leq 2\pi$.

In order to find the field equations, we need to relate the derivatives of cartesian coordinates with those of toroidal coordinates, thus the following formulas can be very useful:

$$\begin{aligned}
\frac{\partial}{\partial x} &= -\frac{\cos\varphi(\cosh\eta\cos\xi - 1)}{a}\frac{\partial}{\partial\eta} - \frac{\sin\xi\sinh\eta\cos\varphi}{a}\frac{\partial}{\partial\xi} - \frac{D\sin\varphi}{a\sinh\eta}\frac{\partial}{\partial\varphi}\\
\frac{\partial}{\partial y} &= -\frac{\sin\varphi(\cosh\eta\cos\xi - 1)}{a}\frac{\partial}{\partial\eta} - \frac{\sin\xi\sinh\eta\sin\varphi}{a}\frac{\partial}{\partial\xi} + \frac{D\cos\varphi}{a\sinh\eta}\frac{\partial}{\partial\varphi}\\
\frac{\partial}{\partial z} &= -\frac{\sin\xi\sinh\eta}{a}\frac{\partial}{\partial\eta} + \frac{\cosh\eta\cos\xi - 1}{a}\frac{\partial}{\partial\xi}\\
\nabla^2 \equiv \partial_x^2 + \partial_y^2 + \partial_z^2 &= -\frac{D}{a^2}\Bigg[(\cos\xi - \cosh\eta)\left(\frac{1}{\sinh^2\eta}\frac{\partial^2}{\partial\varphi^2} + \frac{\partial^2}{\partial\xi^2}\right) +\\
&\quad + sin\xi\frac{\partial}{\partial\xi} + (\cos\xi\cosh\eta - 1)\frac{1}{\sinh\eta}\frac{\partial}{\partial\eta} - D\frac{\partial^2}{\partial\eta^2}\Bigg]
\end{aligned}$$

The relations between unitary vectors of the toroidal and the cartesian coordinate system follow:

$$\begin{aligned}
\hat{h} &= \frac{1}{D}\Big[\cos\varphi(1 - \cosh\eta\cos\xi)\,\hat{i} + \sin\varphi(1 - \cosh\eta\cos\xi)\,\hat{j} - \sinh\eta\sin\xi\,\hat{k}\Big]\\
\hat{\xi} &= \frac{1}{D}\Big[-\sinh\eta\sin\xi(\cos\varphi\,\hat{i} + \sin\varphi\,\hat{j}) + (\cos\xi\cosh\eta - 1)\,\hat{k}\Big]\\
\hat{\varphi} &= -\sin\varphi\,\hat{i} + \cos\varphi\,\hat{j}
\end{aligned}$$

### 5.8.3 Part III: Cylindrical coordinate system

The cylindrical coordinates $(\rho, \varphi, z)$ are related to the cartesian $(x, y, z)$ through the following definition:

$$x = \rho\cos\varphi,\quad y = \rho\sin\varphi,\quad z = z \tag{5.42}$$

In order to find the field equations, we need to relate the derivatives of cartesian coordinates with those of cylindrical coordinates thus, the following formulas can be very useful:

$$\begin{aligned}
\frac{\partial}{\partial x} &= \cos\varphi\frac{\partial}{\partial\rho} - \frac{\sin\varphi}{\rho}\frac{\partial}{\partial\varphi} \\
\frac{\partial}{\partial y} &= \sin\varphi\frac{\partial}{\partial\rho} + \frac{\cos\varphi}{\rho}\frac{\partial}{\partial\varphi} \\
\frac{\partial^2}{\partial x^2} &= \cos^2\varphi\frac{\partial^2}{\partial\rho^2} + \frac{\sin 2\varphi}{\rho^2}\frac{\partial}{\partial\varphi} - \frac{\sin 2\varphi}{\rho}\frac{\partial^2}{\partial\rho\partial\varphi} + \frac{\sin^2\varphi}{\rho}\frac{\partial}{\partial\rho} + \frac{\sin^2\varphi}{\rho^2}\frac{\partial^2}{\partial\varphi^2} \\
\frac{\partial^2}{\partial y^2} &= \sin^2\varphi\frac{\partial^2}{\partial\rho^2} - \frac{\sin 2\varphi}{\rho^2}\frac{\partial}{\partial\varphi} - \frac{\sin 2\varphi}{\rho}\frac{\partial^2}{\partial\rho\partial\varphi} + \frac{\cos^2\varphi}{\rho}\frac{\partial}{\partial\rho} + \frac{\cos^2\varphi}{\rho^2}\frac{\partial^2}{\partial\varphi^2} \\
\frac{\partial^2}{\partial x\partial y} &= \frac{\sin 2\varphi}{2}\frac{\partial^2}{\partial\rho^2} - \frac{\cos 2\varphi}{\rho^2}\frac{\partial}{\partial\varphi} + \frac{\cos 2\varphi}{\rho}\frac{\partial^2}{\partial\rho\partial\varphi} - \frac{\sin^2\varphi}{2\rho}\frac{\partial}{\partial\rho} - \frac{\sin^2\varphi}{2\rho^2}\frac{\partial^2}{\partial\varphi^2} \\
\nabla^2 &= \frac{1}{\rho}\frac{\partial}{\partial\rho}\left(\rho\frac{\partial}{\partial\rho}\right) + \frac{1}{\rho^2}\frac{\partial^2}{\partial\varphi^2} + \frac{\partial^2}{\partial z^2}
\end{aligned}$$

The relations between unitary vectors of the cylindrical and the cartesian coordinate system follow:

$$\begin{aligned}
\hat{\rho} &= \cos\varphi\,\hat{i} + \sin\varphi\,\hat{j} \\
\hat{\varphi} &= -\sin\varphi\,\hat{i} + \cos\varphi\,\hat{j} \\
\hat{z} &= \hat{k}
\end{aligned}$$

### 5.8.4 Part IV: Field profiles in different $z$ levels

Here, we present the dependence of the fields of the $U(1) \times U(1)$ model examined above, on $z$ variable. For that reason, we plot the fields of fig.5.8 for the same parameters, but in different $z$ levels in order to observe their behavior.

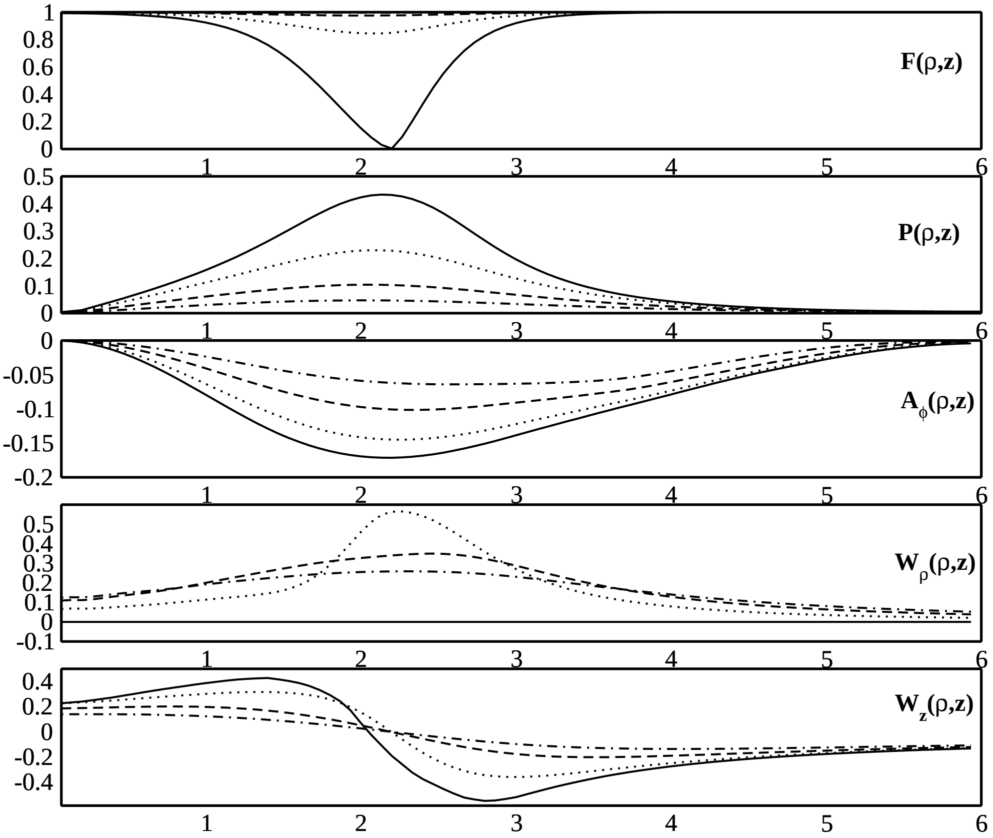

Figure 5.13: $U(1)_A \times U(1)_W$ **model:** Typical plot of the final configuration of fields. Solid line: $z = 0$, dotted line: $z = 0.6$, dashed line: $z = 1.2$, dashed and dotted line: $z = 1.8$. Parameters are $M = 1$, $N = 1$, $e = 5$, $q = m_W = 2$, $g_1 = 14$, $m_\phi = \sqrt{g_1} = 3.74$, $g_2 = 12$, $g_3 = 14$, $u = 1$, $m_\psi = \sqrt{(g_3 - g_2 u^2)/2} = 1$, $v_1 = 7.5 \cdot 10^{-3}$. Energy $E = 0.72$ and virial is $1.5 \cdot 10^{-3}$.

# Chapter 6

# The extended $U(1) \times U(1)$ model for vortex rings

## 6.1 Introduction

Stable strings of the previous $U(1)$ model (examined in chapter 4) could be useful in order to create vortex rings and study their stability. It could also be relatively helpful numerically, as we would have four fields for minimization in the energy functional instead of five we had in [90] (chapter 5). This is not as easy as it might seem, since there are two instability modes. The vortex itself is not necessarily stable while forming a torus, and the latter has the tendency to shrink due to its tension. The first instability can be avoided in a $U(1)\times U(1)$ model as the one presented in [90] (chapter 5), where a numerical search for bosonic superconducting static vortex rings in a $U(1)_A \times U(1)_W$ model is examined. There, the existence of straight strings is ensured for topological reasons. The superconductivity of the loop though, does not seem to prevent shrinking. The conclusion there, is that current quenching takes place before stabilization.

Here we deal with an extended version of the previously discussed model of chapter 5. We add appropriate higher derivative terms which might help the ring to stabilize. We present and analyze our results.

## 6.2 The $U(1)_A \times U(1)_W$ model

The model discussed in [90] (chapter 5), is being described by the Lagrangian density

$$\mathcal{L}_0 = -\frac{1}{4}F_{\mu\nu}^2 - \frac{1}{4}W_{\mu\nu}^2 + |D_\mu\psi|^2 + |\tilde{D}_\mu\phi|^2 - U(|\phi|, |\psi|) \tag{6.1}$$

where the covariant derivatives are $D_\mu\psi \equiv \partial_\mu\psi + ieA_\mu\psi$, $\tilde{D}_\mu\phi \equiv \partial_\mu\phi + iqW_\mu\phi$, the strength of the fields are $F_{\mu\nu} = \partial_\mu A_\nu - \partial_\nu A_\mu$, $W_{\mu\nu} = \partial_\mu W_\nu - \partial_\nu W_\mu$, while $e$ and $q$ stand as the relevant $U(1)$ charges. The potential $U$ is

$$U(|\phi|, |\psi|) = \frac{g_1}{4}\big(|\phi|^2 - v_1^2\big)^2 + \frac{g_2}{4}\big(|\psi|^2 - v_2^2\big)^2 + \frac{g_3}{2}|\phi|^2|\psi|^2 - \frac{g_2}{4}v_2^4 \tag{6.2}$$

The vacuum of this theory is $|\phi| = v_1 \neq 0$, $|\psi| = 0$ and breaks $U(1)_W \times U(1)_A \to U(1)_A$, giving non-zero mass to $W$. The photon field stays massless. There, $U(v_1, 0) = 0$. The vacuum manifold $\mathcal{M}$ in this theory is a circle $S^1$ and the first homotopy group of $\mathcal{M}$ is $\pi_1(\mathcal{M}) = \pi_1(S^1) = \mathbf{Z}$ which signals the existence of strings. In regions where $|\phi| = 0$, the field $|\psi|$ is arranged to be non-vanishing and $U(1)_W \times U(1)_A \to U(1)_W$. Thus, $U(1)_A \to \mathbf{1}$ and electric current flows along regions with vanishing $|\phi|$. Hence, this theory has superconducting strings [103]. The vacuum of the theory leaves unbroken the electromagnetic $U(1)_A$. For $g_3 v_1^2 > g_2 v_2^2$ this vacuum is stable, while $g_1 v_1^4 > g_2 v_2^4$ ensures that it is the global minimum of the potential. The mass spectrum is

$$m_A = 0, \;\; m_W = q v_1, \;\; m_\phi^2 = g_1 v_1^2, \;\; m_\psi^2 = \frac{1}{2}\big(g_3 v_1^2 - g_2 v_2^2\big) \tag{6.3}$$

## 6.3 The extended $U(1)_A \times U(1)_W$ model

We intend to modify the above model by adding higher derivative terms of the fields $\phi$ and $\psi$ and find out whether such changes can stabilize the ring. By following Derrick's scaling argument [98], one can argue that terms such as $|D_\mu \psi|^4$ or $|\tilde{D}_\mu \phi|^4$ or $|\tilde{D}_\mu \phi|^2 |D_\mu \psi|^2$ could be helpful. Also, in an investigation of a similar model [97], the conclusions lead to the same path, in order to search for possibilities of stabilizing such solitons against radial shrinking. Thus, we have the following **Lagrangian density**:

$$\mathcal{L} = \mathcal{L}_0 + c_\phi |\tilde{D}_\mu \phi|^4 + c_\psi |D_\mu \psi|^4 + c_{\phi\psi} |\tilde{D}_\mu \phi|^2 |D_\mu \psi|^2 \tag{6.4}$$

where $c_\phi$, $c_\psi$, $c_{\phi\psi}$ constants. This Lagrangian (6.4) with the extra terms, exhibits the symmetries of the original Lagrangian $\mathcal{L}_0$ (6.1).

Configurations with torus-like shape, representing a piece of a $U(1)_W \rightarrow \mathbf{1}$ Nielsen-Olesen string, closed to form a loop, are of interest in this search. Thus, we will require $\phi$ to vanish on a circle of radius $a$ (the torus radius) $\phi(\rho = a, z = 0) = 0$. At infinity $(\rho \rightarrow \infty, z \rightarrow \infty)$, we have the vacuum of the theory. This translates to $|\phi| \rightarrow v_1$, $|\psi| \rightarrow 0$. The **ansatz** for the fields is:

$$\begin{aligned}
\phi(\rho, \varphi, z) &= F(\rho, z) e^{iM\Theta(\rho, z)} \\
\psi(\rho, \varphi, z) &= P(\rho, z) e^{iN\varphi} \\
\mathbf{A}(\rho, \varphi, z) &= \frac{A_\varphi(\rho, z)}{\rho}\, \hat{\varphi} \\
\mathbf{W}(\rho, \varphi, z) &= W_\rho(\rho, z)\, \hat{\rho} + W_z(\rho, z)\, \hat{z}
\end{aligned}$$

where $M$, $N$ are the winding numbers of the relevant fields, $\hat{\rho}$, $\hat{\varphi}$, $\hat{z}$ are the cylindrical unit vectors and the phase

$$\Theta(\rho, z) \equiv \arctan\left(\frac{z}{\rho - a}\right) \tag{6.5}$$

We use cylindrical coordinates $(t,\rho,\varphi,z)$, with space-time metric that has the form $g_{\mu\nu}{=}diag(1,-1,-\rho^2,-1)$. We work in the $A^0=0=W^0$ gauge. We follow the ansatz of [90].

With the above ansatz, the **energy functional** to be minimized takes the form:

$$\begin{aligned}
E &= 2\pi v_1 \int_0^\infty \rho d\rho \int_{-\infty}^{\infty} dz \Bigg[ \frac{1}{2\rho^2}\Big((\partial_\rho A_\varphi)^2+(\partial_z A_\varphi)^2\Big)+\frac{1}{2}(\partial_\rho W_z-\partial_z W_\rho)^2+ \\
&+ (\partial_\rho P)^2+(\partial_z P)^2+(\partial_\rho F)^2+(\partial_z F)^2+\frac{P^2}{\rho^2}(eA_\varphi+N)^2+ \\
&+ \Big((qW_\rho+M\partial_\rho\Theta)^2+(qW_z+M\partial_z\Theta)^2\Big)F^2+ \\
&+ c_\phi\Bigg\{(\partial_\rho F)^2+(\partial_z F)^2+\Big((qW_\rho+M\partial_\rho\Theta)^2+(qW_z+M\partial_z\Theta)^2\Big)F^2\Bigg\}^2+ \\
&+ c_\psi\Bigg\{(\partial_\rho P)^2+(\partial_z P)^2+\frac{P^2}{\rho^2}(eA_\varphi+N)^2\Bigg\}^2+ \\
&+ c_{\phi\psi}\Bigg\{\Bigg((\partial_\rho F)^2+(\partial_z F)^2+\Big((qW_\rho+M\partial_\rho\Theta)^2+(qW_z+M\partial_z\Theta)^2\Big)F^2\Bigg) \\
&\cdot \Bigg((\partial_\rho P)^2+(\partial_z P)^2+\frac{P^2}{\rho^2}(eA_\varphi+N)^2\Bigg)\Bigg\}+U(F,P)\Bigg]
\end{aligned} \tag{6.6}$$

and the potential $U$ follows:

$$U(F,P)=\frac{g_1}{4}\big(F^2-1\big)^2+\frac{g_2}{4}\big(P^2-u^2\big)^2+\frac{g_3}{2}F^2P^2-\frac{g_2}{4}u^4 \tag{6.7}$$

where $u\equiv v_2/v_1$. This is the energy functional we use for our numerical analysis. The conditions to be satisfied by the parameters become:

$$g_1>g_2u^4 \quad , \quad g_3>g_2u^2 \tag{6.8}$$

The magnetic fields are

$$\nabla\times\mathbf{A}=\mathbf{B_A}=\frac{1}{\rho}\left(\frac{\partial A_\varphi}{\partial\rho}\,\hat{z}-\frac{\partial A_\varphi}{\partial z}\,\hat{\rho}\right)$$

$$\nabla\times\mathbf{W}=\mathbf{B_W}=-\left(\frac{\partial W_z}{\partial\rho}-\frac{\partial W_\rho}{\partial z}\right)\hat{\varphi}$$

while the currents associated with $\phi$ field, namely $j^{\phi}_{\rho}$ and $j^{\phi}_{z}$ and the total current $\mathcal{I}^{\phi}$ out of these as well as the supercurrent $\mathcal{I}^{\psi}$ associated with the $\psi$ field are

$$\mathcal{I}^{\phi} = \sqrt{(j^{\phi}_{\rho})^2 + (j^{\phi}_{z})^2}\ , \quad \mathcal{I}^{\psi} = -\frac{2eP^2}{\rho}(eA_{\varphi} + N) \tag{6.9}$$

where

$$j^{\phi}_{\rho} = -2qF^2(qW_{\rho} + M\partial_{\rho}\Theta), \quad j^{\phi}_{z} = -2qF^2(qW_z + M\partial_z\Theta) \tag{6.10}$$

Finally, in order to check our numerical results, we can derive **virial** relations through Derrick's scaling argument. Below we present the virial relations we use in our search. Consider the rescalings $\rho \to \rho$, $z \to \kappa z$, $F_{\kappa} \to F$, $P_{\kappa} \to P$, $A_{\varphi_{\kappa}} \to A_{\varphi}$, $W_{\rho,z_{\kappa}} \to \kappa W_{\rho,z}$. By demanding $\frac{\partial E}{\partial \kappa} = 0$ when $\kappa = 1$ and if we define

$$\begin{aligned}
I_1 \ &= \ 2\pi v_1 \int_0^{\infty} \rho d\rho \int_{-\infty}^{\infty} dz \Bigg[ \frac{1}{2}(\partial_{\rho}W_z - \partial_z W_{\rho})^2 + \frac{1}{2\rho^2}(\partial_z A_{\varphi})^2 + (\partial_z P)^2 + \\
&+ \ (\partial_z F)^2 + 2F^2\Bigg( qW_{\rho}(qW_{\rho} + M\partial_{\rho}\Theta) + (qW_z + M\partial_z\Theta)^2 \Bigg) + \\
&+ \ c_{\phi}\Bigg\{ 4F^2(\partial_z F)^2 \Bigg( (qW_{\rho} + M\partial_{\rho}\Theta)^2 + (qW_z + M\partial_z\Theta)^2 \Bigg) + \\
&+ \ 3(\partial_z F)^4 + 2(\partial_{\rho}F)^2(\partial_z F)^2 + \\
&+ \ \Bigg( 4F^4 \Bigg( (qW_{\rho} + M\partial_{\rho}\Theta)^2 + (qW_z + M\partial_z\Theta)^2 \Bigg) \\
&\cdot \ \Big( qW_{\rho}(qW_{\rho} + M\partial_{\rho}\Theta) + (qW_z + M\partial_z\Theta)^2 \Big) \Bigg) + \\
&+ \ 4F^2\Big( (\partial_{\rho}F)^2 + (\partial_z F)^2 \Big)\Big( qW_{\rho}(qW_{\rho} + M\partial_{\rho}\Theta) + (qW_z + M\partial_z\Theta)^2 \Big) \Bigg\} + \\
&+ \ c_{\psi}\Bigg\{ 3(\partial_z P)^4 + 2(\partial_{\rho}P)^2(\partial_z P)^2 + \frac{2P^2}{\rho^2}(\partial_z P)^2(eA_{\varphi} + N)^2 \Bigg\} +
\end{aligned}$$

$$
\begin{aligned}
+ \quad & c_{\phi\psi}\Bigg\{(\partial_z P)^2(\partial_\rho F)^2 + (\partial_\rho P)^2(\partial_z F)^2 + 3(\partial_z P)^2(\partial_z F)^2 + \\
+ \quad & \frac{P^2}{\rho^2}(eA_\varphi + N)^2(\partial_z F)^2 + \left(\frac{2P^2F^2}{\rho^2}(eA_\varphi + N)^2 + 2F^2\Big((\partial_\rho P)^2 + (\partial_z P)^2\Big)\right) \\
\cdot \quad & \Big(qW_\rho(qW_\rho + M\partial_\rho\Theta) + (qW_z + M\partial_z\Theta)^2\Big) + \\
+ \quad & (\partial_z P)^2F^2\left((qW_\rho + M\partial_\rho\Theta)^2 + (qW_z + M\partial_z\Theta)^2\right)\Bigg\}\Bigg]
\end{aligned}
$$

$$
\begin{aligned}
I_2 \quad = \quad & -2\pi v_1 \int_0^\infty \rho d\rho \int_{-\infty}^\infty dz \Bigg[\frac{1}{2\rho^2}(\partial_\rho A_\varphi)^2 + (\partial_\rho F)^2 + (\partial_\rho P)^2 + \\
+ \quad & \frac{P^2}{\rho^2}(eA_\varphi + N)^2 + (\partial_z W_\rho)(\partial_\rho W_z - \partial_z W_\rho) + \\
+ \quad & F^2\left((qW_\rho + M\partial_\rho\Theta)^2 + (qW_z + M\partial_z\Theta)^2\right) + \\
+ \quad & c_\phi\Bigg\{(\partial_\rho F)^4 + F^4\left((qW_\rho + M\partial_\rho\Theta)^2 + (qW_z + M\partial_z\Theta)^2\right)^2 + \\
+ \quad & 2F^2\Big((\partial_\rho F)^2 + (\partial_z F)^2\Big)\left((qW_\rho + M\partial_\rho\Theta)^2 + (qW_z + M\partial_z\Theta)^2\right)\Bigg\} + \\
+ \quad & c_\psi\left\{(\partial_\rho P)^4 + \frac{P^4}{\rho^4}(eA_\varphi + N)^4 + \frac{2P^2}{\rho^2}(\partial_\rho P)^2(eA_\varphi + N)^2\right\} + \\
+ \quad & c_{\phi\psi}\Bigg\{(\partial_\rho P)^2(\partial_\rho F)^2 + \frac{P^2}{\rho^2}(eA_\varphi + N)^2(\partial_\rho F)^2 + \\
+ \quad & \left(\frac{P^2F^2}{\rho^2}(eA_\varphi + N)^2 + F^2(\partial_\rho P)^2\right) \\
\cdot \quad & \left((qW_\rho + M\partial_\rho\Theta)^2 + (qW_z + M\partial_z\Theta)^2\right)\Bigg\} + \\
+ \quad & \frac{g_1}{4}(F^2 - 1)^2 + \frac{g_2}{4}(P^2 - u^2)^2 + \frac{g_3}{2}F^2P^2 - \frac{g_2}{4}u^4\Bigg]
\end{aligned}
$$

we must have $I_1 + I_2 = 0$. We define the index $V = \frac{||I_1| - |I_2||}{|I_1| + |I_2|}$ and we want its value to be as small as possible. We can have many other virial relations by assuming generally for a field $\phi$, the "double" rescaling $\phi(\vec{x}) \rightarrow \kappa\phi(\mu\vec{x})$ and then demand $\frac{\partial E}{\partial \kappa}|_{\kappa=1=\mu} = 0 = \frac{\partial E}{\partial \mu}|_{\kappa=1=\mu}$. For example, we check our results through the following relations as well. Consider the following rescalings $\rho \rightarrow \rho$, $z \rightarrow \mu z$, $F_\kappa \rightarrow F$, $P_\kappa \rightarrow \kappa P$, $A_{\varphi_\kappa} \rightarrow A_\varphi$, $W_{\rho,z_\kappa} \rightarrow W_{\rho,z}$. We define

$$\begin{aligned}
I_3 &= 2\pi v_1 \int_0^\infty \rho d\rho \int_{-\infty}^\infty dz \Bigg[ \frac{1}{2\rho^2}(\partial_z A_\varphi)^2 + (\partial_z P)^2 + (\partial_z F)^2 + \\
&+ \frac{1}{2}(\partial_\rho W_z - \partial_z W_\rho)^2 + 2F^2 \Bigg( M\partial_z\Theta(qW_z + M\partial_z\Theta) \Bigg) + \\
&+ c_\phi \Bigg\{ 3(\partial_z F)^4 + 2(\partial_\rho F)^2(\partial_z F)^2 + \\
&+ 4F^4 \Bigg( (qW_\rho + M\partial_\rho\Theta)^2 + (qW_z + M\partial_z\Theta)^2 \Bigg) \Big( M\partial_z\Theta(qW_z + M\partial_z\Theta) \Big) + \\
&+ 4F^2(\partial_z F)^2 \Bigg( (qW_\rho + M\partial_\rho\Theta)^2 + (qW_z + M\partial_z\Theta)^2 \Bigg) + \\
&+ 4F^2 \Big( (\partial_\rho F)^2 + (\partial_z F)^2 \Big) \Big( M\partial_z\Theta(qW_z + M\partial_z\Theta) \Big) \Bigg\} + \\
&+ c_\psi \Bigg\{ 3(\partial_z P)^4 + 2(\partial_\rho P)^2(\partial_z P)^2 + \frac{2P^2}{\rho^2}(\partial_z P)^2(eA_\varphi + N)^2 \Bigg\} + \\
&+ c_{\phi\psi} \Bigg\{ (\partial_\rho P)^2(\partial_z F)^2 + (\partial_z P)^2(\partial_\rho F)^2 + 3(\partial_z P)^2(\partial_z F)^2 + \\
&+ \frac{P^2}{\rho^2}(eA_\varphi + N)^2(\partial_z F)^2 + \\
&+ 2F^2 \Bigg( (\partial_\rho P)^2 + (\partial_z P)^2 + \frac{P^2}{\rho^2}(eA_\varphi + N)^2 \Bigg)(M\partial_z\Theta(qW_z + M\partial_z\Theta)) + \\
&+ (\partial_z P)^2 F^2 \Bigg( (qW_\rho + M\partial_\rho\Theta)^2 + (qW_z + M\partial_z\Theta)^2 \Bigg) \Bigg\} \Bigg]
\end{aligned}$$

$$
\begin{array}{rcl}
I_4 & = & -2\pi v_1 \int_0^\infty \rho d\rho \int_{-\infty}^{\infty} dz \left[ \frac{1}{2\rho^2}(\partial_\rho A_\varphi)^2 + (\partial_\rho P)^2 + (\partial_\rho F)^2 + \right. \\
& + & \frac{P^2}{\rho^2}(eA_\varphi + N)^2 + \partial_\rho W_z(\partial_\rho W_z - \partial_z W_\rho) + \\
& + & F^2 \left( (qW_\rho + M\partial_\rho \Theta)^2 + (qW_z + M\partial_z \Theta)^2 \right) + \\
& + & c_\phi \left\{ (\partial_\rho F)^4 + F^4 \left( (qW_\rho + M\partial_\rho \Theta)^2 + (qW_z + M\partial_z \Theta)^2 \right)^2 + \right. \\
& + & \left. 2F^2 \Big( (\partial_\rho F)^2 + (\partial_z F)^2 \Big) \left( (qW_\rho + M\partial_\rho \Theta)^2 + (qW_z + M\partial_z \Theta)^2 \right) \right\} + \\
& + & c_\psi \left\{ (\partial_\rho P)^4 + \frac{P^4}{\rho^4}(eA_\varphi + N)^4 + \frac{2P^2}{\rho^2}(\partial_z P)^2 (eA_\varphi + N)^2 \right\} + \\
& + & c_{\phi\psi} \left\{ (\partial_\rho P)^2 (\partial_\rho F)^2 + \frac{P^2}{\rho^2}(eA_\varphi + N)^2 (\partial_\rho F)^2 + \right. \\
& + & \left( \frac{P^2 F^2}{\rho^2}(eA_\varphi + N)^2 + (\partial_\rho P)^2 F^2 \right) \\
& \cdot & \left. \left( (qW_\rho + M\partial_\rho \Theta)^2 + (qW_z + M\partial_z \Theta)^2 \right) \right\} + \\
& + & \left. \frac{g_1}{4}(F^2 - 1)^2 + \frac{g_2}{4}(P^2 - u^2)^2 + \frac{g_3}{2} F^2 P^2 - \frac{g_2}{4} u^4 \right]
\end{array}
$$

together with

$$\begin{aligned}
I_5 &= 4\pi v_1 \int_0^\infty \rho d\rho \int_{-\infty}^\infty dz \Bigg[ (\partial_\rho P)^2 + (\partial_z P)^2 + \frac{P^2}{\rho^2}(eA_\varphi + N)^2 + \\
&+ c_\psi \Bigg\{ 2(\partial_\rho P)^4 + 2(\partial_z P)^4 + \frac{2P^4}{\rho^4}(eA_\varphi + N)^4 + 4(\partial_\rho P)^2(\partial_z P)^2 + \\
&+ \frac{4P^2}{\rho^2}\Big((\partial_\rho P)^2 + (\partial_z P)^2\Big)(eA_\varphi + N)^2 \Bigg\} + \\
&+ c_{\phi\psi} \Bigg\{ (\partial_\rho P)^2(\partial_\rho F)^2 + (\partial_\rho P)^2(\partial_z F)^2 + (\partial_z P)^2(\partial_\rho F)^2 + (\partial_z P)^2(\partial_z F)^2 + \\
&+ F^2 \left( (\partial_\rho P)^2 + (\partial_z P)^2 + \frac{P^2}{\rho^2}(eA_\varphi + N)^2 \right) \\
&\cdot \left( (qW_\rho + M\partial_\rho \Theta)^2 + (qW_z + M\partial_z \Theta)^2 \right) + \\
&+ \frac{P^2}{\rho^2}(eA_\varphi + N)^2 \Big( (\partial_\rho P)^2 + (\partial_z P)^2 \Big) \Bigg\} \Bigg] \\
I_6 &= 2\pi v_1 \int_0^\infty \rho d\rho \int_{-\infty}^\infty dz \Big[ g_2 \Big(P^2 - u^2\Big) P^2 + g_3 F^2 P^2 \Big]
\end{aligned}$$

where, as above, we must have $I_3 + I_4 = 0 = I_5 + I_6$.

In the energy functional (6.6), the terms that come from the $|\tilde{D}_i\phi|^4$ extra term, are multiplied with $c_\phi$. In fact, these terms are proportional to $\partial_\rho F$ and $\partial_z F$. Thus, if one chooses $(c_\phi, c_\psi, c_{\phi\psi}) = (1, 0, 0)$, then there are more $F$-derivative terms in the functional. Energy minimization lowers these terms, something which one expects to lead to a thicker string. This is a wanted feature in order to stabilize the ring. This would have another consequence. The extra "$F$-terms", enforce the $F$ field to stay away from its vacuum expectation value within a larger area. This means that $F \approx 0$ inside a bigger area. There, the potential becomes

$$U(0, P) = \frac{g_1}{4} - \frac{g_2 u^4}{4} + \frac{g_2}{4}\Big(P^2 - u^2\Big)^2 \tag{6.11}$$

and its value increases because of the term $g_1(F^2 - 1)^2/4$, as $F \to 0$. Minimization tends to make $P \to u$, which tries to compensate for that increase. The latter means that $P$ will increase and this is another wanted feature since the supercurrent $\mathcal{I}^\psi \propto P^2$.

On the other hand, in (5.15), the terms that come from the $|D_i\psi|^4$ extra term, are multiplied with $c_\psi$. In fact, these terms are proportional to $\partial_\rho P$ and $\partial_z P$. Thus, if one chooses $(c_\phi, c_\psi, c_{\phi\psi}) = (0, 1, 0)$, then the $P$-derivative terms become more. The minimization of them is expected to decrease the charge condensate $P$. This decrease is an unwanted feature.

Finally, the terms that come from the $|\tilde{D}_i\phi|^2|D_i\psi|^2$ term, are multiplied with $c_{\phi\psi}$. The consequences of the addition of this term can be seen if we observe that the extra terms are of the form

$$(\partial P)^2 \left[ (\partial_\rho F)^2 + (\partial_z F)^2 + \cdots \right] \tag{6.12}$$

where the dots represent the rest of the terms which are positive as well. We expect a stronger decrease of the charge condensate $P$. This is because $\partial P < 1$ which means that $(\partial P)^2 > (\partial P)^4$. Thus, the need for minimizing the derivative terms of $P$ becomes stronger than in the case of $(c_\phi, c_\psi, c_{\phi\psi}) = (0, 1, 0)$. Apart from this, it is also the fact that, since $\partial F \sim 1$, the weight of the $P$-derivative terms is now greater than unity and this is another factor which would tend to make $P \to 0$ or, at least, smaller than in the case $(c_\phi, c_\psi, c_{\phi\psi}) = (0, 1, 0)$.

Theoretically, the fact that the terms $|D_i\psi|^4$ and $|\tilde{D}_i\phi|^2|D_i\psi|^2$ tend to shrink the charge condensate $P$, can also be seen from the virial relation $I_5 + I_6 = 0$ above. The integral $I_6$ is negative (since $P < u$) and the addition of extra terms leaves it unchanged. On the other hand, $I_5$ is a sum of positive terms and the above two extra derivative terms rise the value of $I_5$. Thus, the only way to satisfy that virial relation is either to increase $g_2$ and/or to decrease $P$. If $I_5$ is large enough, then $P$ will be enforced to become zero in order to satisfy the $I_5 + I_6 = 0$ relation.

## 6.4 The extended $U(1)_A \times U(1)_W$ model: Numerical results

We use the same minimization algorithm, as in [90], to minimize the energy functional presented in (6.6). A $90 \times 20$ grid for every of the five functions is used, that is, 90 points on $\rho$-axis and 20 on $z$. We begin with fixed torus radius $a$. Then, the configuration with minimum energy for this $a$ is found. Other values of $a$ are chosen as well and the same process goes on until we plot the energy vs. the torus radius $E(a)$. It would be very interesting to find a non-trivial minimum of the energy (in $a_{min} \neq 0$), which would correspond to stable toroidal defects with radius $a_{min}$. One crucial check of our results is done through virial relations.

.

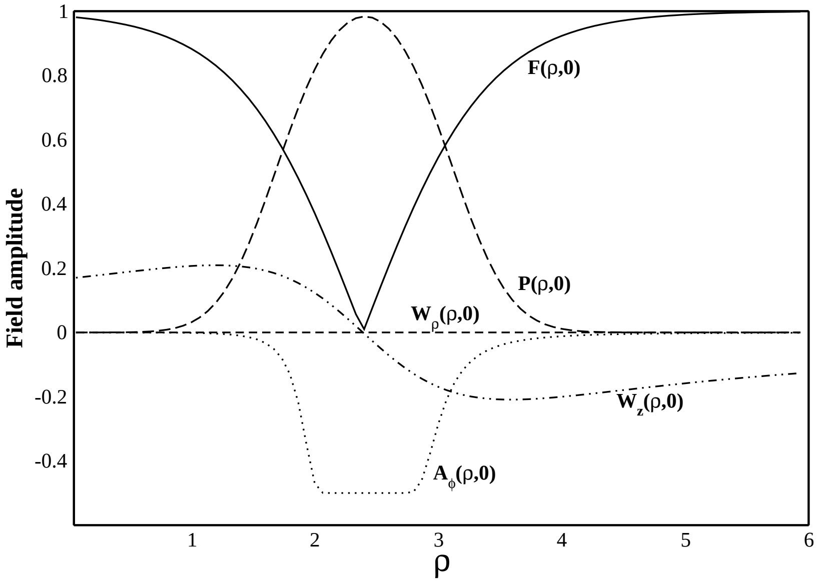

Figure 6.1: **Extended $U(1)_A \times U(1)_W$ model:** A typical plot of the initial guess we use, for the lowest winding state $M = 1, N = 1$ on $z = 0$ plane.

The **initial guess** (fig.6.1) we use for our computation is:

$$F(\rho,z) = \tanh((\rho-a)^2+z^2)^{M/2}$$
$$P(\rho,z) = \tanh(\rho^N)(1-\tanh((\rho-a)^2+z^2)$$
$$A_\varphi(\rho,z) = -\frac{N}{e}\tanh\left(\frac{\rho^2}{((\rho-a)^2+z^2)^2}\right)$$
$$W_\rho(\rho,z) = \frac{Mz\cos^2\Theta}{q(\rho-a)^2}\left(\frac{(\rho-a)^2+z^2}{(\rho-a)^2+z^2+(a^2/4)}\right)^2$$
$$W_z(\rho,z) = -\frac{M\cos^2\Theta}{q(\rho-a)}\left(\frac{(\rho-a)^2+z^2}{(\rho-a)^2+z^2+(a^2/4)}\right)$$

This initial guess also satisfies the appropriate asymptotics

- near $\rho = 0$:
$$F \neq 0, \;\; P \sim \rho^N, \;\; A_\varphi \sim \rho^2 f(z) \tag{6.13}$$
- near $(\rho = a, z = 0)$:
$$F \sim \tilde{\rho}^{M/2}, \;\; W_\rho = 0 = W_z \tag{6.14}$$

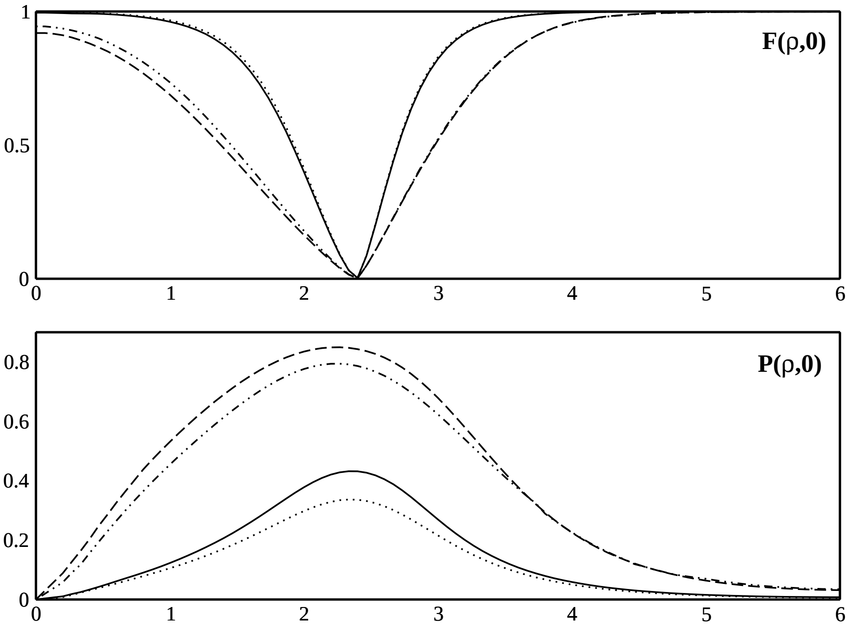

Figure 6.2: **Extended $U(1)_A \times U(1)_W$ model:** A typical graph which exhibits the effects of the higher derivative terms on the scalar fields. Solid line is for $(c_\phi, c_\psi, c_{\phi\psi})$=$(0,0,0)$, dotted line for $(c_\phi, c_\psi, c_{\phi\psi})$=$(0,1,0)$, dashed for $(c_\phi, c_\psi, c_{\phi\psi})$=$(1,0,0)$ while dashed and dotted for $(c_\phi, c_\psi, c_{\phi\psi})$=$(1,1,0)$. In the case $(c_\phi, c_\psi, c_{\phi\psi})$=$(0,0,1)$, $P$ is trivial. Parameters in this figure are $(g_1, g_2, g_3, e, q, u, v_1, M, N)$= $(14, 12, 14, 6, 2, 1, 7.5 \cdot 10^{-3}, 1, 1)$.

- at infinity:

$$F \sim 1 - \mathcal{O}(e^{-\sqrt{\tilde\rho}}), \quad P \sim \mathcal{O}(e^{-\sqrt{\rho^2+z^2}})$$
$$W_\rho \sim -\frac{M}{q}\partial_\rho \Theta|_\infty + \mathcal{O}(e^{-\sqrt{\tilde\rho}}), \quad W_z \sim -\frac{M}{q}\partial_z \Theta|_\infty + \mathcal{O}(e^{-\sqrt{\tilde\rho}}) \quad (6.15)$$

where $\tilde\rho \equiv (\rho - a)^2 + z^2$.

Based on [90] (chapter 5), we search on parameter areas where $e$ acquires relatively large values, but they are interesting concerning the possible stability of the loop. The reason was analyzed in that paper (chapter) and stems from the need to have string thickness greater than the penetration depth as well as strong supercurrent.

The results confirm our expectations stated previously. For example, in fig.6.2, one can observe that when the extra higher derivative term is

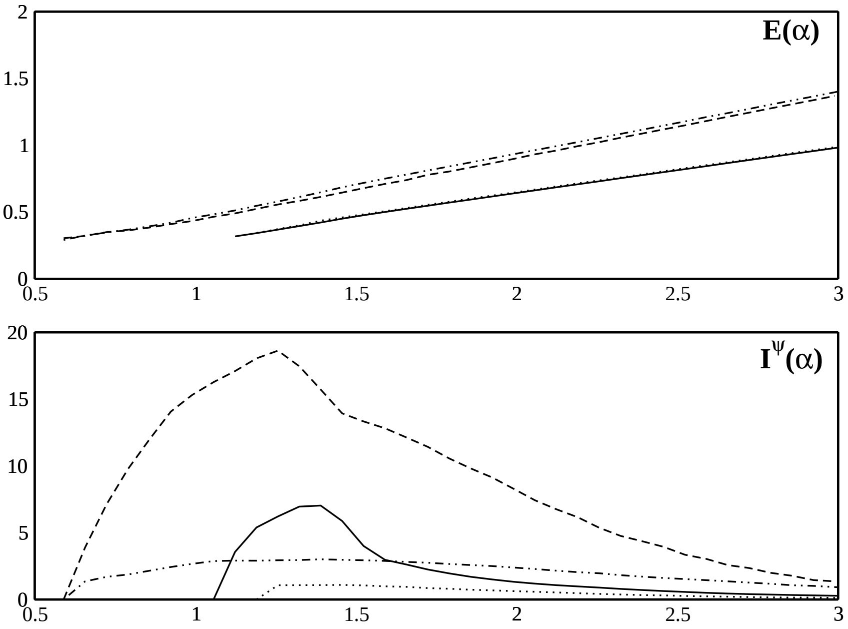

Figure 6.3: **Extended $U(1)_A \times U(1)_W$ model:** The effect of the higher derivative terms on the energy and the supercurrent when these are plotted vs. the radius of the torus. Solid line is for $(c_\phi, c_\psi, c_{\phi\psi})$=$(0,0,0)$, dotted line for $(c_\phi, c_\psi, c_{\phi\psi})$=$(0,1,0)$, dashed for $(c_\phi, c_\psi, c_{\phi\psi})$=$(1,0,0)$ while dashed and dotted for $(c_\phi, c_\psi, c_{\phi\psi})$=$(1,1,0)$. For $(c_\phi, c_\psi, c_{\phi\psi})$=$(0,0,1)$, the supercurrent as well as the charge condensate, are trivial. Parameters in this figure are $(g_1, g_2, g_3, e, q, u, v_1, M, N)$=$(14, 12.5, 14, 10, 2, 1, 7.5 \cdot 10^{-3}, 1, 1)$.

$|D_i\psi|^4$, then $F$ exhibits no change while the charge condensate $P$ decreases (dotted line in fig.6.2). In this case, the consequence is the reduction of the supercurrent (dotted line in fig.6.3) when compared to the case of the original model without extra terms ($(c_\phi, c_\psi, c_{\phi\psi}) = (0,0,0)$, see solid line in fig.6.3). On the other hand, when the extra term is $|\tilde{D}_i\phi|^4$, then $F$ widens and this leads to the broadening of $P$ as well. The latter increases (compare dashed and solid lines of fig.6.2) and the supercurrent increases too (dashed line of fig.6.3). Finally, when the extra term is $|\tilde{D}_i\phi|^2|D_i\psi|^2$, then $P = 0$ for the values of $g_2$ we use. In general, the charge condensate can be non-trivial for higher $g_2$. This happens due to the term $g_2(P^2 - u^2)^2/4$ of the potential. When $g_2$ grows, $P$ tends to reach $u$. This is also numerically observed.

One can combine two extra terms to see what happens. In example, we add both $|\tilde{D}_i\phi|^4$ and $|D_i\psi|^4$, (case $(c_\phi, c_\psi, c_{\phi\psi})$=$(1,1,0)$ in fig.6.2). This results to the addition of the "favorable" $F$-derivative terms, but also $P$-derivative terms would be present. This translates to the growth of $P$ but not as much as in the case $(c_\phi, c_\psi, c_{\phi\psi})$=$(1,0,0)$. We also observed that the combination of either $|\tilde{D}_i\phi|^4$ or $|D_i\psi|^4$ or even both, with the $|\tilde{D}_i\phi|^2|D_i\psi|^2$ term, leads to shrinking of $P$ because of the strong effect of the last term. After the theoretical and numerical analysis, we conclude that the most "interesting" extra term is $|\tilde{D}_i\phi|^4$.

It is clear that current quenching is present here as well (fig.6.3). The extra term $|\tilde{D}_i\phi|^4$, can increase the supercurrent and can make the penetration of the magnetic field more difficult, as the string increases its diameter, but this increase is not enough in order for the ring to stabilize. For the shake of research, we also tried higher values of $c_\phi$ in order to make the favorable term more significant. We also tried higher values of $e$, but the ring could not stabilize in a non-trivial radius.

## 6.5 Discussion

The most crucial terms of the energy functional which could provide for the stability of the ring in a non-zero radius $a$, are:

$$\begin{aligned} A &= \int_0^\infty \rho d\rho \int_{-\infty}^\infty dz \ \frac{B_A^2}{2} = \int_0^\infty \rho d\rho \int_{-\infty}^\infty dz \ \frac{1}{2\rho^2}\Big((\partial_\rho A_\varphi)^2 + (\partial_z A_\varphi)^2\Big) \\ B &= \int_0^\infty \rho d\rho \int_{-\infty}^\infty dz \ \frac{P^2}{\rho^2}(eA_\varphi + N)^2 \end{aligned}$$

These two terms have an explicit total $1/\rho$ behavior which helps them to increase as the torus radius decreases. The problem is that they are not increasing at a satisfactory rate in order to overcome all the rest terms of the energy which are decreasing with $\rho$. This is also numerically observed. Under some radius $a$, the ideal would be to have a strongly increasing charge condensate $P$. Then, as the radius decreases and at the same time $P$ increases, the above two terms would start to increase with sufficient rate in order to lift the energy of the system. The magnetic term would increase because as $P^2/\rho^2$ increases, $|A_\varphi| \to |A_{\varphi_{\mathbf{max}}}| \to N/e$. The latter would make the derivatives of $A_\varphi$ (and $B_A$ as well) to increase as $\rho$ decreases.

This is what we tried to do here, especially with the help of the $|\tilde{D}_i\phi|^4$ extra term. The charge condensate became more robust but that was not enough. This supports the conclusion of [90] which states that very high values of supercurrent are needed for stabilization. It seems that such highly increasing currents can not be produced, despite the help of extra terms. In fact, numerical details reveal that the rate of increase of the terms $A, B$ above, is $\Delta(A+B) \sim 10^{-3}$, while the rate of decrease of all the rest terms is $\Delta(E-(A+B)) \sim 3{\cdot}10^{-2}$. This means that the rate of increase of $A, B$ should be $\sim$ 30 times bigger. That case would require $P \geq u$ which is something that does not seem to satisfy $I_5 + I_6 = 0$ virial relation. But even if that was possible, current quenching would be another "obstacle".

## 6.6 Conclusions

We are based on the model of [90] (the previous chapter) and analyze an extended version of it, by adding higher derivative terms in order to check whether they can stabilize the superconducting ring or not. Although the $|\tilde{D}_i\phi|^4$ term is helpful on that direction, it turns out to be insufficient and current quenching prevails. Finally, we discuss what one would need for a stable ring. This discussion in combination with the results of [90], seems to exclude the possibility of existence of such vortex rings in this model.

# Chapter 7

# Conclusions

## 7.1 Conclusions

Bosonic superconducting cosmic strings and solitons were the main subject of research in this Thesis. Firstly, we examined a Goldstone model for antiperiodic solitons on $S^1$. An analytical study as well as stability analysis are performed. Classically stable solitons were identified. Such model can be connected and can give us the experience to deal with realistic particle physics models in our search for possible metastable localized solitons.

Then, a detailed numerical search for bosonic superconducting straight strings in a $U(1)$ model with Ginzburg-Landau potential with a cubic term added to it, is done. Such strings exist in a small, numerically determined region. We fully analyze and explain the reasons of stability there, as well as the reasons of instability in the rest of the parameter space. Such models can be found in Condensed Matter Physics as well. On the other hand, this model can provide the basis for searching torus-shaped solitons in the framework of High-Energy Physics.

The stable strings of the above $U(1)$ model though, are not necessarily stable while forming a torus. Thus, we worked in a $U(1) \times U(1)$ model which admits straight bosonic superconducting strings due to topological reasons. We cut a piece out of these strings in order to create a torus and examine its stability. We performed a detailed numerical study which showed that such solitons seem to be unstable. An explanation concerning this instability is given with the help of theoretical predictions about current quenching as well. There are strong indications that current quenching is the main reason of instability.

After the above conclusion, we searched further the model by extending it. We add higher derivative terms which could be in favor of stability of this vortex ring. We analyze and explain our expectations. Despite the fact that the results are improved, we again have non-stable objects. We discuss the reason for this and explain what it would be necessary for stability. Out of this discussion, the conclusion which states that these objects are unstable, is strongly supported. Current quenching seems to be the obstacle, while there are indications that the vortex rings of this theory, need some specific extreme conditions in order to be stable. Conditions which can *not* be satisfied by the $U(1) \times U(1)$ model we examined, even if current quenching phenomenon was absent.

LHC experiments, which are about to start in early 2008, can answer whether metastable particle-like solitons exist in MSSM or 2HSM. In the framework of 2HSM, the existence of spherically symmetric solitons was examined but the result was negative. The next step was to search for the possibility of the existence of axially symmetric solitons with mass of the order of TeV. The confirmation or rejection of the existence of such solitons, would be a very interesting, important as well as urgent task, since LHC will start working in a few months in a very promising energy range. The work appeared in this Thesis, gives an answer and completes the above mentioned search on solitons with axial symmetry.

Apart from this, search for such solitons can be done in other models with higher symmetries or extended models [92]-[96]. Experimental condensed matter physics is another branch where these gauge theories can apply. Some examples can be found in [3]-[12] and [100, 101]. On the other hand, such theories can give detailed and useful hints for cosmological observation of strings in general and of loops in particular [27]-[31], [64]-[80], [83], [118]-[120]. Finally, another interest comes from the recent developments in Superstring theory. In the framework of large extra dimensions, long superstrings may be stable and appear at the same energy scale as GUT scale cosmic strings. More can be found in [81, 82], [129]-[133].

# PART III

## NUMERICAL METHODS

In this part, we present details of the numerical methods used in models of Part I. Then, we present full details of the algorithm we finally chose for our research in Part II. We tested the algorithms on models with known solutions such as, the Nielsen-Olesen vortex and the straight superconducting string. Newton-Raphson and energy minimization were comparatively easier to handle, while the latter was faster and quite helpful as it concerns the physics of the model and for that reason we chose it for our research.

# Chapter 8

# Summary of the algorithms used

## 8.1 Relaxation

- *How it works*

In relaxation methods, ODE's (Ordinary Differential Equations) are replaced by approximate FDE's (Finite-Difference Equations) on a grid or mesh of points that fills the domain of interest. The general rule is:

$$\frac{dy}{dx} \to \frac{y_k - y_{k-1}}{h}, \quad (x, y) \to \Big(\frac{x_k + x_{k-1}}{2}, \frac{y_k + y_{k-1}}{2}\Big) \tag{8.1}$$

where $h = (x_{max} - x_{min})/N$ and $N$ stands for the number of points used to divide the region we are interested in. In other words it is the step on $x$-axis. The information the algorithm needs as input in order to start computing the final configuration of fields are, the initial and final conditions as well as an initial guess for the solution. It is important to have an, as good as possible, initial guess. This can be done by using the results of an asymptotical analysis on the behavior of the differential equations around $x_{min}$ and $x_{max}$. An iterative process is used and the initial guess improves step by step, while every next step uses the improved configuration produced by the previous one. Finally, the result is said to relax to the true solution.

- *Concluding remarks for Relaxation*

The satisfactory output for Nielsen-Olesen was created after many difficulties since the algorithm was very sensitive on very small changes of the boundary conditions. This had effect on the model of superconducting bosonic string where the method did not led us to a satisfactory result. In general this algorithm was not easy to use and it's not efficient [104] especially in problems which have solutions with oscillatory parts. We continue by working with Runge-Kutta.

## 8.2 Runge-Kutta

- *How it works*

This method advances a solution from $x_n$ to $x_{n+1} \equiv x_n + h$ through the formula $y_{n+1} = y_n + h\, f(x_n, y_n)$. User supplies the code with the initial boundary conditions only. This means that the values of $y_{x_{min}}$ and its derivative at that point are necessary. The ”core” of the code of a fourth-order Runge-Kutta method follows:

$$
\begin{aligned}
k_1 &= h\, f(x_n, y_n) && (8.2)\\
k_2 &= h\, f\Big(x_n + \frac{h}{2}, y_n + \frac{k_1}{2}\Big) && (8.3)\\
k_3 &= h\, f\Big(x_n + \frac{h}{2}, y_n + \frac{k_2}{2}\Big) && (8.4)\\
k_4 &= h\, f(x_n + h, y_n + k_3) && (8.5)\\
y_{n+1} &= y_n + \frac{k_1}{6} + \frac{k_2}{3} + \frac{k_3}{3} + \frac{k_4}{6} + \mathcal{O}(h^5) && (8.6)
\end{aligned}
$$

which means that every step $h$ involves four evaluations of the right hand side as one can see. Apart from that, we also used the fifth-order Runge-Kutta method in order to achieve greater accuracy although our problems involve smooth functions, thus one could support that it might not be necessary. The ”core” of the fifth-order Runge-Kutta method is presented below:

$$
\begin{aligned}
k_1 &= h\, f(x_n, y_n) && (8.7)\\
k_2 &= h\, f(x_n + a_2 h, y_n + b_{21} k_1) && (8.8)\\
k_3 &= h\, f(x_n + a_3 h, y_n + b_{31} k_1 + b_{32} k_2) && (8.9)\\
k_4 &= h\, f(x_n + a_4 h, y_n + b_{41} k_1 + b_{42} k_2 + b_{43} k_3) && (8.10)\\
k_5 &= h\, f(x_n + a_5 h, y_n + b_{51} k_1 + b_{52} k_2 + b_{53} k_3 + b_{54} k_4) && (8.11)\\
k_6 &= h\, f(x_n + a_6 h, y_n + b_{61} k_1 + b_{62} k_2 + b_{63} k_3 + b_{64} k_4 + b_{65} k_5) && (8.12)\\
y_{n+1} &= y_n + c_1 k_1 + c_2 k_2 + c_3 k_3 + c_4 k_4 + c_5 k_5 + c_6 k_6 + \mathcal{O}(h^6) && (8.13)
\end{aligned}
$$

where $a_i,\ b_{ij},\ c_i$ are the Cash-Karp parameters and can be found on page 717 of [104].

- *Concluding remarks for Runge-Kutta*

Runge-Kutta was easier to use in comparison to Relaxation but the results were poor in the “test”-models we tried to use it. Thus, we proceed on Newton-Raphson and energy minimization algorithms.

## 8.3 Newton-Raphson

- *How it works*

The algorithm that follows, was created in 2004, in collaboration with Dr. E.D.M.Kavoussanaki.

Suppose a differential equation written in the form of matrices: $A{\cdot}x = B$, where $A$ is a $N \times N$ matrix, $x$ is a $N \times 1$ matrix of the unknown function and $B$ is a $N \times 1$ matrix as well. In that formulation, the solution of a differential equation involves is the root of the function $F = A \cdot x - B$. This means $F(x_{new}) = 0$, where *new* means the matrix $x$ after an iteration. Thus $F(x_{new}) = F(x_{old}) + F'(x_{old})(x_{new} - x_{old}) + \cdots$, which is in fact a Taylor expansion where terms beyond linear are considered unimportant. Solving in terms of $\delta = x_{new} - x_{old}$, we have:

$$\delta = -\frac{F(x_{old})}{F'(x_{old})} \tag{8.14}$$

where the prime denotes differentiation with respect to $x$. The above equation is the correction to our initial guess $x$ and iteratively leads us to the solution. Practically, one does the following steps:

(i) **Write the equation**. In our case we have second-order differential equations. The derivatives are replaced in the following way:

$$x' \rightarrow \frac{x_{k+1} - x_{k-1}}{2h}, \quad x'' \rightarrow \frac{x_{k+1} + x_{k-1} - 2x_k}{h^2} \tag{8.15}$$

(ii) **Write matrices $A$ and $B$**. In this case, matrix $A$ is tri-diagonal. $B$ is initially zero unless the equation is non-homogeneous with respect to $x$. Otherwise, it contains these non-homogeneous terms. If the equation is non-linear, then $A = A_L + A_{NL}$, where $L$ and $NL$ stands for Linear an Non-Linear respectively.

(iii) **Compute the inverse of the Jacobian of $A$**. A general formula for the calculation of the Jacobian of a matrix is:

$$J_{ij} = \frac{\partial F_i}{\partial x_j} \tag{8.16}$$

The Jacobian, and its inversion can also be done at once with *clapack* [1] routine package in order to achieve greater efficiency [2].

---

[1] More information at www.netlib.org

[2] In fact it was observed that by using this package, the program needed at most 1/3 of the time it needed before in order to run. The difference was greater by increasing the grid points.

(iv) **Compute correction**. The above step does the correction and this is added to our initial guess in the first iteration. Thus, our initial guess is improved in every iteration.

(v) **Find solution**. When the correction $\delta$ becomes smaller than a user-defined small value, the program stops and we get the numerical solution.

- *Concluding remarks for Newton-Raphson*

This method, as one can observe in Part I, is one of the two methods which gives satisfactory results on both models described there. A result is satisfactory when we have proofs [3] that we found the solution, such as the appropriate asymptotics, the satisfaction of the equations of motion/field equations and of virial theorem. Apart from this, other advantages of this algorithm is the relatively short time it took us to get the results shown for both "test-models" and it is also the fact that it is relatively easy (compared with Relaxation and Runge-Kutta) to use.

## 8.4 Energy minimization

- *How it works*

The general idea is this. Suppose the energy functional of a model of interest. This can involve two or more functions of one or more variables. One can start with an initial guess for these functions approximating the true solution. A standard minimization algorithm such as the one we used, adds a correction to the fields but having as a criterion that every such step will reduce the energy functional value. Thus, it is called energy minimization. The output is a field configuration for which the energy functional value is minimum. The algorithm needs as input the function as well as the derivative of that function at every point.

Details of the specific algorithm can be found on page 428 of [104]. There are used two subroutines, the first of them called DFPMIN which has as target to find the so-called “Newton” direction which is a direction that makes the value of the energy smaller. Then, after this direction is calculated, subroutine LNSRCH is called and finds an appropriate step of correction for every point of every function on the "Newton" direction. When the correction is done, DFPMIN calculates a new "Newton" direction based on the new corrected data. When the corrections are smaller than the machine tolerance ($\approx 10^{-8}$) or the derivative of our function is very small then we are on a minimum.

---

[3] In Part I, one can find in detail, explanation of ways of how to check if a final configuration is the solution of a system of differential equations, with the help of virial relations.

To determine the next iteration point in this algorithm we do the following: Consider finding a minimum by using Newton's method to search for a zero on the gradient of the function. Near the current point $\mathbf{x}_i$ we have to second order:

$$f(\mathbf{x}) = f(\mathbf{x}_i) + (\mathbf{x} - \mathbf{x}_i) \cdot \nabla f(\mathbf{x}_i) + \frac{1}{2}(\mathbf{x} - \mathbf{x}_i) \cdot \mathbf{A} \cdot (\mathbf{x} - \mathbf{x}_i) \tag{8.17}$$

so

$$\nabla f(\mathbf{x}) = \nabla f(\mathbf{x}_i) + \mathbf{A} \cdot (\mathbf{x} - \mathbf{x}_i) \tag{8.18}$$

In Newton's method we set $\nabla f(\mathbf{x}) = 0$ to determine the next iteration step and finally we have:

$$\mathbf{x}_{i+1} = \mathbf{x}_i + \mathbf{A}^{-1} \cdot (\nabla f(\mathbf{x}_{i+1}) - \nabla f(\mathbf{x}_i)) \tag{8.19}$$

The DFPMIN subroutine provides the appropriate formulas for calculating $\mathbf{A}^{-1}$. One can find more details on p.428 of [104].

- *Numerical details*

A point we need to mention here is that one has to be very careful when inserting the derivatives (below denoted as $g_i$) of functions (below denoted as $p_i$) such as the one we have in our model. One must write down explicitly the first two or three terms of the double sum which constitutes our energy functional, as well as the last two in order to see the sequence of appearance of $p_i$ in order to compute the relevant $g_i$. Then, we choose the variable of differentiation and gather the terms which include that variable in order to find the derivative. In numerical language, the notion of the term "variable" is not necessarily the same as in mathematical language.

In this model, as we have five functions of two variables, we firstly have to divide the $\rho$-coordinate which has $n$ points, into five parts representing the functions: $1 \rightarrow k_1$ for $F$, $k_1 + 1 \rightarrow k_2$ for $P$, $k_2 + 1 \rightarrow k_3$ for $A_\varphi$, $k_3 + 1 \rightarrow k_4$ for $W_\rho$ and $k_4 + 1 \rightarrow n$ for $W_z$. We also have to divide the $z$-coordinate in, say, $n_z$ points. Because of the fact that now we have derivatives of these functions also in the $z$-direction we have to find a way to connect a point of a function in $z_{ii}$ level with the same point in the $z_{ii_+}$ level. Well, according to our formulation, this happens when we add $n$ to the index of a point. Thus, if $i$ is for $\rho$ and $ii$ is for $z$, then we can represent a derivative of a function $f$ in $z$ direction as

$$\frac{df}{dz} = \frac{f[i+n] - f[i]}{h_z} \tag{8.20}$$

with

$$h_z = \frac{z_{max} - z_{min}}{n_z} \tag{8.21}$$

Also, differentiation of $f$ with respect to $\rho$ is

$$\frac{df}{d\rho} = \frac{f[i+1] - f[i]}{h_\rho} \tag{8.22}$$

with

$$h_\rho = \frac{\rho_{max} - \rho_{min}}{n} \tag{8.23}$$

In the formulation below, for simplicity, we represent with $ii_+$ the next $z$ level and with $ii_-$ the previous $z$ level. For example if we are at $z = d$ level then $ii = d \cdot n$ and $ii_+ = (d+1) \cdot n$, while $ii_- = (d-1) \cdot n$, where $d$ an integer. The energy functional in numerical language, follows:

$$\begin{aligned}
\mathbf{E}_{\mathbf{i:\,1\to k_1-1,\;\; ii:\,0\to n(z_{max}-1)}} = 2\pi v_1 h_\rho h_z \rho_i \Bigg[ \frac{1}{2\rho_i^2} \Bigg( \left( \frac{p_{k_2+i+1+ii} - p_{k_2+i+ii}}{h_\rho} \right)^2 + \\
+ \left( \frac{p_{k_2+i+ii_+} - p_{k_2+i+ii}}{h_z} \right)^2 \Bigg) + \frac{1}{2} \Bigg( \frac{p_{k_4+i+1+ii} - p_{k_4+i+ii}}{h_\rho} - \\
- \frac{p_{k_3+i+ii_+} - p_{k_3+i+ii}}{h_z} \Bigg)^2 + \\
+ \left( \frac{p_{k_1+i+1+ii} - p_{k_1+i+ii}}{h_\rho} \right)^2 + \left( \frac{p_{k_1+i+ii_+} - p_{k_1+i+ii}}{h_z} \right)^2 + \\
+ \left( \frac{p_{i+1+ii} - p_{i+ii}}{h_\rho} \right)^2 + \left( \frac{p_{i+ii_+} - p_{i+ii}}{h_z} \right)^2 + \frac{p_{k_1+i+ii}^2}{\rho_i^2} \Big( e p_{k_2+i+ii} + N \Big)^2 + \\
+ \left[ \left( q p_{k_3+i+ii} - M \frac{z_{ii} cos^2\Theta}{(\rho_i - a)^2} \right)^2 + \left( q p_{k_4+i+ii} + M \frac{cos^2\Theta}{\rho_i - a} \right)^2 \right] p_{i+ii}^2 + \\
+ \frac{g_1}{4} \Big( p_{i+ii}^2 - 1 \Big)^2 + \frac{g_2}{4} \Big( p_{k_1+i+ii}^2 - u^2 \Big)^2 + \frac{g_3}{2} p_{i+ii}^2 p_{k_1+i+ii}^2 \Bigg]
\end{aligned}$$

Below we write down the derivatives of the above energy functional for every "variable". We start with the $i = 1$ level for all functions and all $z$-levels except for the first and the last one. In fact $i = 1$ means $\rho = 0$.

$$\begin{aligned}
\mathbf{g_{1+ii}} = 2\pi v_1 h_\rho h_z \rho_1 \Bigg[ & \frac{2}{h_z^2}(p_{1+ii} - p_{1+ii_-}) - \frac{2}{h_\rho^2}(p_{2+ii} - p_{1+ii}) - \frac{2}{h_z^2}(p_{1+ii_+} - p_{1+ii}) + \\
& + 2p_{1+ii}\left[\left(qp_{k_3+1+ii} - M\frac{z_{ii}cos^2\Theta}{(\rho_1 - a)^2}\right)^2 + \left(qp_{k_4+1+ii} + M\frac{cos^2\Theta}{\rho_1 - a}\right)^2\right] + \\
& + g_1(p_{1+ii}^2 - 1)p_{1+ii} + g_3 p_{1+ii} p_{k_1+1+ii}^2 \Bigg]
\end{aligned}$$

$$\begin{aligned}
\mathbf{g_{k_1+1+ii}} = 2\pi v_1 h_\rho h_z \rho_1 \Bigg[ & \frac{2}{h_z^2}(p_{k_1+1+ii} - p_{k_1+1+ii_-}) - \frac{2}{h_\rho^2}(p_{k_1+2+ii} - p_{k_1+1+ii}) - \\
& - \frac{2}{h_z^2}(p_{k_1+1+ii_+} - p_{k_1+1+ii}) + \\
& + \frac{2}{\rho_1^2}p_{k_1+1+ii}(ep_{k_2+1+ii} + N)^2 + g_2\left(p_{k_1+1+ii}^2 - u^2\right)p_{k_1+1+ii} + g_3 p_{1+ii}^2 p_{k1+1+ii} \Bigg]
\end{aligned}$$

$$\begin{aligned}
\mathbf{g_{k_2+1+ii}} = 2\pi v_1 h_\rho h_z \rho_1 \Bigg[ & \frac{1}{2\rho_1^2}\Bigg( - \frac{2}{h_\rho^2}(p_{k_2+2+ii} - p_{k_2+1+ii}) - \\
& - \frac{2}{h_z^2}(p_{k_2+1+ii_+} - p_{k_2+1+ii}) + \\
& + \frac{2}{h_z^2}(p_{k_2+1+ii} - p_{k_2+1+ii_-})\Bigg) + \frac{2ep_{k_1+1+ii}^2}{\rho_1^2}(ep_{k_2+1+ii} + N) \Bigg]
\end{aligned}$$

$$\begin{aligned}
\mathbf{g_{k_3+1+ii}} = 2\pi v_1 h_\rho h_z \rho_1 \Bigg[ & \frac{1}{h_z}\left(\frac{p_{k_4+2+ii} - p_{k_4+1+ii}}{h_\rho} - \frac{p_{k_3+1+ii_+} - p_{k_3+1+ii}}{h_z}\right) - \\
& - \frac{1}{h_z}\left(\frac{p_{k_4+2+ii_-} - p_{k_4+1+ii_-}}{h_\rho} - \frac{p_{k_3+1+ii} - p_{k_3+1+ii_-}}{h_z}\right) + \\
& + 2qp_{1+ii}^2\left(qp_{k_3+1+ii} - M\frac{z_{ii}cos^2\Theta}{(\rho_1 - a)^2}\right) \Bigg]
\end{aligned}$$

$$\begin{aligned}
\mathbf{g_{k_4+1+ii}} = 2\pi v_1 h_\rho h_z \rho_1 \Bigg[ & - \frac{1}{h_\rho}\left(\frac{p_{k_4+2+ii} - p_{k_4+1+ii}}{h_\rho} - \frac{p_{k_3+1+ii_+} - p_{k_3+1+ii}}{h_z}\right) + \\
& + 2qp_{1+ii}^2\left(qp_{k_4+1+ii} + M\frac{cos^2\Theta}{\rho_1 - a}\right) \Bigg]
\end{aligned}$$

The derivatives of all functions on all the $\rho$ and $z$ levels apart from the first and the last level follow.

$$
\begin{aligned}
\mathbf{g}_{(\mathbf{i}:\ \mathbf{2}\to\mathbf{k_1-1})\ \ \mathbf{i+ii}} &= 2\pi v_1 h_\rho h_z \rho_{i-1}\left[\frac{2}{h_\rho^2}(p_{i+ii}-p_{i-1+ii})\right]+\\
&+2\pi v_1 h_\rho h_z \rho_i \Bigg[\frac{2}{h_z^2}(p_{i+ii}-p_{i+ii_-})-\frac{2}{h_\rho^2}(p_{i+1+ii}-p_{i+ii})-\frac{2}{h_z^2}(p_{i+ii_+}-p_{i+ii})+\\
&+2p_{i+ii}\left[\left(qp_{k_3+i+ii}-M\frac{z_{ii}cos^2\Theta}{(\rho_i-a)^2}\right)^2+\left(qp_{k_4+i+ii}+M\frac{cos^2\Theta}{\rho_i-a}\right)^2\right]+\\
&+g_1(p_{i+ii}^2-1)p_{i+ii}+g_3p_{i+ii}p_{k_1+i+ii}^2\Bigg]
\end{aligned}
$$

$$
\begin{aligned}
\mathbf{g}_{(\mathbf{i}:\ \mathbf{2}\to\mathbf{k_1-1}),\ \ \mathbf{k_1+i+ii}} &= 2\pi v_1 h_\rho h_z \rho_{i-1}\left[\frac{2}{h_\rho^2}(p_{k_1+i+ii}-p_{k_1+i-1+ii})\right]+\\
&+2\pi v_1 h_\rho h_z \rho_i \Bigg[\frac{2}{h_z^2}(p_{k_1+i+ii}-p_{k_1+i+ii_-})-\frac{2}{h_\rho^2}(p_{k_1+i+1+ii}-p_{k_1+i+ii})-\\
&-\frac{2}{h_z^2}(p_{k_1+i+ii_+}-p_{k_1+i+ii})+\\
&+\frac{2}{\rho_i^2}p_{k_1+i+ii}(ep_{k_2+i+ii}+N)^2+g_2\left(p_{k_1+i+ii}^2-u^2\right)p_{k_1+i+ii}+g_3p_{i+ii}^2p_{k_1+i+ii}\Bigg]
\end{aligned}
$$

$$
\begin{aligned}
\mathbf{g}_{(\mathbf{i}:\ \mathbf{2}\to\mathbf{k_1-1}),\ \ \mathbf{k_2+i+ii}} &= 2\pi h_\rho h_z \rho_{i-1}\left[\frac{1}{2\rho_{i-1}^2}\left(\frac{2}{h_\rho^2}(p_{k_2+i+ii}-p_{k_2+i-1+ii})\right)\right]+\\
&+2\pi v_1 h_\rho h_z \rho_i \Bigg[\frac{1}{2\rho_i^2}\Bigg(-\frac{2}{h_\rho^2}(p_{k_2+i+1+ii}-p_{k_2+i+ii})-\frac{2}{h_z^2}(p_{k_2+i+ii_+}-p_{k_2+i+ii})+\\
&+\frac{2}{h_z^2}(p_{k_2+i+ii}-p_{k_2+i+ii_-})\Bigg)+\frac{2ep_{k_1+i+ii}^2}{\rho_i^2}(ep_{k_2+i+ii}+N)\Bigg]
\end{aligned}
$$

$$\begin{aligned}\mathbf{g_{(i:\,2\rightarrow k_1-1),\ k_3+i+ii}} = 2\pi v_1 h_\rho h_z \rho_i \Bigg[ \frac{1}{h_z}\Bigg( & \frac{p_{k_4+i+1+ii}-p_{k_4+i+ii}}{h_\rho} - \\ & - \frac{p_{k_3+i+ii_+}-p_{k_3+i+ii}}{h_z}\Bigg) - \\ - \frac{1}{h_z}\Bigg(\frac{p_{k_4+i+1+ii_-}-p_{k_4+i+ii_-}}{h_\rho} - \frac{p_{k_3+i+ii}-p_{k_3+i+ii_-}}{h_z}\Bigg) & + \\ + 2qp^2_{i+ii}\Bigg(qp_{k_3+i+ii} - M\frac{z_{ii}cos^2\Theta}{(\rho_i-a)^2}\Bigg)\Bigg] &\end{aligned}$$

$$\begin{aligned}\mathbf{g_{(i:\,2\rightarrow k_1-1),\ k_4+i+ii}} = 2\pi v_1 h_z \rho_{i-1} \Bigg[\Bigg( & \frac{p_{k_4+i+ii}-p_{k_4+i-1+ii}}{h_\rho} - \\ & - \frac{p_{k_3+i-1+ii_+}-p_{k_3+i-1+ii}}{h_z}\Bigg)\Bigg] - \\ 2\pi v_1 h_\rho h_z \rho_i \Bigg[\frac{1}{h_\rho}\Bigg(\frac{p_{k_4+i+1+ii}-p_{k_4+i+ii}}{h_\rho} - \frac{p_{k_3+i+ii_+}-p_{k_3+i+ii}}{h_z}\Bigg) & + \\ + 2qp^2_{i+ii}\Bigg(qp_{k_4+i+ii} + M\frac{cos^2\Theta}{\rho_i-a}\Bigg)\Bigg] &\end{aligned}$$

The derivatives of all functions on the last $\rho$ level and all $z$ levels apart from the first and the last level follow.

$$\mathbf{g_{k_1+ii}} = 2\pi v_1 h_\rho h_z \rho_{k_1-1}\Bigg[\frac{2}{h_\rho^2}(p_{k_1+ii}-p_{k_1-1+ii})\Bigg]$$

$$\mathbf{g_{k_2+ii}} = 2\pi v_1 h_\rho h_z \rho_{k_1-1}\Bigg[\frac{2}{h_\rho^2}(p_{k_2+ii}-p_{k_2-1+ii})\Bigg]$$

$$\mathbf{g_{k_3+ii}} = 2\pi v_1 h_\rho h_z \rho_{k_1-1}\Bigg[\frac{1}{2\rho_{k_1-1}^2}\Bigg(\frac{2}{h_\rho^2}(p_{k_3+ii}-p_{k_3-1+ii})\Bigg)\Bigg]$$

$$\mathbf{g_{k_4+ii}} = 0$$

$$\mathbf{g_{n+ii}} = 2\pi v_1 h_z \rho_{k_1-1}\Bigg[\Bigg(\frac{p_{n+ii}-p_{n-1+ii}}{h_\rho} - \frac{p_{k_4-1+ii_+}-p_{k_4-1+ii}}{h_z}\Bigg)\Bigg]$$

The derivatives of all functions on all the $\rho$ levels apart from the first and the last level and the $ii = 0$ level follow. The $ii = 0$ level is in fact the $z = -z_0$.

$$\begin{aligned}
\mathbf{g}_{(\mathbf{i}:\ \mathbf{2}\to\mathbf{k_1-1}),\ \mathbf{i+0}} &= 2\pi v_1 h_\rho h_z \rho_{i-1}\left[\frac{2}{h_\rho^2}(p_{i+0}-p_{i-1+0})\right]+\\
&+ 2\pi v_1 h_\rho h_z \rho_i \Bigg[-\frac{2}{h_z^2}(p_{i+ii_+}-p_{i+0})-\frac{2}{h_\rho^2}(p_{i+1+0}-p_{i+0})+\\
&+2p_{i+0}\left(\left(qp_{k_3+i+0}-\frac{Mz\cos^2\Theta}{(\rho_i-a)^2}\right)^2+\left(qp_{k_4+i+0}-\frac{M\cos^2\Theta}{\rho_i-a}\right)^2\right)+\\
&+g_1p_{i+0}\left(p_{i+0}^2-1\right)+g_3p_{i+0}p_{k_1+i+0}^2\Bigg]
\end{aligned}$$

$$\begin{aligned}
\mathbf{g}_{(\mathbf{i}:\ \mathbf{2}\to\mathbf{k_1-1}),\ \mathbf{k_1+i+0}} &= 2\pi v_1 h_\rho h_z \rho_{i-1}\left[\frac{2}{h_\rho^2}(p_{k_1+i+0}-p_{k_1+i-1+0})\right]+\\
&+ 2\pi v_1 h_\rho h_z \rho_i \Bigg[-\frac{2}{h_\rho^2}(p_{k_1+i+1+0}-p_{k_1+i+0})-\frac{2}{h_z^2}(p_{k_1+i+ii_+}-p_{k_1+i+0})+\\
&+\frac{2p_{k_1+i+0}}{\rho_i^2}(ep_{k_2+i+0}+N)^2+g_2p_{k_1+i+0}\left(p_{k_1+i+0}^2-u^2\right)+g_3p_{i+0}^2p_{k_1+i+0}\Bigg]
\end{aligned}$$

$$\begin{aligned}
\mathbf{g}_{(\mathbf{i}:\ \mathbf{2}\to\mathbf{k_1-1}),\ \mathbf{k_2+i+0}} &= 2\pi v_1 h_\rho h_z \rho_{i-1}\left[\frac{1}{2\rho_{i-1}^2}\left(\frac{2}{h_\rho^2}(p_{k_2+i+0}-p_{k_2+i-1+0})\right)\right]+\\
&+ 2\pi v_1 h_\rho h_z \rho_i \Bigg[\frac{1}{2\rho_i^2}\left(-\frac{2}{h_\rho^2}(p_{k_2+i+1+0}-p_{k_2+i+0})-\frac{2}{h_z^2}(p_{k_2+i+ii_+}-p_{k_2+i+0})\right)+\\
&+\frac{2ep_{k_1+i+0}^2}{\rho_i^2}(ep_{k_2+i+0}+N)\Bigg]
\end{aligned}$$

$$\begin{aligned}
\mathbf{g}_{(\mathbf{i}:\ \mathbf{2}\to\mathbf{k_1-1}),\ \mathbf{k_3+i+0}} &= 2\pi v_1 h_\rho h_z \rho_i\Bigg[\frac{1}{h_z}\Bigg(\frac{p_{k_4+i+1+0}-p_{k_4+i+0}}{h_\rho}-\\
&-\frac{p_{k_3+i+ii_+}-p_{k_3+i+0}}{h_z}\Bigg)+2qp_{i+0}^2\left(qp_{k_3+i+0}-\frac{Mz\cos^2\Theta}{(\rho_i-a)^2}\right)\Bigg]
\end{aligned}$$

$$\begin{aligned}\mathbf{g}_{(\mathbf{i}:\ \mathbf{2}\rightarrow\mathbf{k_1}-\mathbf{1}),\ \mathbf{k_4}+\mathbf{i}+\mathbf{0}} = 2\pi v_1 h_\rho h_z \rho_{i-1}\Bigg[\frac{1}{h_\rho}\Bigg(\frac{p_{k_4+i+0}-p_{k_4+i-1+0}}{h_\rho} - \\ - \frac{p_{k_3+i-1+ii_+}-p_{k_3+i-1+0}}{h_z}\Bigg)\Bigg] \\ + 2\pi v_1 h_\rho h_z \rho_i\Bigg[-\frac{1}{h_\rho}\Bigg(\frac{p_{k_4+i+1+0}-p_{k_4+i+0}}{h_\rho} - \frac{p_{k_3+i+ii_+}-p_{k_3+i+0}}{h_z}\Bigg) + \\ + 2qp_{i+0}^2\Bigg(qp_{k_4+i+0} + \frac{M\cos^2\Theta}{\rho_i - a}\Bigg)\Bigg]\end{aligned}$$

The derivatives of all functions on all the $\rho$ levels except for the last level and the last $z$ level follow. The last $z$ level $ii_{max}$ is in fact the $z = z_0$.

$$\mathbf{g}_{(\mathbf{i}:\ \mathbf{1}\rightarrow\mathbf{k_1}-\mathbf{1}),\ \mathbf{i}+\mathbf{ii_{max}}} = 2\pi v_1 h_\rho h_z \rho_i\Bigg[\frac{2}{h_z^2}(p_{i+ii_{max}} - p_{i+ii_{max-1}})\Bigg]$$

$$\mathbf{g}_{(\mathbf{i}:\ \mathbf{1}\rightarrow\mathbf{k_1}-\mathbf{1}),\ \mathbf{k_1}+\mathbf{i}+\mathbf{ii_{max}}} = 2\pi v_1 h_\rho h_z \rho_i\Bigg[\frac{2}{h_z^2}(p_{k_1+i+ii_{max}} - p_{k_1+i+ii_{max-1}})\Bigg]$$

$$\mathbf{g}_{(\mathbf{i}:\ \mathbf{1}\rightarrow\mathbf{k_1}-\mathbf{1}),\ \mathbf{k_2}+\mathbf{i}+\mathbf{ii_{max}}} = 2\pi v_1 h_\rho h_z \rho_i\Bigg[\frac{1}{2\rho_i^2}\Bigg(\frac{2}{h_z^2}(p_{k_1+i+ii_{max}} - p_{k_1+i+ii_{max-1}})\Bigg)\Bigg]$$

$$\begin{aligned}\mathbf{g}_{(\mathbf{i}:\ \mathbf{1}\rightarrow\mathbf{k_1}-\mathbf{1}),\ \mathbf{k_3}+\mathbf{i}+\mathbf{ii_{max}}} = 2\pi v_1 h_\rho h_z \rho_i\Bigg[-\frac{1}{h_z}\Bigg(\frac{p_{k_4+i+1+ii_{max-1}}-p_{k_4+i+ii_{max-1}}}{h_\rho} - \\ - \frac{p_{k_3+i+ii_{max}}-p_{k_3+i+ii_{max-1}}}{h_z}\Bigg)\Bigg]\end{aligned}$$

$$\mathbf{g}_{(\mathbf{i}:\ \mathbf{1}\rightarrow\mathbf{k_1}-\mathbf{1}),\ \mathbf{k_4}+\mathbf{i}+\mathbf{ii_{max}}} = 0$$

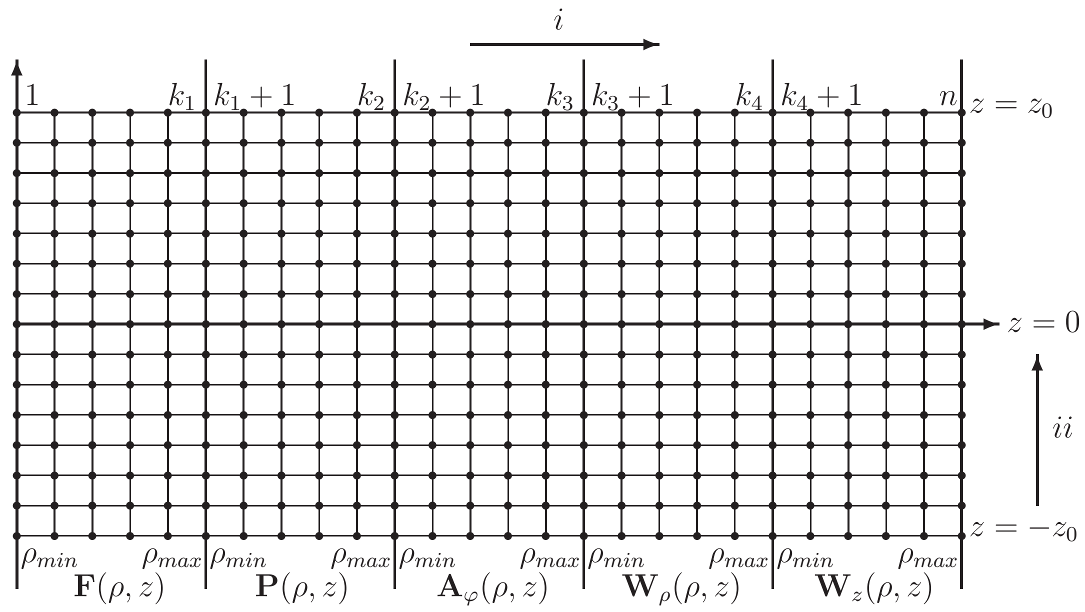

Above one can see how a grid, like the one we use, looks like. The five areas where the data points of every function are stored, is clear as well as the $\rho$ and $z$ levels. A brief diagram of the program we use follows. Subroutines DFPMIN and LNSRCH are provided by [104]. In the following diagram $\mathbf{x}$ is the matrix that has all the points of the five functions and is the matrix on which the corrections are applied until we have the final position of these points, the final configuration for the fields and the value of the total energy.

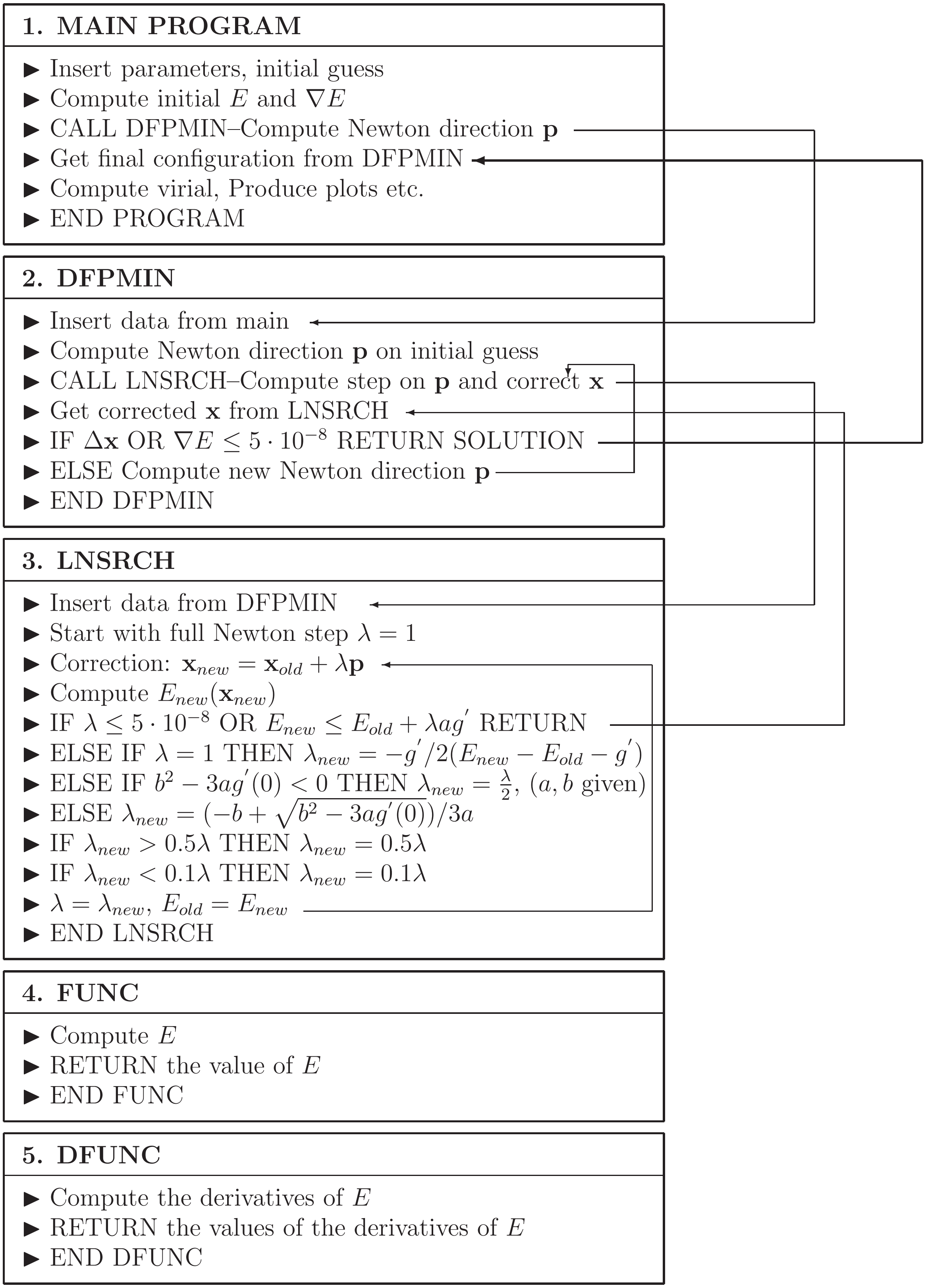

**1. MAIN PROGRAM**

- Insert parameters, initial guess
- Compute initial $E$ and $\nabla E$
- CALL DFPMIN–Compute Newton direction $\mathbf{p}$
- Get final configuration from DFPMIN
- Compute virial, Produce plots etc.
- END PROGRAM

**2. DFPMIN**

- Insert data from main
- Compute Newton direction $\mathbf{p}$ on initial guess
- CALL LNSRCH–Compute step on $\mathbf{p}$ and correct $\mathbf{x}$
- Get corrected $\mathbf{x}$ from LNSRCH
- IF $\Delta\mathbf{x}$ OR $\nabla E \leq 5 \cdot 10^{-8}$ RETURN SOLUTION
- ELSE Compute new Newton direction $\mathbf{p}$
- END DFPMIN

**3. LNSRCH**

- Insert data from DFPMIN
- Start with full Newton step $\lambda = 1$
- Correction: $\mathbf{x}_{new} = \mathbf{x}_{old} + \lambda\mathbf{p}$
- Compute $E_{new}(\mathbf{x}_{new})$
- IF $\lambda \leq 5 \cdot 10^{-8}$ OR $E_{new} \leq E_{old} + \lambda a g^{'}$ RETURN
- ELSE IF $\lambda = 1$ THEN $\lambda_{new} = -g^{'}/2(E_{new} - E_{old} - g^{'})$
- ELSE IF $b^2 - 3ag^{'}(0) < 0$ THEN $\lambda_{new} = \frac{\lambda}{2}$, $(a, b$ given)
- ELSE $\lambda_{new} = (-b + \sqrt{b^2 - 3ag^{'}(0)})/3a$
- IF $\lambda_{new} > 0.5\lambda$ THEN $\lambda_{new} = 0.5\lambda$
- IF $\lambda_{new} < 0.1\lambda$ THEN $\lambda_{new} = 0.1\lambda$
- $\lambda = \lambda_{new}$, $E_{old} = E_{new}$
- END LNSRCH

**4. FUNC**

- Compute $E$
- RETURN the value of $E$
- END FUNC

**5. DFUNC**

- Compute the derivatives of $E$
- RETURN the values of the derivatives of $E$
- END DFUNC

- *Concluding remarks for Energy minimization algorithm*

It was an algorithm which successfully generated the expected results for our test models in the shortest time and the output for every model is exhibited in the appropriate section. It is the easiest to handle, even when compared to Newton-Raphson, and the results again were multi-tested as one can see in detail. Thus, it is used in our research models and provides the solutions we found there.

# List of Figures

1.1 String intercommutation in a nemantic liquid crystal. Further details can be found in [11]. . . . . . . . . . . . . . . . . . . . . . . 15

1.2 Vortex-antivortex formation in a nematic liquid crystal. Further details can be found in [12]. . . . . . . . . . . . . . . . . . . . . . 16

1.3 Higgs field space and physical space. Above $T_c$ the potential has a minimum at $\phi_1 = 0 = \phi_2$, but below $T_c$ the new form of the potential has its minima on a circle. If $m$ is an element of the coset space $G/H$ and $\Psi_1$ and $\Psi_2$ two different states at that circle, then $m\Psi_1 = \Psi_2$. Generally, every element of the coset space $G/H$ can produce all the other minimum energy states when acting on any of them. Thus, $G/H = \mathcal{M}$ where $\mathcal{M}$ stands for the vacuum manifold. On the right side of the figure one can have a picture of how a cosmic string forms when different regions of space met, having their Higgs field phases as above. Picture from astro-ph/0303504 (A.Gangui). . . . . . . . . . . . . . . . . . . . . . . . . . . 17

1.4 Cosmic string formation. Picture from astro-ph/0303504 (A.Gangui). 18

1.5 Temperature dependent potential. Here is an example of such potential and how it changes shape as temperature falls. It is clearly visible that above $T_c$ the system has one stable minimum at $\phi_c = 0$. As $T \to 0$ the potential develops a minimum at $\phi_c \neq 0$ and when the system settles there, we say that the initial symmetry of the system is broken. The ground state of the model does not respect the original symmetry of the Lagrangian. Picture from astro-ph/0303504 (A.Gangui). . . . . . . . . . . . . . . . . . . . . 19

1.6 Apart from the intersection of two different strings (a), self-intersection of a cosmic string can be another mechanism of loop production (b). Picture from [135]. . . . . . . . . . . . . . . . . . . . . . . 22

2.1 An example of a first order phase transition. The plots are for $\beta = 2 < \beta_{crit}$, $\beta = \beta_{crit}$, $\beta = 2.2 > \beta_{crit}$. Parameter is $a = 1$. . . . . . 31

2.2 An example of a second order phase transition. The plots are for $T = \sqrt{0.5} < T_{crit}$, $T = T_{crit}$, $T = \sqrt{12} > T_{crit}$. Parameters are $\eta = 1,\ \lambda = 1$. . . . . . . . . . . . . . . . . . . . . . . . . . . 32

2.3 The magnetic field drops exponentially inside the superconductor. 35

2.4 Nielsen-Olesen string. The graph on top is the output of a relaxation program. The graph in the middle is the result of a Newton-Raphson algorithm and the bottom graph is done through energy minimization. All graphs show $f(\rho)$ and $a(\rho)$, for $n = 1,\ \lambda = 2e^2 = 4$. 42

2.5 Straight bosonic superconducting string. Both graphs on top are the output of energy minimization algorithm. Parameters are $(\bar{\lambda}, \bar{m}^2, \bar{g}^2, \bar{v}, e)$ =$(1, 0.65, 0.25, 0.75, 1)$. Bottom graphs are the output of Newton-Raphson algorithm. Parameters are $(\bar{\lambda}, \bar{m}^2, \bar{g}^2, \bar{v}, e)$ =$(1, 0.62, 0.25, 0.75, 1)$. Letter $a$ denotes the scalar field, $b$ the charge condensate and $c$ the magnetic field associated with the $a$ field. . . . . . . . . . . . . . . . . . . . . . . . . . . . . . 48

3.1 **Goldstone model:** The solutions of equations (3.25) and (3.26) are plotted as functions of $k^2$ for two values of $(n, m)$. The dashed curve indicates the limit (3.24). . . . . . . . . . . . . . . . . . 55

3.2 **Goldstone model:** The energies of some of the solutions are plotted as functions of the parameter $L$. The four stars on the upper branch indicate the four bifurcation points on the $N = 2$ type-I solution. The two lower stars indicate the two bifurcation points on the $N = 1$ type-I solution. The two numbers in parentheses refer to the number of negative and zero modes of the corresponding solution. . . . . . . . . . . . . . . . . . . . . . . . . . . . . 58

3.3 **Goldstone model:** The values (3.11) are plotted as functions of $L$ for $j = 0, 1, 2$ (solid curves), together with the values $\omega_1^2(1, 1, -1)$, $\omega_2^2(1, 0, -1)$, $\omega_3^2(1, 0, 1)$, $\omega_4^2(1, 2, -1)$, $\omega_5^2(1, 1, 1)$, $\omega_6^2(1, 3, -1)$ of (3.46) (dashed and dotted curves). The numbers indicate the multiplicity of the eigenvalues. . . . . . . . . . . . . . . . . . . . . . . . . 60

4.1 $U(1)_A$ **model:** The relative position of the supercurrent as well as of the magnetic field on a $xy$-profile of the system on the right. The left picture is strongly reminiscent of an infinite solenoid. . . . 68

4.2 $U(1)_A$ **model:** The potential for $a = 1$ and $\beta = 2$, $\beta = \beta_{crit} = \frac{3}{\sqrt{2}}$ (dashed line) and $\beta = 2.17$ (bottom line). The plot is $U$ vs. $P$. . . 69

4.3 $U(1)_A$ **model:** In the first two graphs we have the initial guess (dashed lines - - - ) as well as the final configuration of fields (solid lines — ) $P(\rho)$, $A_\varphi(\rho)$. We chose $M = 1$, $e = 1$, $\beta = 2.17$, $a = 43.7$. The energy $E = 35.3$ and virial is $10^{-4}$. The bottom graph gathers all the fields. For the field $P$, the area between the horizontal lines $P_3$ and $P_4$ is energetically favorable (see also fig.4.6). . . . . . . . 72

4.4 $U(1)_A$ **model:** In the first two graphs we have the initial guess (dashed lines - - - ) as well as the final configuration of fields (solid lines — ) $P(\rho)$, $A_\varphi(\rho)$. We chose $M = 1$, $e = 1$, $\beta = 2.13$, $a = 1104$. The energy $E = 115.2$ and virial is $2 \cdot 10^{-3}$. The bottom graph gathers all the fields. For the field $P$, the area between the horizontal lines $P_1$ and $P_2$ is energetically favorable (see also fig.4.6). . . . . . . . . . . . . . . . . . . . . . . . . . . . . . 73

4.5 $U(1)_A$ **model:** Here we have a plot in order to compare the changes of $P(\rho)$ and $B_A(\rho)$ as $a$ goes from 2.17 (dashed and dotted - · - ), to 2.15 (dashed - - - ) and 2.13 (dotted $\cdots$). . . . . . . . . . . . . 74

4.6 $U(1)_A$ **model:** The $P_+$ and $P_-$ solution of eq.(4.5), for which the potential becomes zero. Between these lines the potential gets negative values (see also fig.4.2). The plot is $P$ vs. $\beta$ for $\beta > \beta_{crit.} = \frac{3}{\sqrt{2}}$. . . . . . . . . . . . . . . . . . . . . . . . . . . . . . 76

4.7 $U(1)_A$ **model:** The plot exhibits the relation of the parameter $a$ with respect to $\beta$. We observe that as we approach the limit $\beta_{crit}$, we need an increasingly deeper minimum of the potential which is expressed through the fastly increasing value of $a$. The dashed vertical line signals the position of $\beta_{crit} = \frac{3}{\sqrt{2}}$. . . . . . . . . . . . 77

5.1 $U(1)_A \times U(1)_W$ **model:** Step 1: Infinite straight string. Step 2: Cut a piece of it. Step 3: Periodically connect its ends together to form a loop. Step 4A: Rings without current shrink due to their tension... Step 5A: ...and finally collapse. Step 4B: Superconducting vortex rings can be stabilized?... Step 5B: ... or not? . . . . . 81

5.2 $U(1)_A \times U(1)_W$ **model:** A $x - y$ profile of the superconducting ring (left) as well as a $y - z$ profile (right) where one can view how the mechanism we propose, against shrinking, works. . . . . . . . 85

5.3 $U(1)_A \times U(1)_W$ **model:** A wider view of the “Mexican hat” potential (eq.5.16) for $(g_1, g_2, u) = (10, 8, 1)$. . . . . . . . . . . . . . 87

5.4 $U(1)_A \times U(1)_W$ **model:** For different values of $\sqrt{g_1}$, we plot the lower bound over which the condition (5.20) is satisfied. The plot is $P_{max}$ vs. $e$ and we plot the function $P_{max} = \frac{\sqrt{g_1}}{e}$. . . . . . . . 88

5.5 $U(1)_A \times U(1)_W$ **model:** A typical plot of the initial guess we use for the five fields, for the lowest winding state $M = 1, N = 1$ on $z = 0$ plane. . . . . . . . . . . . . . . . . . . . . . . . . . . 94

5.6 $U(1)_A \times U(1)_W$ **model:** This is a typical picture of the toroidal soliton we are after. . . . . . . . . . . . . . . . . . . . . . . . . 94

5.7 $U(1)_A \times U(1)_W$ **model:** The profile of the torus has two identical cycles. The initial configuration of fields (plotted in fig.5.5) is the same in both of them thus, we choose to plot only the right side. . 95

5.8 $U(1)_A \times U(1)_W$ **model:** Typical plot of the final configuration of fields. Parameters are $M = 1$, $N = 1$, $e = 5$, $q = m_W = 2$, $g_1 = 14$, $m_\phi = \sqrt{g_1} = 3.74$, $g_2 = 12$, $g_3 = 14$, $u = 1$, $m_\psi = \sqrt{(g_3 - g_2 u^2)/2} = 1$, $v_1 = 7.5 \cdot 10^{-3}$. Energy $E = 0.72$ and virial is $1.5 \cdot 10^{-3}$. . . . . . . . . . . . . . . . . . . . . . . . . . . 96

5.9 $U(1)_A \times U(1)_W$ **model:** The top graph is the energy vs. the torus radius $E(a)$. The middle graph is the supercurrent $I^\psi$ vs. $a$. In that graph one can clearly see current quenching. The bottom graph is the quantity $e^2 P_{max}^2$ vs. $a$ (or $m_{\mathbf{A}}$ vs. $a$) where one can see the area in which the condition of eq.5.20 holds (lines over the $g_1$-limit line). The resistance from the magnetic field can be seen as a sharp increase on the supercurrent. Dotted lines are for $e = 6$, dashed for $e = 8$ while dashed and dotted for $e = 10$. All plots are for $(M, N, u, g_1, g_2, g_3)$=$(1, 1, 1, 14, 12.5, 14)$. . . . . . . . . . . . 97

5.10 $U(1)_A \times U(1)_W$ **model:** The top graph is the energy vs. the torus radius $E(a)$. The middle graph is the supercurrent $I^\psi$ vs. $a$. In that graph one can clearly see current quenching. The bottom graph is the quantity $e^2 P_{max}^2$ vs. $a$ (or $m_{\mathbf{A}}$ vs. $a$) where one can see the area in which the condition of eq.5.20 holds (lines over the $g_1$-limit line). The resistance from the magnetic field can be seen as a sharp increase on the supercurrent. Dotted lines are for $g_2 = 12$, dashed for $g_2 = 12.5$ while dashed and dotted for $g_2 = 13$. All plots are for $(M, N, u, e, g_1, g_3)$=$(1, 1, 1, 6, 14, 14)$. . . . . . . . . 98

5.11 $U(1)_A \times U(1)_W$ **model:** The plot of the energy of the system vs. the radius of the torus for four different sets of parameters. Dotted is for $(g_1, g_2, g_3)$= $(14, 12.5, 14)$, dashed is for $(18, 15, 18)$, dashed and dotted is for $(25, 20, 25)$ while dashed with two dots is for $(30, 24, 30)$. For all data sets we have $(e, M, N, u)$=$(10, 1, 1, 1)$. As one can observe, there exists no minimum. . . . . . . . . . . . 99

5.12 $U(1)_W$ **model:** Profiles for the scalar field $F(\rho, z)$ on the left and for the magnetic field $B_W$ on the right side, for three random values of $a$. On the bottom graph there is the energy vs. radius of the torus $a$. Parameters are $(M, m_\phi, m_W, v_1)$=$(1, 4.47, 2, 0.01)$. Black solid line is for $z = 0$. . . . . . . . . . . . . . . . . . . . . . . . . 101

5.13 $U(1)_A \times U(1)_W$ **model:** Typical plot of the final configuration of fields. Solid line: $z = 0$, dotted line: $z = 0.6$, dashed line: $z = 1.2$, dashed and dotted line: $z = 1.8$. Parameters are $M = 1$, $N = 1$, $e = 5$, $q = m_W = 2$, $g_1 = 14$, $m_\phi = \sqrt{g_1} = 3.74$, $g_2 = 12$, $g_3 = 14$, $u = 1$, $m_\psi = \sqrt{(g_3 - g_2 u^2)/2} = 1$, $v_1 = 7.5{\cdot}10^{-3}$. Energy $E = 0.72$ and virial is $1.5 \cdot 10^{-3}$. . . . . . . . . . . . . . . . . . . . . . . . . 106

6.1 **Extended** $U(1)_A \times U(1)_W$ **model:** A typical plot of the initial guess we use, for the lowest winding state $M = 1, N = 1$ on $z = 0$ plane. . . . . . . . . . . . . . . . . . . . . . . . . . . . . . 117

6.2 **Extended** $U(1)_A \times U(1)_W$ **model:** A typical graph which exhibits the effects of the higher derivative terms on the scalar fields. Solid line is for $(c_\phi, c_\psi, c_{\phi\psi})$=$(0, 0, 0)$, dotted line for $(c_\phi, c_\psi, c_{\phi\psi})$=$(0, 1, 0)$, dashed for $(c_\phi, c_\psi, c_{\phi\psi})$=$(1, 0, 0)$ while dashed and dotted for $(c_\phi, c_\psi, c_{\phi\psi})$=$(1, 1, 0)$. In the case $(c_\phi, c_\psi, c_{\phi\psi})$=$(0, 0, 1)$, $P$ is trivial. Parameters in this figure are $(g_1, g_2, g_3, e, q, u, v_1, M, N)$= $(14, 12, 14, 6, 2, 1, 7.5{\cdot}10^{-3}, 1, 1)$.118

6.3 **Extended** $U(1)_A \times U(1)_W$ **model:** The effect of the higher derivative terms on the energy and the supercurrent when these are plotted vs. the radius of the torus. Solid line is for $(c_\phi, c_\psi, c_{\phi\psi})$=$(0, 0, 0)$, dotted line for $(c_\phi, c_\psi, c_{\phi\psi})$=$(0, 1, 0)$, dashed for $(c_\phi, c_\psi, c_{\phi\psi})$=$(1, 0, 0)$ while dashed and dotted for $(c_\phi, c_\psi, c_{\phi\psi})$=$(1, 1, 0)$. For $(c_\phi, c_\psi, c_{\phi\psi})$=$(0, 0, 1)$, the supercurrent as well as the charge condensate, are trivial. Parameters in this figure are $(g_1, g_2, g_3, e, q, u, v_1, M, N)$=$(14, 12.5, 14, 10, 2, 1, 7.5{\cdot} 10^{-3}, 1, 1)$. . . . . . . . . . . . . . . . . . . . . . . . . . . . 119

# Bibliography

[1] N.Papanicolaou, T.N.Tomaras, *Nucl.Phys.* **B 360** (1991) 425.

[2] N.Papanicolaou, T.N.Tomaras, *Phys.Lett.* **A 179** (1993) 33; G.Stratopoulos, T.N.Tomaras, *Phys.Rev.* **B 54** (1996) 12493; *Physica* **D 89** (1995) 136.

[3] K.B.W.Buckley, M.A.Metlitski and A.R.Zhitnitsky, *hep-ph*/**0212074**.

[4] K.B.W.Buckley and A.R.Zhitnitsky, *cond-mat*/**0211245**.

[5] I.Chuang et.al., *Science* **2351** (1991) 1336.

[6] M.Bowick et.al., *Science* **2360** (1994) 943.

[7] V.M.H.Ruutu et.al., *Nature* **382** (1996) 334.

[8] N.S.Ginsberg, J.Brand, L.V.Hau, *Phys.Rev.Lett.* **94** (2005) 040403 and references therein.

[9] "Topological Defects and the Non-Equilibrium Dynamincs of Symmetry Breaking Phase Transitions", Y.M.Bunkov, H.Godfrin, (NATO Science Serious-Vol. 549, 1999).

[10] C.Winkelmann, J.Elbs, Y.Bunkov and H.Godfrin, *Phys.Rev.Lett.* **96** (2006) 205301.

[11] I.Chuang, N.Turok, B.Yurke, *Phys.Rev.Lett.* **66** (1991) 2472.

[12] S.Digal, R.Ray and A.M.Srivastava, *Phys.Rev.Lett.* **83** (1999) 5030.

[13] C.Bachas and T.N.Tomaras, *Nucl.Phys.* **B 428** (1994) 209; conference proceedings, *hep-ph*/**9501264**.

[14] C.Bachas and T.N.Tomaras, *Phys.Rev.* **D 51**, 5356 (1995); *Phys.Rev.Lett.* **76**, (1996) 356; C.Bachas, B.Rai and T.N.Tomaras, *Phys.Rev.Lett.* **82** (1999) 2443; T.N.Tomaras in conference proceedings, *hep-ph*/**9612341**; *hep-ph*/**9707236**.

[15] C.Bachas, P.Tinyakov and T.N.Tomaras, *Phys.Lett.* **B 385** (1996) 237; L.Perivolaropoulos and T.N.Tomaras, *Phys.Rev.* **D 62** (2000) 025012; *hep-ph*/**9911227**.

[16] T.W.B.Kibble, *J.Phys.* **A 9** (1976) 1387.

[17] T.H.R.Skyrme, *Proc.Roy.Soc.* **262** (1961) 233.

[18] H.B.Nielsen and P.Olesen, *Nucl.Phys.* **B 61** (1973) 45.

[19] G.'t Hooft, *Nucl.Phys.* **B 79** (1974) 276.

[20] C.P.Dokos and T.N.Tomaras, *Phys.Rev.* **D 21** (1980) 2940.

[21] D.A.Kirzhnits, *JETP Lett.* **15** (1972) 745.

[22] Zel'dovich, Ya.B.Kozbarev, I.Yu and L.B.Okun, *Sov.Phys.JETP* **40** (1974) 1.

[23] S.Weinberg, *Phys.Rev.* **D 9** (1974) 3357.

[24] A.E.Everett, *Phys.Rev.* **D 10** (1974) 3161.

[25] T.Vachaspati and A.Vilenkin, *Phys.Rev.* **D 31** (1985) 3052.

[26] R.R.Caldwell and B.Allen, *Phys.Rev.* **D 45** (1992) 3447.

[27] C.Ringeval, M.Sakellariadou, F.Bouchet, *JCAP* **0702** (2007) 023.

[28] M.Donaire, A.Rajantie, *Phys.Rev.* **D 73** (2006) 063517.

[29] V.Vanchurin, K.D.Olum, A.Vilenkin, *Phys.Rev.* **D 74** (2006) 063527.

[30] V.Vanchurin, K.Olum and A.Vilenkin, *Phys.Rev.* **D 72** (2005) 063514.

[31] T.Matsuda, *JCAP* **0604** (2006) 005.

[32] T.W.B.Kibble, N.Turok, *Phys.Lett.* **B 116** (1982) 141.

[33] E.Copeland, D.Haws, M.Hindmarsh, N.Turok, *Nucl.Phys.* **B 306** (1988) 908.

[34] A.Babul, T.Piran, D.N.Spergel, *Phys.Lett.* **B 202** (1988) 307.

[35] P.Peter, *Phys.Rev.* **D 46** (1992) 3335.

[36] P.Peter, *Phys.Rev.* **D 47** (1993) 3169.

[37] Y.Shnir, *Phys.Rev.* **D 72** (2005) 055016.

[38] A.B.Gadde and U.A.Jajnik, *hep-th*/**0511235**.

[39] J.J.Blanco-Pillado and A.Iglesias, *Phys.Lett.* **B 636** (2006) 207.

[40] Y.Lemperiere, E.P.S.Shellard, *Nucl.Phys.* **B 649** (2003) 511.

[41] R.L.Davis, E.P.S.Shellard, *Nucl.Phys.* **B 323** (1989) 209.

[42] R.L.Davis, *Phys.Rev.* **D 38** (1988) 3722.

[43] E.Copeland, M.Hindmarsh, N.Turok, *Phys.Rev.Lett.* **58** (1987) 1910.

[44] C.T.Hill, H.M.Hodges, M.S.Turner, *Phys.Rev.Lett.* **59** (1987) 2493.

[45] C.T.Hill, H.M.Hodges, M.S.Turner, *Phys.Rev.* **D 37** (1988) 263.

[46] R.L.Davis, E.P.S.Shellard, *Phys.Lett.* **B 209** (1988) 485.

[47] X.Martin, P.Peter, *Phys.Rev.* **D 51** (1995) 4092.

[48] B.Carter, X.Martin, *Ann.Phys.* **227** (1993) 151.

[49] B.Carter, P.Peter, A.Gangui, *Phys.Rev.* **D 55** (1997) 4647.

[50] M.Nagasawa, J.Yokoyama, *Phys.Lett.* **B 345** (1995) 416.

[51] E.J.Copeland, T.W.B.Kibble, D.A.Steer, *Phys.Rev.* **D 58** (1998) 043508.

[52] D.Haws, M.Hindmarsh, N.Turok, *Phys.Lett.* **B 209** (1988) 255.

[53] R.H.Brandenberger and L.Perivolaropoulos and A.Stebbins, *Int.J.Mod.Phys.***A5** (1990) 1633.

[54] D.P.Bennett, *Phys.Rev.* **D 33** (1986) 872.

[55] N.Turok, *Phys.Lett.* **B 126** (1983) 437.

[56] A.Vilenkin, Q.Shafi, *Phys.Rev.Lett.* **51** (1983) 1716.

[57] N.Turok, *Nucl.Phys.* **B 242** (1984) 520.

[58] J.Silk, A.Vilenkin, *Phys.Rev.Lett.* **53** (1984) 1700.

[59] N.Turok, R.H.Brandenberger, *Phys.Rev.* **D33** (1986) 2175.

[60] A.Vilenkin, *Phys.Rev.Lett.* **46** (1981) 1169.

[61] A.Albrecht, N.Turok, *Phys.Rev.Lett.* **54** (1985) 1868.

[62] P.Laguna, R.Matzner, *Phys.Rev.* **D 41** (1990) 1751.

[63] D.P.Bennett, F.R.Bouchet, *Phys.Rev.* **D 41** (1990) 2408.

[64] P.P.Avelino, C.Martins, C.Santos, E.P.S.Shellard, *Phys.Rev.* **D 68** (2003) 123502.

[65] P.P.Avelino, C.J.A.P.Martins, C.Santos, E.P.S.Shellard, *Phys.Rev.Lett.* **89** (2002) 271301.

[66] C.J.A.P.Martins and E.P.S.Shellard, *Phys.Rev.* **D 73** (2006) 043515.

[67] P.P.Avelino, C.J.A.P.Martins, J.Menezes, R.Menezes and J.C.R.E.Oliveira, *Phys.Rev.* **D 73** (2006) 123519.

[68] C.T.Hill, D.N.Schramm, T.P.Walker, *Phys.Rev.* **D 36** (1987) 1007.

[69] A.de Laix, T.Vachaspati, *Phys.Rev.* **D 54** (1996) 4780.

[70] A.de Laix, L.M.Krauss, T.Vachaspati, *Phys.Rev.Lett.* **79** (1997) 1968.

[71] B.Allen, R.R.Caldwell, S.Dodelson, L.Knox, E.P.S.Shellard, A.Stebbins, *Phys.Rev.Lett.* **79** (1997) 2624.

[72] M.Oguri and K.Takahashi, *Phys.Rev.* **D 72** (2005) 085013.

[73] F.Ferrer and T.Vachaspati, *Phys.Rev.Lett.* **95** (2005) 261302.

[74] J.P.Ostriker, C.Thompson, E.Witten, *Phys.Lett.* **B 180** (1986) 231.

[75] C.T.Hill, D.N.Schramm, T.P.Walker, *Phys.Rev.* **D 36** (1987) 1007.

[76] R.Schild, I.S.Masnyak, B.I.Hnatyk, V.I.Zhdanov, *Astron.Astrophys.* **422** (2004) 477.

[77] M.Sazhin et.al., *MNRAS* **343** (2003) 353.

[78] M.Sazhin et.al., *astro-ph*/**0406516**.

[79] M.Fairbairn, *astro-ph*/**0511085**.

[80] M.V.Sazhin, M.Capaccioli, G.Longo, M.Paolillo, O.S.Khovanskaya, N.A.Grogin, E.J.Schreier, G.Covone, *astro-ph*/**0601494**.

[81] M.J.Jackson, N.T.Jones, J.Polchinski, *JHEP* **0510** (2005) 013.

[82] J.Polchinski, *hep-th*/**0412244**.

[83] K.J.Mack, D.H.Wesley, L.J.King, *astro-ph*/**0702648**.

[84] S.Coleman and E.Weinberg, *Phys.Rev.***D 7** (1973) 1887.

[85] T.D.Lee, *Phys.Rep.***23 C** (1976) 254.

[86] R.L.Davis and E.P.S.Shellard, *Phys.Rev.Lett.***63** (1989) 2021.

[87] P.Amsterdamski and P.Laguna-Castillo, *Phys.Rev.* **D 37** (1988) 877.

[88] Y.Brihaye and T.N.Tomaras, *Nonlinearity* **12** (1999) 867.

[89] C.G.Doudoulakis, *Nonlinearity* **17** (2004) 2293; ArXiv: hep-th/0404146 .

[90] C.G.Doudoulakis, *Physica* **D 228** (2007) 159; ArXiv: hep-ph/0612095 .

[91] C.G.Doudoulakis, *Physica* **D 234** (2007) 1; ArXiv: hep-ph/0702243 .

[92] M.S.Volkov, *Phys.Lett.* **B 644** (2007) 203.

[93] A.Achucarro, T.Vachaspati, *Phys.Rept.* **327** (2000) 347.

[94] B.Kleihaus, J.Kunz, Ya.Shnir, *Phys.Rev.* **D 68** (2003) 101701.

[95] P.Forgacs, S.Reuiller, M.S.Volkov, *Phys.Rev.Lett.***96** (2006) 041601; P.Forgacs, S.Reuiller, M.S.Volkov, *Nucl.Phys.***B 751** (2006) 390.

[96] Y.Koma, H.Suganuma and H.Toki, *Phys.Rev.* **D 60** (1999) 074024.

[97] J.Jäykkä and J.Hietarinta, *cond-mat*/**0608424**.

[98] G.H. Derrick, *J. Math. Phys.* **5** (1964) 1252.

[99] W.H.Zurek, *Phys.Rep.* **276** (1996) 177.

[100] A.D.Linde, *Rep.Prog.Phys.* **42** (1979) 294 and references therein.

[101] J.Paramos, O.Bertolami, T.A.Girard and P.Valko, *Phys.Rev.* **B 67** (2003) 134511.

[102] M.Hindmarsh, A.Davis, R.Brandenberger, *Phys.Rev.* **D 49** (1994) 1944.

[103] E.Witten, *Nucl.Phys.* **B 249** (1985) 557.

[104] W.H.Press, B.P.Flannery, S.A.Teukolsky, W.T.Vetterling, "Numerical Recipes", Cambridge University Press 1986.

[105] A.Vilenkin, E.P.S.Shellard, "Cosmic Strings and other topological defects", Cambridge University Press 1994.

[106] T.W.B.Kibble, *Phys.Rev.* **D 67** (1980) 183; T.W.B.Kibble, M.Hindmarsh, *Rep.Prog.Phys.* **58** (1995) 477.

[107] S.J.Avis and C.J.Isham, *Proc.R.Soc.A* **363** (1978) 571.

[108] N.S.Manton and T.M.Samols, *Phys.Lett.B* **207** (1988) 179.

[109] Y.Brihaye, S.Giller, P.Kosinski and J.Kunz, *Phys.Lett.* **B 293** (1992) 383.

[110] J-Q.Liang, H.J.W.Muller-Kirsten and D.T.Tchrakian, *Phys.Lett.* **B 282** (1992) 105.

[111] H.W.Braden, *J.Phys.A: Math.Gen.* **18** (1985) 2127.

[112] H.W.Braden, *J.Math.Phys.* **28** (1987) 929.

[113] J-Q.Liang, H.J.W.Muller-Kirsten, D.K.Park and F.Zimmerschied, *Phys.Rev.Lett.* **81** (1998) 216.

[114] Y.Brihaye, B.Hartmann, *Mod.Phys.Lett.* **A16** (2001) 1895.

[115] M.Sakamoto, M.Tachibana, K.Takenaga, *Phys.Lett.* **B 457** (1999) 33.

[116] M.Sakamoto, M.Tachibana, K.Takenaga, *Phys.Lett.* **B 458** (1999) 231.

[117] M.Sakamoto, M.Tachibana, K.Takenaga, *Prog.Theor.Phys.* **104** (2000).

[118] A.Albrecht, R.A.Battye, J.Robinson, *Phys.Rev.Lett.* **79** (1997) 4736.

[119] A.Vilenkin, A.E.Everett, *Phys.Rev.Lett.* **48** (1982) 1867.

[120] A.Albrecht, R.A.Battye, J.Robinson, *Phys.Rev.* **D 59** (1999) 023508.

[121] T.Vachaspati, *Contemp.Phys.* **39** (1998) 225.

[122] T.W.B.Kibble, *astro-ph*/**0410073**.

[123] J.Preskill, *Vortices and monopoles*, Lectures presented at the 1985 *Les Houches Summer School*, Les Houches, France.

[124] A.A.Abrikosov, *Sov.Phys. JETP* **5** (1957) 1174.

[125] R.L.Davis, *Mod.Phys.Lett.* **A 5** (1990) 853.

[126] R.L.Davis, *Mod.Phys.Lett.* **A 6** (1991) 73.

[127] L.Perivolaropoulos, *astro-ph*/**0501590**.

[128] A.Vilenkin, *hep-th*/**0508135**.

[129] A.C.Davis and T.W.B.Kibble, *Contemp.Phys.* **46** (2005) 313.

[130] M.Sakellariadou, *Annalen Phys.* **15** (2006) 264.

[131] M.Sakellariadou, *hep-th*/**0602276**.

[132] M.Majumbar, *hep-th*/**0512062**.

[133] A.Achucarro, A.Celi, M.Esole, J.V.den Bergh and A.V.Proeyen, *JHEP* **0601** (2006) 102.

[134] M. Donaire, *J.Phys.* **A 39** (2006) 15013.

[135] http://www.damtp.cam.ac.uk/user/gr/public/cs_interact.html.

[136] Y.M.Bunkov and H.Godfrin, "Topological defects and the non-equilibrium dynamics of symmetry breaking phase transitions", Kluwer Academic Publishers 2000.

[137] J.Polchinski, "String Theory. Vol.2: Superstring Theory and beyond", Cambridge University Press 1998.